PhD Program in Biomolecular Sciences

Department of Cellular, Computational and Integrative Biology – CIBIO

38th Cycle

"Deciphering tranSNPs: functional genetic variants shaping protein output and cancer-related phenotypes"

Tutor

Prof. Alberto Inga

University of Trento

Advisor

Prof. Alessandro Romanel

University of Trento

Ph.D. Thesis of

Laura Alunno

University of Trento

Academic Year 2024-2025

Declaration of Original Authorship

I, Laura Alunno, confirm that this is my own work and the use of all material from other sources has been properly and fully acknowledged.

In particular, I shared the work on the initial characterization of HCT116 edited clones (DDIT4 protein levels and DDIT4 protein stability; polysome profiling and global protein synthesis; cell proliferation and cell cycle) and the co-culture experiments with Meriem H. Hamadou from the Laboratory of Transcriptional Networks. Indeed, we are co-first authors of two preprints related to this work.

Collaborations with external laboratories are clearly mentioned in the text.

Table of Contents

List of Abbreviations

Abbreviation	***Definition***
AF/dAF	Allelic Fraction/Delta Allelic Fraction
CDS	Coding Sequence
COAD	Colorectal Adenocarcinoma
DFI	Disease-Free Interval
DPF	Days Post Fertilization
ER	Endoplasmic Reticulum
GWAS	Genome-Wide Association Study
HDR	Homology-Directed Repair
IFN	Interferon
Kd	Dissociation Constant
MAF	Minor Allelic Fraction
POL	Polysomal mRNA fraction
RBP	RNA Binding Protein
REMSA	RNA Electromobility Shift Assay
RIP	RNA/RBP immunoprecipitation
RNP	Ribonucleoprotein particle
rs	Reference SNP cluster ID
smiFISH	Single-molecule inexpensive Fluorescence In Situ Hybridization
SNP	Single Nucleotide Polymorphism
SNV	Single Nucleotide Variant
TCGA	The Cancer Genome Atlas
TE	Translation Efficiency
TF	Transcription Factor
TME	Tumor Microenvironment
TOT	Total mRNA fraction
UTR	Untranslated Region

Abstract

This study investigates the impact of genetic diversity, in the form of single-nucleotide polymorphisms (SNPs), on the post-transcriptional control of gene expression, to identify a novel class of functional SNPs, named tranSNPs, with potential applications as biomarkers for cancer diagnosis, prognosis, or targeted therapy; tranSNPs are defined as SNPs whose allelic fraction is significantly imbalanced across polysome-bound and total mRNAs.

We provide a comprehensive characterization of tranSNPs and their implications by exploring their cell line and cancer-type specificity, as well as their mechanistic insights focusing on the rs1053639 tranSNP (T/A) on DDIT4 3'UTR. This example demonstrated that a 3'UTR SNP can significantly affect mRNA localization, modification, and polysomal recruitment through allele-specific interaction with the trans-factor RBMX, eventually causing allele-specific differences in protein levels and downstream phenotypes related to cancer. Indeed, autophagy, cell competition, and *in vivo* xenotransplantation were significantly affected across TT and AA clones homozygous for the SNP.

Furthermore, analysis of TCGA colorectal cancer data revealed that rs1053639 alleles are prognostic for disease-free interval (DFI), and we uncovered allele-specific sensitivities to a number of compounds. When further explored, tranSNPs could become an uncharted source of SNPs to be used as biomarkers for cancer prognosis and to guide treatments based on SNP genotype in the context of personalized medicine.

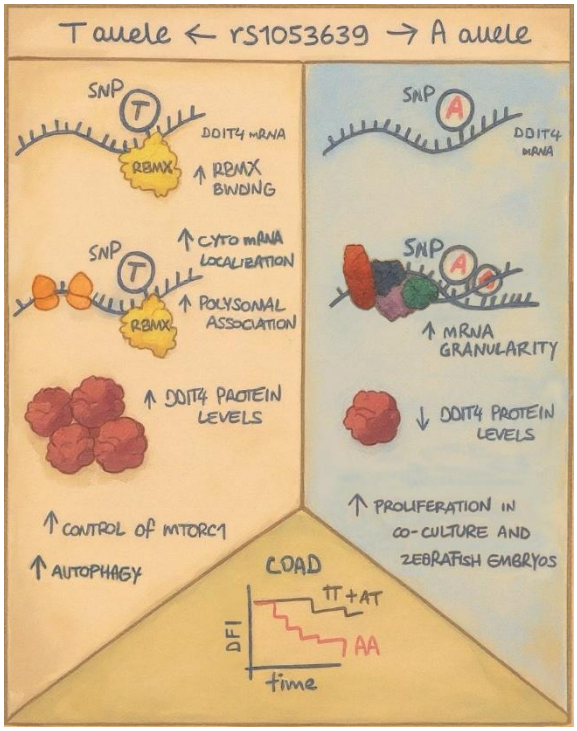

Introduction

A notable layer of gene expression regulation occurs post-transcriptionally

Gene expression is a complex and finely modulated process that allows the temporal, level, and tissue-specific expression of genes, enabling the generation of diverse phenotypes from the same genome and ultimately establishing cell identities (Buccitelli and Selbach, 2020). Indeed, the complexity of an organism is better reflected by the number of different cell types and is driven by how genes are finely tuned, rather than by the haploid genome size (C-value paradox) or the number of genes (G-value paradox) (Buccitelli and Selbach, 2020; Hahn and Wray, 2002; Thomas, 1971). Consequently, the dysregulation of such a central process is one of the most relevant topics in biomedicine.

Traditionally, transcription was considered the primary, if not the unique, regulator of gene expression, with transcription factors (TFs), enhancers, and epigenetic marks being regarded as the main regulatory components (Lee and Young, 2013; Maston et al., 2006). Although transcription represents the initial step of gene expression and is undoubtedly critical, it does not fully account for the diversity of gene output.

Over the past decades, post-transcriptional regulation emerged as another layer in tuning gene expression. The mRNA splicing, modification, degradation, export, polyadenylation, translation, and protein degradation are key events underlying post-transcriptional regulation (Bertram and Schuster, 2014; Corbett, 2018) (**Figure 1**).

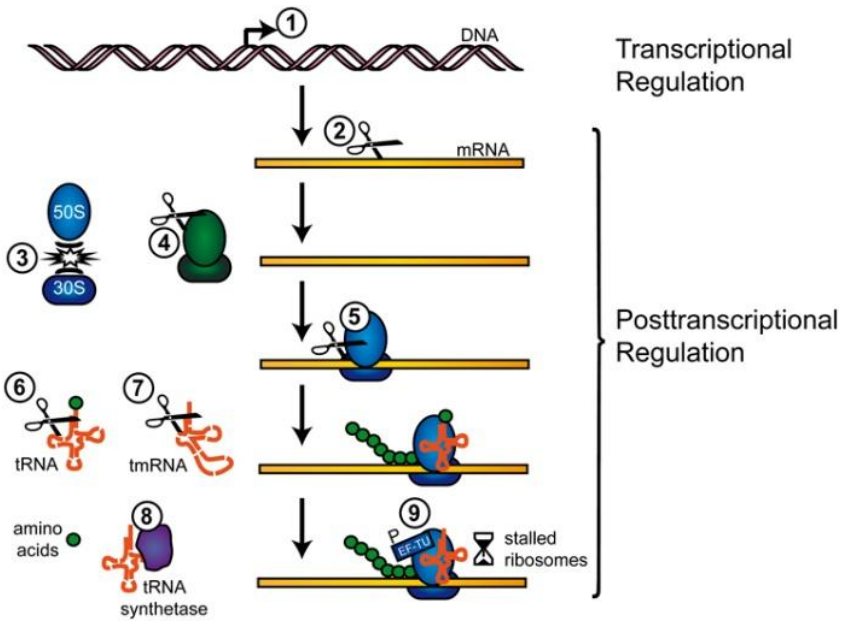

Figure 1. Gene expression is dynamically regulated by transcriptional and post-transcriptional events. The attention towards post-transcriptional events has grown in the last decade and includes mRNA processing, modification, and translation (Bertram and Schuster, 2014).

While in some cases mRNA levels are mere proxies for protein levels, in other cases post-transcriptional regulation can set protein levels independently from mRNA levels (Franks et al., 2017). This is frequently observed for the regulators of metabolic fluxes, whose protein levels must be rapidly adjusted in response to environmental changes (Daran-Lapujade et al., 2007; Kim and Kyung Lee, 2012). The activation of the mTOR pathway itself, which is a master regulator of cell metabolism, has been associated to the shortening of the 3' untranslated regions (UTRs) of its target mRNAs through alternative polyadenylation, which in turn reduces the space for the RNA-binding protein (RBP) and microRNA (miRNA)-mediated control of gene expression (Yeh and Yong, 2020). Similarly, cells need a preponderance of post-transcriptional regulation for genes involved in cell division to tightly couple cell cycle progression with cell growth (Mulas, 2024; Polymenis and Schmidt, 1997). The most abundant modification on messenger RNAs (mRNAs), N6-methyl-adenosine, referred to as m6A, has also been found to control cell fate transitions in stem cells, highlighting a role for post-transcriptional regulation in development as well (Batista et al., 2014; Chen et al., 2015; Jalkanen and Wilusz, 2014; Li et al., 2021).

This renewed interest and awareness were stimulated by the development of RNA sequencing and its variants, and studies highlighting that transcription and translation should not be considered as completely distinct processes, but as interconnected and coordinated, although they occur in separate cellular compartments in eukaryotes. Interestingly, the mTOR pathway is considered a master coordinator of transcription and translation, eventually shaping various cell responses (Adams-Brown and Reid, 2025). The mTOR can indeed modulate the translation of transcription factors but also influence the activity of chromatin remodelling complexes such as NURD and CoREST (Dufour et al., 2022). Conversely, p53, which is considered a central transcription factor, can transcriptionally induce translation initiation factors such as 4EBP1, affect ribosome biogenesis and transfer RNAs (tRNAs) production by acting on the activity of the RNA Polymerases I and III and broadly modulate translation by acting as an RBP itself (Crighton et al., 2003; Marcel et al., 2018, 2015; Tiu et al., 2021); p53 can also inhibit mTORC1 through its transcriptional targets Sestrin1 and Sestrin2 (Loayza-Puch et al., 2013), and perform protein-protein interactions with the m6A writer METTL3 to be stabilized, promote the epitranscriptomic modification of p53 target genes and reinforce p53-mediated effect as a tumour suppressor (Raj et al., 2022). There is now solid evidence that splicing occurs co-transcriptionally and is, in turn, regulated by RNA folding (Buratti and Baralle, 2004; Shenasa and Bentley, 2023). Moreover, dynamic interplays exist between transcription, RNA decay, and ribosome dynamics (Heck and Wilusz, 2018; Murakami et al., 2025).

Overall, there is strong literature evidence indicating that transcription, RNA processing, and translation cannot be considered as separate events, but are intertwined, so that the interpretations deriving from static RNA steady-state level analyses will need to be revised (Furlan et al., 2020) and opened to the concepts of RNA decay rate and translation. The evidence that post-transcriptional events matter in collectively regulating gene expression is mounting, and there are already multiple examples of new therapeutic strategies arising from the study of post-transcriptional events (Laham-Karam et al., 2020). Great effort is being made to modulate the splicing of the SMN2 gene, to boost the levels of SMN protein, which in Spinal Muscular Atrophy (SMA) are low due to mutations in SMN1 (Fitzgerald et al., 2018). Major global health challenges such as diabetes, obesity, and hypercholesterolemia are also currently being tackled by inhibiting target miRNAs (Hennessy and Moore, 2013). Chemotherapeutic drugs

such as Synribo are currently in clinical use for Chronic Myeloid Leukemia (CML) as translation elongation inhibitors (Gandhi et al., 2014).

Single-nucleotide polymorphisms are crucial regulators of gene expression

A substantial proportion of the genetic contribution to complex disorders, including cancer, is still unexplained. Multiple types of genetic variants exist and can be classified based on their allelic frequency and effect size (**Figure 2**). Variants with a minor allele frequency (MAF) of 5% or higher are defined as common variants, whereas those below this threshold are considered rare. Rare variants often have large effects (e.g., in Mendelian disorders), while rare variants of small effect remain challenging to detect with the current genetic tools and approaches. Common variants are typically identified by Genome Wide Association Studies (GWAS) and have modest effects but can synergize to generate complex traits. Importantly, common genetic variants have a considerable potential to be broadly used as disease biomarkers due to the high frequency of both alleles in the population (Yengo et al., 2022).

However, despite the huge effort invested into GWAS over the past decade, a substantial gap persists between known and unknown disease-associated variants, which is named missing heritability. While low-frequency variants with intermediate effect sizes may explain part of the missing heritability in complex diseases, it is also increasingly evident that certain genomic regions (e.g., UTRs), as well as ancestrally diverse populations, are underrepresented in GWAS studies (Chen et al., 2024; Fitipaldi and Franks, 2023; Reshef et al., 2018; Tam et al., 2019). It is therefore possible that common genetic variants in UTRs, which escape detection by GWAS, may play a larger role than currently appreciated and contribute to the missing heritability. These variants must therefore be identified with alternative methods that extend beyond the traditional association studies.

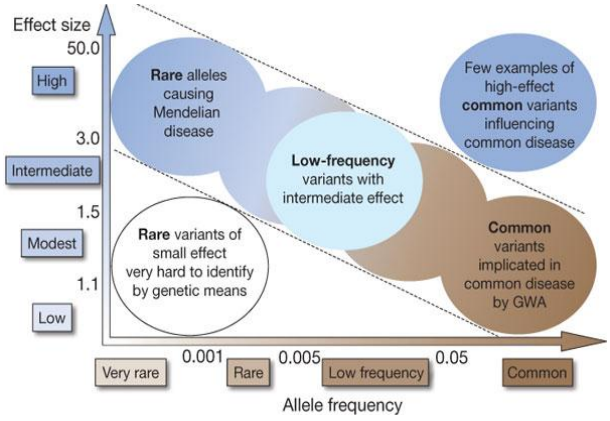

Figure 2. The allele frequency–effect size spectrum illustrates the contribution of genetic variants to disease risk.

The gap between the known and unknown genetic variants is named "missing heritability" (Gandhi et al., 2014; Manolio et al., 2009).

Single-nucleotide polymorphisms (SNPs) are among the most abundant classes of genetic variation in the human genome. SNPs are defined as germline substitutions of a single nucleotide at a specific position in the genome with a minor allelic frequency greater than 1% in the population. This feature makes SNPs particularly amenable to personalized medicine (Ho et al., 2019; Weitzel et al., 2011). SNPs occur, on average, once every 300 base pairs of sequence in the human genome (Kruglyak and Nickerson, 2001).

Over the past decade, GWAS have identified a large number of disease-associated SNPs with low to modest effect sizes. However, as discussed above, such studies systematically underscored the untranslated (UTR) regions of transcripts and largely focused on the association with disease risk, rather than disease prognosis or therapy. Early functional characterization highlighted variants located in promoters and enhancers, where they influence transcription by impinging on the creation or disruption of TF binding sites, or by changing the affinity of the TFs for their sites (Degtyareva et al., 2021; Menendez et al., 2019, 2007).

With the growing awareness and recognition of the post-transcriptional control of gene expression, some studies have begun to explore SNPs affecting the post-transcriptional regulation as well. Notably, one of the first studies described riboSNitches, which are functional RNA structures disrupted by SNPs, while other studies reported specific examples of functional SNPs in the 5' and 3' UTRs that altered microRNA-binding sites (Landi et al., 2008;

Solem et al., 2015). Despite these advances, SNPs affecting post-transcriptional regulation have remained comparatively understudied, largely due to the limited availability of experimental and computational tools for interrogating UTR-mediated regulation compared to transcriptional regulatory regions (Bahrami-Samani et al., 2015; de Klerk and 't Hoen, 2015). Furthermore, these pioneering studies proved the importance of SNPs in modulating post-transcriptional processes, but they did not provide a pipeline for systematically identifying instances of SNPs involved in post-transcriptional regulation.

A pipeline for the identification of SNPs involved in post-transcriptional regulation

To this regard, a few years ago, the Laboratory of Transcriptional Networks (headed by Prof. A. Inga) in which I am working – in collaboration with the Laboratory of Bioinformatics and Computational Genomics (headed by Prof. Alessandro Romanel, University of Trento) – published a pipeline for the identification of tranSNPs, where tranSNPs were defined as "a class of functional SNPs affecting the mRNA translation potential" (Valentini et al., 2021). The pipeline relies on the comparative analysis of the allelic fraction (AF) of the alternative allele across polysome-bound mRNAs (POL) and total mRNAs (TOT) for the SNPs that are heterozygous and transcribed in a certain cell line. Polysome-bound mRNAs are considered a proxy for the actively translated mRNAs, while total mRNAs are a proxy for less translated mRNAs. We assume that when two SNP alleles are significantly imbalanced in the polysomal compared to the total RNA, one allele is enriched in the polysomes; therefore, the SNP is identified as a putative tranSNP (**Figure 3**).

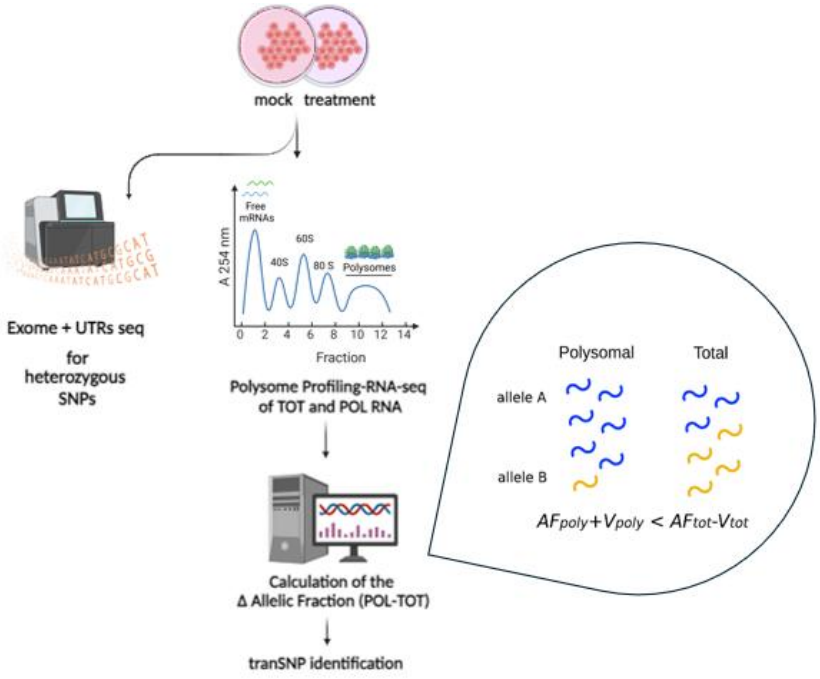

Figure 3. The pipeline for the identification of tranSNPs: RNA-seq-based quantification of allelic fraction across polysome-bound and total mRNAs.

The pipeline captures instances of allelic imbalances in polysome-bound compared to total mRNAs.

Firstly, the requirement for SNP heterozygosity is addressed by performing (or using publicly available) exome sequencing datasets covering the UTRs. SNPs with allelic fraction (AF) values between 0.2 and 0.8 are classified as heterozygous. This wide range of allelic fractions, divergent from the expected 0.5 allelic fraction, has been observed across all the datasets, attributed to potential technical biases in the RNA-seq workflow, such as position-specific sequencing properties.

Polysome-bound mRNAs are subsequently isolated by polysome profiling, a method based on sucrose gradient ultracentrifugation that separates polysome-associated mRNAs from those bound to monosomes or to the ribosomal subunits or ribosome-free mRNAs, which together constitute the total mRNA pool in the cytoplasm (Chassé et al., 2017; Rodriguez-Martinez and Young-Baird, 2025). The total mRNA fraction thus includes the polysome-bound mRNAs, which might dilute the magnitude of the observed effect. Alternatively, the free mRNA fraction, which contains poorly translated mRNAs, may be used instead of total mRNA. However, previous reports as well as our data (see **Figure 12A-C** in the Results section) have shown that this fraction contains a relatively low amount of mRNA (Panda et al., 2017), which may negatively

affect the subsequent library preparation and sequencing quality. Indeed, both polysome-bound and total mRNAs are then subjected to RNA sequencing (RNA-seq).
Only the SNPs identified in the preliminary genotyping are then interrogated in the RNA-seq data, overcoming the intrinsic noise in SNP calling and coverage. Quality controls, such as a depth of coverage of at least 20 reads at the SNP site across all biological replicates and fractions, are subsequently applied, generating a more restricted set of "analyzable" SNPs.
Paired t-test statistics is performed to compare AF measures between matched polysomal and total mRNA samples across biological replicates. Analyzable SNPs displaying nominal p-values ≤0.05 are considered as putative tranSNPs.

Aside from mock conditions, the pipeline can also be applied to treated cells. The use of RNA-seq data for identifying instances of allele-specific gene expression is consolidated (Mayba et al., 2014; Pandey et al., 2013; Romanel, 2019), but this is the first example in which RNA sequencing data is used to identify SNPs potentially affecting gene expression specifically at the post-transcriptional level. Notably, new insightful technologies for studying translation, such as Ribo-seq (Limbu et al., 2024), have recently come out. However, Ribo-seq does not provide enough coverage of UTR regions, because the method captures ribosome-protected fragments (footprints), and ribosome footprints are generally restricted to the coding region (Brar and Weissman, 2015; Wang et al., 2020). Instead, the UTRs, which are the prominent regulatory regions for translation, hold a huge potential for harbouring SNPs potentially affecting gene expression at the post-transcriptional level; therefore, our pipeline for tranSNPs identification sticks with the polysome-sequencing. Moreover, the whole study was originally stimulated by the observation that some melanoma patients' samples showed 5' UTR variants of uncertain significance rather than mutations in the typical predisposing genes for melanoma, such as CDKN2A (Andreotti et al., 2016).

Three tranSNP catalogues: MCF7, HCT116 and RPE-1

Our tranSNP-identifying pipeline was applied to the breast cancer cell line MCF7 in the earliest work (Valentini et al., 2021). This dataset relies on high coverage (80 million reads, minimal local depth of 10X), pair-end RNA sequencing, but only two biological replicates. Cells were exposed to either 10 μM Nutlin or 1 μM Doxorubicin for 16 hours, in addition to the mock condition, to activate p53, given its emerging role in the regulation of translation. Overall, 147

SNPs, corresponding to about 4% of the analyzable SNPs, were identified as putative tranSNPs. Imbalances were almost equally divided between constitutive, doxorubicin-dependent, and Nutlin-dependent. A slight overlap of only three tranSNPs was observed between mock and treatments; it can probably be ascribed to differences in local coverage and quality control thresholds, since a consistent subset of SNPs exhibited comparable imbalance across two or three conditions, maintaining the same directional trend even when statistical significance was not reached. The average global minor allele frequency (MAF) among tranSNPs was favorable, not restricted to particularly rare or common variants. No enrichment for specific pathways was observed among the genes harboring the tranSNPs. About 25% of tranSNPs were located in the UTRs, with the remainder in coding regions. In this initial catalogue, statistical analysis was built on variance estimates; indeed, correction for multiple testing was not applied, as the independence of SNPs could not be reliably assessed due to the limited ability to reconstruct haplotypes in this dataset.

To extend the approach to a different cancer cell line and increase the number of biological replicates, the pipeline was applied to the colon cancer cell line HCT116 in the next work (Hamadou and Alunno et al., 2025). This dataset consists of lower coverage than the previous (20 million reads, minimum local depth of 20X), single-end sequencing, but four biological replicates. Cells were untreated or exposed to 10 μM Nutlin for 16 hours. A total of 40 putative tranSNPs, corresponding to approximately 7% of the analyzable SNPs, were identified. As in the MCF7 dataset, no enrichment for specific pathways or gene networks was observed among the putative tranSNPs. Statistical analysis was implemented compared to the MCF7 dataset by using paired t-tests with nominal p-values, providing a more robust assessment. After a first step of validation through Sanger sequencing on new biological replicates and luciferase reporter assays, two tranSNPs were selected for an in-depth validation: rs1053639 on DDIT4 3' UTR and the rs1554710467 missense variant on EIF4H coding sequence (CDS).
The first case described a UTR variant in a p53 target gene and proposed a mechanism of action in which the tranSNP affects mRNA localization, modification, and translation efficiency, upon modelling the tranSNP in cells exploiting CRISPR/Cas9-mediated knock-in (Ghetti et al., 2021). In addition, the clinical impact of this tranSNP was assessed by analyzing the disease-free interval (DFI) in colorectal cancer cohorts from TCGA.

The second case leveraged the use of proteomics to quantify the peptides derived from either the alternative or the reference allele of a missense tranSNP at the endogenous level in a heterozygous cell line. This approach represents an initial step towards exploiting the still underscored power of allele-specific proteomics in the field of genetics.

The pipeline was subsequently applied to the human retinal pigment epithelial RPE-1 cell line to explore the tranSNP phenomenon in non-cancer cells. Further, we compared polysome-bound mRNAs to 80S-bound mRNAs in order to clarify the role of the 80S monosome in translation. Overall, the three tranSNP datasets provided a deeper understanding of the tranSNP phenomenon (**Figure 4**).

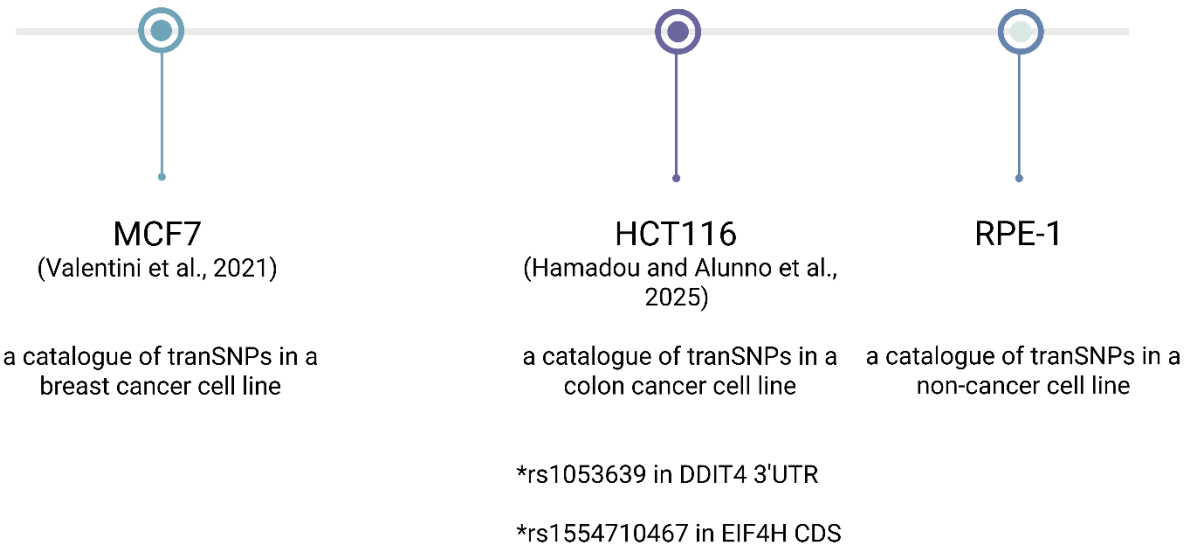

Figure 4. Schematic of the timeline and features of the three tranSNPs catalogues.

Allele-specific mRNA fate: the example of rs1053639 in the 3' UTR of DDIT4

In the HCT116 dataset, the rs1053639 tranSNP in DDIT4 mRNA emerged as the most promising and was deeply characterized. The rs1053639 is a T>A SNP, in which the T allele represents the ancestral (or reference) allele, and the A allele represents the alternative allele. According to the 1000 Genome Project Phase 3, this SNP displays a MAF of 0.46 globally, with the lowest frequency (0.2) among African populations and the highest (0.8) among East Asian populations. The SNP-containing region of DDIT4 is quite conserved across species. The high prevalence of both alleles across populations makes this variant a strong candidate biomarker for

personalized medicine. The computed allelic fraction imbalance from the RNA-seq data is -0.136 for the alternative allele, indicating that the A allele is relatively more represented in the total compared to the polysomal mRNA fraction. The rs1053639 is located approximately 90 nucleotides downstream of the stop codon, therefore, in the proximal region of DDIT4 3' UTR, which is about 0.85 kbp long. This feature is particularly relevant when considering that DDIT4 mRNA is only about 2.1 kbp long. Long 3'UTRs are generally associated with increased post-transcriptional regulation, as they tend to contain a higher density of regulatory elements, such as RBP and miRNA binding sites, or alternative polyadenylation sites (Navarro et al., 2021). Indeed, there is evidence that the 3'UTR of DDIT4 is targeted by multiple miRNAs (Sun et al., 2021; Wang et al., 2018).

The SNP host gene is DDIT4 (DNA-damage-inducible transcript 4), which is also known as REDD1 or RTP801. DDIT4 is located on the long arm of chromosome 10 and contains three exons and two introns, resulting in three splice variants (Ellisen et al., 2002; Shoshani et al., 2002). The two protein-coding isoforms share the SNP-containing region. DDIT4 has an important paralog, with similar functions, named DDIT4L. The DDIT4 protein is a 25 kDa protein (migrating at 33 kDa in western blot gels due to the multiple C-terminal lysine residues) characterized by low tissue specificity (Shoshani et al., 2002). DDIT4 protein is predominantly localized in the cytoplasm; a few studies reported that nuclear and membrane DDIT4 protein expression was associated with aggressive pancreatic and colon cancer samples (Dehghan Manshadi et al., 2025; Fattahi et al., 2021; Tajik et al., 2023), suggesting that DDIT4 protein may relocalize to the nucleus under specific conditions related to aggressive cancer behavior. Structurally, the DDIT4 protein consists of two chains, each containing antiparallel α-helices followed by four β-strands (Vega-Rubin-de-Celis et al., 2010). DDIT4 protein is degraded by the proteasome system via a cascade starting with DDIT4 phosphorylation by GSK3-β and continuing through CUL4A. The cascade is triggered by mTOR since DDIT4 degradation is crucially required for the restoration of mTOR signalling as cells recover from stress (Katiyar et al., 2009).

Indeed, functionally, DDIT4 is mostly known as a negative regulator of mTORC1 (**Figure 5**). The mTORC1 inhibition by DDIT4 was widely observed and shown in HCT116 cells as well (Wang et al., 2015). The inhibition occurs via multiple routes, such as the release of TSC1/2 from the inhibitory 14-3-3 proteins, which impedes the TSC1/2-mediated blockage of Rheb, the GTPase,

which in turn activates mTORC1 (Tirado-Hurtado et al., 2018). DDIT4 can also recruit the phosphatase-2A to inhibit the phosphorylation of Akt, which occurs upstream in the mTOR pathway (Gordon et al., 2016). Overall, DDIT4 does not act as an enzyme but rather as a stress-responsive regulatory adaptor protein that interacts with the 14-3-3 proteins or phosphatase-2A, ultimately inhibiting mTORC1. This function on the mTORC1 pathway has positioned DDIT4 as a putative tumor suppressor gene by inhibiting uncontrolled proliferation, growth, and survival, which are features of active mTORC1. Moreover, DDIT4 mediates p53 functions relative to metabolism and DNA damage response (Ellisen et al., 2002). It is debated whether DDIT4 is a direct target of p53 or if the induction of DDIT4 by p53 occurs through the intermediate RFX7 (Coronel et al., 2022). Indeed, while reporter assays supported the existence of a putative p53-responsive element (RE) in the promoter of DDIT4, p53 ChIP-seq data never confirmed the binding of p53 just upstream of the DDIT4 transcription start site (TSS) (Coronel et al., 2022). Nevertheless, recent studies positioned DDIT4 as one of the major mediators of the tumor suppressor functions of p53, comparable to the most well-known CDKN2A and PUMA (Janic et al., 2018). However, the expression of DDIT4 is rapidly induced upon different types of stresses, ranging from hypoxia (via HIF-1α) to DNA damage (via p53), nutrient starvation, and endoplasmic reticulum (ER) stress (via ATF4) (Canal et al., 2014; Sofer et al., 2005; Tirado-Hurtado et al., 2018; Whitney et al., 2009a). This role of DDIT4 in supporting cellular adaptation to stress, which is further described with examples of DDIT4 promoting autophagy (Ho et al., 2020; Wang et al., 2023; Y. Zhang et al., 2023), may instead sustain the cellular transformation, giving DDIT4 oncogenic features as well. Indeed, the elevated expression of DDIT4 correlates with worse outcomes compared to low DDIT4 expression in acute myeloid leukemia, glioblastoma, and lung cancer (Cheng et al., 2020; Fattahi et al., 2021), while the opposite association has been reported in breast, colorectal, and sporadic clear cell renal cancer carcinoma (Chen et al., 2023; Kucejova et al., 2011). Conversely, DDIT4 expression is negatively regulated by YAP/TAZ (Hwang et al., 2024). DDIT4 knock-out is not generally lethal.

Overall, these findings highlight the paradoxical role of DDIT4 in cancer, in which high expression levels can be detrimental despite the expected inhibitory effect on mTORC1 signaling.

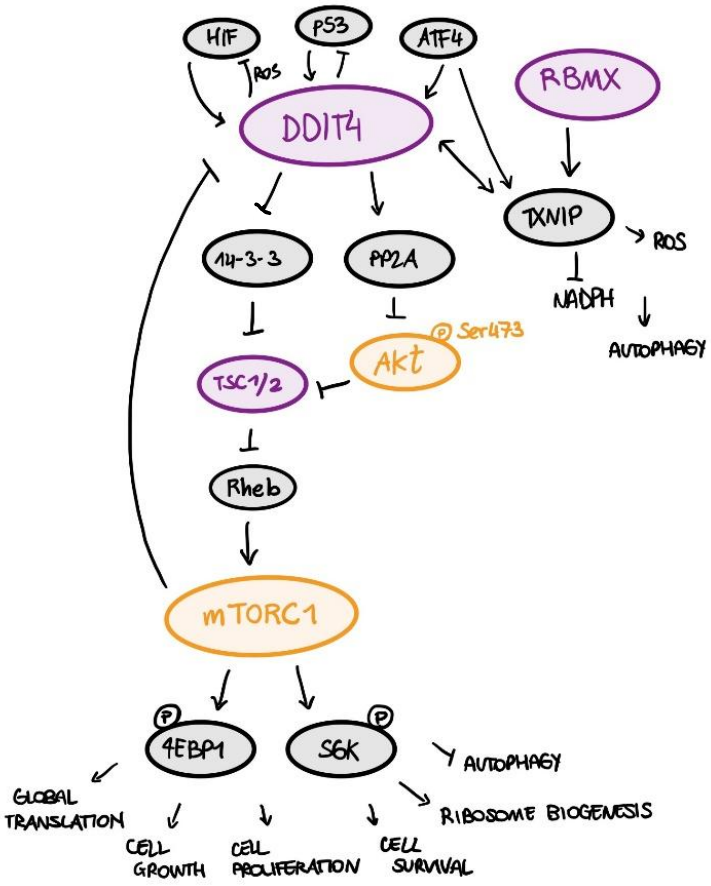

Figure 5. Schematic representation of the DDIT4 network.

DDIT4 is a central stress-responsive regulator of cellular metabolism upstream of mTORC1. While DDIT4 inhibits mTORC1 to suppress energy-consuming processes during stress conditions, it also contributes to cellular energy conservation and autophagy activation.

While overexpression or downregulation of DDIT4 is frequently observed in cancer, DDIT4 is not heavily mutated in cancer patients; only a limited number of studies have reported DDIT4 mutations, primarily in pancreatic cancer (Ding et al., 2021). Notably, two of the above-mentioned mutations mapped to DDIT4 3' UTR, and one corresponds to the tranSNP rs1053639 (m.990 T>A). Overall, the 3' UTR of DDIT4 is not very polymorphic; according to the 1000 Genome Project, there are 94 SNPs across DDIT4. The most common haplotype, corresponding to 41% of the observed cases (N=5008), features the alternative alleles for both rs1053639 and rs8316, which is located 256 bp downstream of rs1053639. The reference alleles for those two SNPs are in cis in 27% of the cases. The alleles are in cis in HCT116 cells. The third most common haplotype (11%) contains the reference rs1053639 and the alternative rs8316 alleles. Additional haplotypes exist, in which the alternative alleles of the two mentioned SNPs are in cis with other variants, but with frequencies below 3%. The rs1053639 has been cited in

additional studies: Xu et al., 2019 selected five SNPs related to the mTOR pathway and performed a study involving 441 genotyped osteoarthritis patients and 553 genotyped controls, concluding that rs1053639 in DDIT4 increased the risk of osteoarthritis. In an earlier study, Mas et al., 2015 interrogated mTOR-related SNPs and identified a network involving the rs1053639 and three other SNPs in Akt, Raptor, and FCHSD1, respectively, involved in extrapyramidal symptoms induced by antipsychotic treatment. The double-edged nature of DDIT4 in cancer complicates targeting DDIT4 as a therapeutic strategy, but at the same time, it fuels the research around and upstream of DDIT4 to find novel actionable targets and strategies.

In this regard, the mechanism we will propose in this study for rs1053639 involves the trans-factor RBMX, which holds the potential to be an actionable trans-factor. RBMX, which is also known as hnRNP G, is a ubiquitous 43-kDa RNA-binding protein with multiple roles related to transcriptional and post-transcriptional regulation. The gene coding for RBMX is located on the X chromosome. RBMX protein is primarily found in the nucleus under normal conditions (Heinrich et al., 2009; Johansson et al., 2024; Kanhoush et al., 2010). The DepMap portal reported that RBMX is an essential protein in a large number of cancer cell lines.

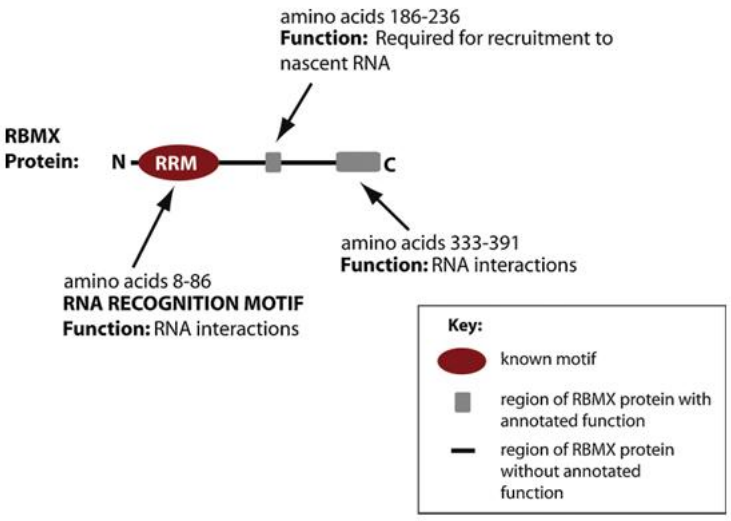

Figure 6. RBMX is a versatile RNA-binding protein with three functional domains.

This figure from Elliott et al., 2019 shows the functional domains of RBMX. Three functional domains have been identified to date.

One of the best-characterized functions of RBMX is the regulation of pre-mRNA splicing through its participation in splice site selection and the repression of cryptic splice sites,

especially within ultra-long exons (Heinrich et al., 2009; Siachisumo et al., 2024a). RBMX also interacts with the C-terminal domain of RNA Polymerase II, increasing its dwell time on chromatin, stabilizing it, and promoting exon inclusion rather than skipping. RBMX was also found to act as a transcription factor, by binding and transactivating the promoter of Txnip *in vivo* (Shin et al., 2008a). RBMX also emerged as an important component of DNA damage response from a genome-wide homologous recombination (HR) screening. RBMX accumulates at sites of DNA damage, recruited by PARP1, and promotes HR through favoring the correct BRCA2 splicing (Adamson et al., 2012). More recently, RBMX has been identified as a secondary reader for m6A in the nucleus through a ribo-switch mechanism involving its low complexity C-terminal domain (Zhou et al., 2019). Biochemical assays showed that m6A can locally alter the RNA secondary structure to favor the binding of RBMX (Liu et al., 2017). This interaction supports the cooperation of RBMX with m6A in the regulation of splicing. Zhou et al., 2019 observed that m6A-modified exons close to splice junctions show enhanced RBMX binding. Liu et al., 2023 also proposed a role for RBMX in maintaining telomere stability by regulating the nuclear stability of telomeric repeat-containing RNA (TERRA), through direct interaction with the nuclear exosome targeting protein ZCCHC8, which directs the transcripts to nuclear degradation. Interestingly, Zuccotti et al., 2020 provided preliminary evidence for RBMX in triggering a cascade of post-transcriptional events related to homeotic gene regulation. They proposed for the first time that RBMX might modulate translation, and they showed that overexpressed RBMX co-sediments with the polysomes in sucrose gradient fractions in HEK293 cells. **Figure 7** summarizes the functions currently described for RBMX based on its putative interacting partners.

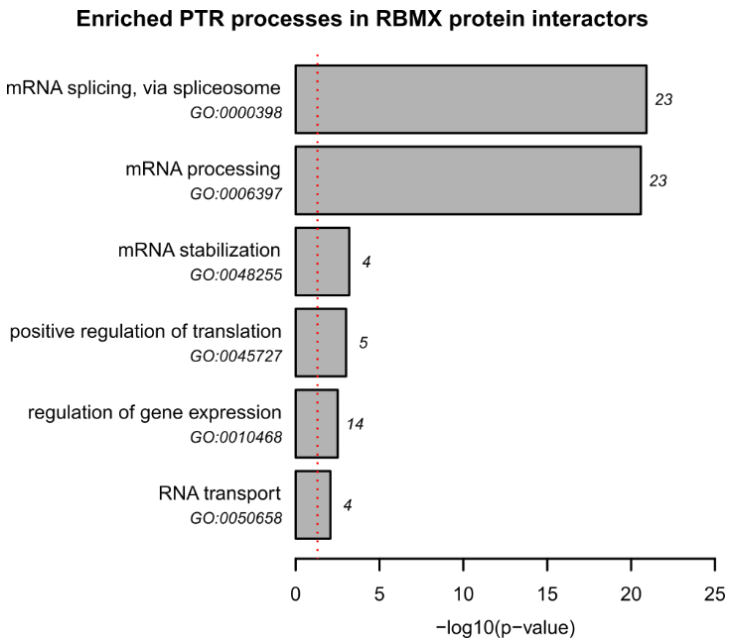

Figure 7. Summary of RBMX functions based on *in silico* RBMX interactors.

This figure from Zuccotti et al., 2020, summarizes putative functions of RBMX spanning mRNA transcription, splicing, processing, stability, and translation based on STRING and IntAct interaction tools, followed by Enrichr for the GO Biological Process ontology for the 83 protein-protein interactors of RBMX. Numbers correspond to the count of RBMX interactors involved in each of the indicated pathways. RBM3, KHDRBS1, FXR2, CIRBP, and HNRNPD are listed among the positive regulators of translation interacting with RBMX.

The rs1554710467 in EIF4H CDS as a proof-of-concept for allele-specific proteomics

The rs1554710467 G>A (R183H) in EIF4H emerged in the HCT116 dataset when extending the analysis from UTR to missense tranSNPs. With the highest MAF being <0.01, rs1554710467 is a single-nucleotide variant (SNV) rather than a SNP, as the alternative allele A is virtually absent in the population. The AF imbalance computed from the RNA-seq data is 0.1397 for the A allele, suggesting that this allele is relatively more represented in the polysomal compared to the total mRNA fraction. The amino acid substitution from arginine (R) to histidine (H) is not predicted to have a severe impact on the protein structure, as it occurs within a loop protein region. However, the CADD score for the alternative allele is 28.2. The CADD (Combined Annotation Dependent Depletion) score is a tool for classifying the deleteriousness of single-nucleotide variants based on the integration of multiple information, including evolutionary sequence conservation, genomic location, and predicted protein effect. CADD scores between 0 and 10 indicate well-tolerated SNPs, while scores around 20 include the 1% most deleterious variants, and scores around 30 correspond to the top 0.1% deleterious variants. Therefore, the CADD

score of 28.2 indicates that the variant is close to the top 0.1% deleterious variants, suggesting a potentially disruptive and deleterious functional impact. EIF4H has two transcript isoforms due to alternative splicing, leading to two proteins of 27 and 25 kDa, respectively, but the tranSNP is contained in both isoforms.

EIF4H encodes a translation initiation factor belonging to the eIF4A/4G/4H complex. EIF4H functions as an activator of the RNA helicase eIF4A, which unwinds inhibitory RNA secondary structures from the 5' UTR to allow the 40S subunit to sit on the mRNA and start scanning (Marintchev et al., 2009; Richter et al., 1999; Rozovsky et al., 2008). Indeed, EIF4H has been described as a key contributor to translation initiation, even in the context of tumor promotion. In lung cancer, EIF4H is considered an oncogene by facilitating the translation of IRES-containing or structured 5' UTR mRNAs such as FGF-2, VEGF, and C-MYC (Vaysse et al., 2015). Notably, the genomic region containing EIF4H belongs to a 1.6 Mbp region that is commonly hemizygously deleted in the Williams-Beuren Syndrome, leading to broad symptoms ranging from growth defects to neuronal and behavioral abnormalities (Capossela et al., 2012). This observation reinforces the fundamental role of translation and how its regulation is relevant and has broad consequences on virtually any cellular process, from development to proliferation to cellular plasticity.

Aims

This study investigates the impact of genetic diversity, in the form of single-nucleotide polymorphisms (SNPs), on the post-transcriptional regulation of gene expression, to identify and comprehensively characterize a novel class of functional SNPs, named *tranSNPs*. In particular, the study aims to refine the tranSNP-identifying pipeline, explore the cell line and cancer-type specificity of tranSNPs, and elucidate their mechanistic insights. Mechanistic studies hold the potential to reveal novel relationships between tranSNP host genes and trans-acting factors (such as RBPs and miRNAs), leading to the identification of actionable trans-factors that could be therapeutically targeted in cancer. Moreover, when further explored, tranSNPs could become an original and poorly explored source of SNPs to be used as biomarkers for prognosis or for informing targeted therapy.

Specifically, this study pursues the following objectives:

- **To improve the tranSNP-identifying pipeline,** through the introduction of the 80S-bound mRNAs as an additional fraction to increase the resolution in tranSNP identification
- **To characterize the molecular mechanisms and trans-factor dependency of tranSNPs,** using the tranSNP rs1053639 in DDIT4 3' UTR as a model
- **To assess the clinical relevance of tranSNPs,** via the analysis of allele-specific drug vulnerabilities and prognosis from TCGA data related to disease-free interval
- **To investigate the cancer specificity of tranSNPs,** by generating a tranSNPs catalogue in the non-cancer cell line RPE-1 and comparing it with the cancer cell line datasets
- **To investigate the cell-line specificity and context dependency of tranSNPs,** by comparing the effect of tranSNPs found in the cancer cell line HCT116 in the non-cancer cell line RPE-1 and the lung cancer cell line A549 using luciferase reporter assays, considering the cell lines as surrogates for the respective tissues, which express trans-factors at different levels, to establish the context-dependent activity of tranSNPs

Results

40 tranSNPs can be identified in HCT116 cells

We computed the allelic fraction imbalance across polysome-bound and total mRNAs for the analyzable heterozygous SNPs to generate a catalogue of tranSNPs in the colon cancer cell line HCT116.

Approximately 7% of the analyzable SNPs showed a significant imbalance, corresponding to 40 putative tranSNPs identified in this dataset. The analyzable SNPs were almost equally distributed between CDS and 3' UTR, and this distribution was preserved in the group of tranSNPs, with 19 tranSNPs located in the CDS and 21 in the 3' UTR (**Figure 6A**). Since the UTRs are prominent regulatory regions for the post-transcriptional and translational regulation, we focused on the 3' UTR tranSNPs for experimental validation at this stage. We applied selection criteria for the choice of the UTR tranSNPs to be validated experimentally: we primarily set a threshold of 0.1 for the absolute magnitude of the imbalance (delta Allelic Fraction, dAF POL-TOT) and 0.3 for the MAF, which indicates the frequency of the less common allele in the population (**Figure 6B**). Subsequently, we prioritized the four resulting candidates (rs1053639, rs3743518, rs137085, and rs763121) for the functional relevance of the gene harboring the SNP, especially in cancer. The rs1053639 in DDIT4 and the rs137085 in POLDIP3 were the most compelling candidates based on the overall criteria.

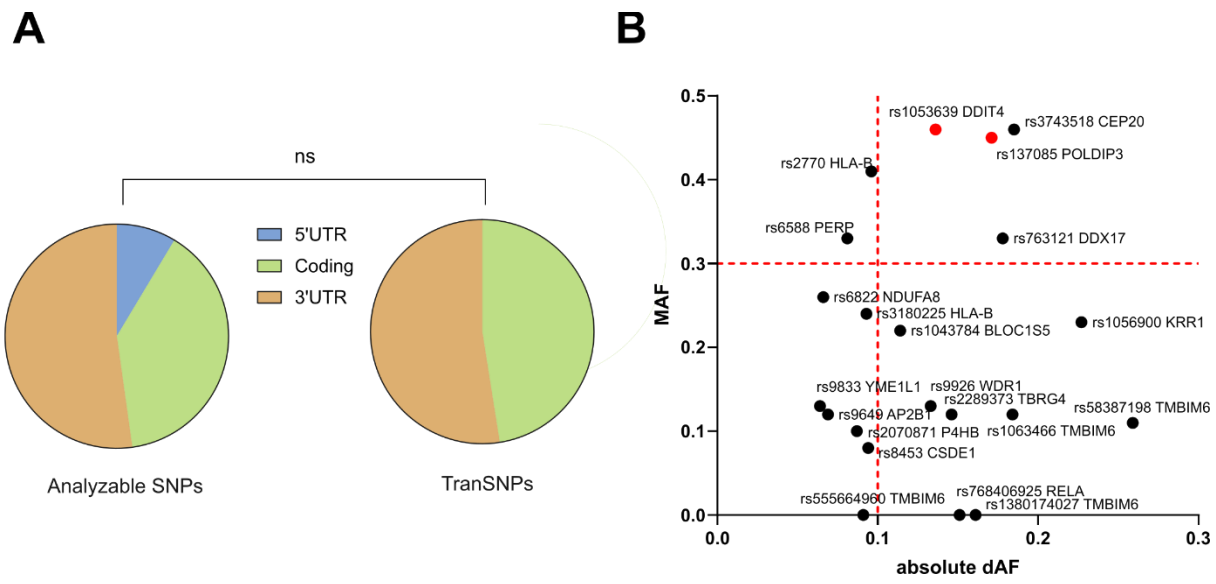

Figure 6. Forty putative tranSNPs were identified in HCT116 cells.

A) Distribution of the analyzable SNPs (left) and tranSNPs (right) across coding and UTR regions. **B)** For the 3'UTR tranSNPs identified in this study, the absolute delta Allelic Fraction, the Minor Allele Frequency in the human population, and the associated gene name are shown. The selected tranSNP candidates for experimental validation appear in red in the upper right quadrant of the chart.

Generating homozygous rs1053639 clones via CRISPR/Cas9-mediated knock-in

While heterozygosity is an essential requirement for identifying transSNPs by our pipeline, we expect that the homozygous state for the alternative and reference alleles would reveal the maximum phenotypic impact. We thus exploited CRISPR/Cas9-mediated knock-in to generate isogenic homozygous HCT116 clones for rs1053639 (T/A) in DDIT4 and rs137085 (T/C) in POLDIP3 and to assess the tranSNP effect at the endogenous loci. We delivered the Cas9 and single-guide RNA (sgRNA) as a ribonucleoprotein particle (RNP) to minimize the off-target potential (Ghetti et al., 2021).

We first screened the gene sequences of the two candidate tranSNPs for the presence of the Cas9 Protospacer Adjacent Motif (PAM) close to the SNP site to evaluate the possibility of editing. We then designed a unique gRNA as close as possible to the tranSNP site to simultaneously cut both alleles and maximize the efficiency of homology-directed repair (HDR). We also used a single donor DNA for each tranSNP, carrying either the reference or the alternative allele at the SNP site (**Figure 7**).

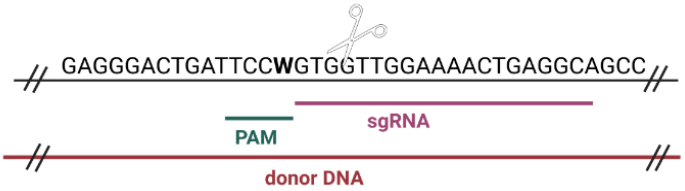

Figure 7. Schematic representation of the sgRNA and donor DNA design at the rs1053639 site.
A unique sgRNA was designed to target both alleles of rs1053639, along with a donor DNA containing W (T or A) at the SNP site.

We initially delivered the RNP in the absence of donor DNA to test for the cutting efficiency at the SNP site, as measured by TIDE analysis (Brinkman and van Steensel, 2019). The rs1053639 gRNA exhibited a cutting efficiency of 79.8%, whereas the rs137085 gRNA reached only 36%. Given the intrinsically low efficiency of the following homology-directed repair (HDR), we set a minimum cut efficiency threshold of ~ 80% as a starting point for HDR and therefore excluded the rs137085 in POLDIP3 for further analyses.

Upon knock-in of the best candidate rs1053639, the HDR efficiency, measured by the ICE Synthego analysis tool (Conant et al., 2022), ranged from 5% to 9% in the initial bulk population. With a single cell cloning efficiency of about 1 in 3, 85 clones were isolated and characterized by Sanger sequencing. **Figure 8** summarizes the workflow for editing the rs1053639 site.

Collectively, we obtained four clones homozygous for the rs1053639 T allele (#2, #3, #12, #13) and four homozygous for the A allele (#5, #6, #7, #10). Despite extensive screening efforts, clone #2 was the only isogenic homozygous T clone, while the remaining clones exhibited additional small indels of variable extent around the SNP site when sequencing the DDIT4 3' UTR (**Table 4**). Interestingly, three clones (#3 TT, #5 AA, and #6 AA) showed the same GGT three-nucleotide deletion, starting three nucleotides downstream of the SNP site. To overcome the possible influence of clonal selection and adaptation, and the above-mentioned editing limitations, we included the clones harboring small indels, named as shown in **Table 4**, but we considered multiple clones per genotype as cellular models to study the tranSNP effects in most experiments.

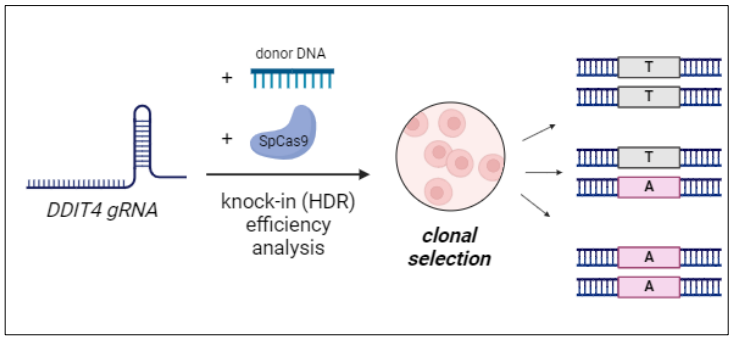

Figure 8. Knock-in strategy for the generation of rs1053639 TT and AA homozygous HCT116 clones.

TT homozygous clones exhibit significantly higher DDIT4 protein levels

The imbalance in the allelic fraction between polysome-bound and total mRNAs from our RNA-seq data showed a significantly lower representation of the alternative rs1053639 A allele in the polysome-bound compared to the total mRNAs, indicating the T allele as enriched in the polysome-bound mRNAs. We asked whether this allele-specific polysomal loading would result in different DDIT4 protein levels across TT and AA homozygous clones.

Interestingly, TT clones exhibited significantly higher steady-state DDIT4 protein levels compared to AA clones, with the AT cells showing intermediate levels (**Figure 9A, Appendix**

Figure 1). We found that the difference in steady-state DDIT4 protein levels was not attributable to allele-specific changes in DDIT4 protein half-life (**Figure 9B**), DDIT4 mRNA turnover (**Figure 9C**), or steady-state DDIT4 mRNA levels across TT and AA clones (**Figure 9D**). We also assessed steady-state DDIT4 mRNA levels by amplifying across all the possible exon junctions to account for potential splicing effects. We did not find significant allele-specific differences in DDIT4 mRNA splicing by amplifying across the two junctions and across TT and AA clones (**Figure 9E**).

To investigate possible contributions by other regulatory elements, and particularly those already described to regulate DDIT4 expression, we measured the levels of the antisense DDIT4-AS1 RNA across our cellular models using published primer sequences. Indeed, a portion of DDIT4-AS1 overlaps with the SNP-containing region of DDIT4 3' UTR. However, we detected very low expression of DDIT4-AS1 in our cellular models, and mostly, we did not find significant differences in the expression of DDIT4-AS1 across TT and AA clones (**Figure 9F**). We also attempted to measure the levels of the circular circDDIT4 RNA, which is generated by back splicing at the DDIT4 3' UTR (Kong et al., 2023), but the expression of the circDDIT4 was undetectable across TT and AA HCT116 cellular models.

Overall, we found that TT homozygous clones exhibit significantly higher DDIT4 protein levels compared to AA clones, which is concordant with the significantly lower relative polysomal loading of the A allele from RNA-seq data. However, we did not find allele-specific DDIT4 mRNA or protein features, nor allele-specific non-coding RNA regulation to mechanistically explain the allele-specific differences in DDIT4 protein levels.

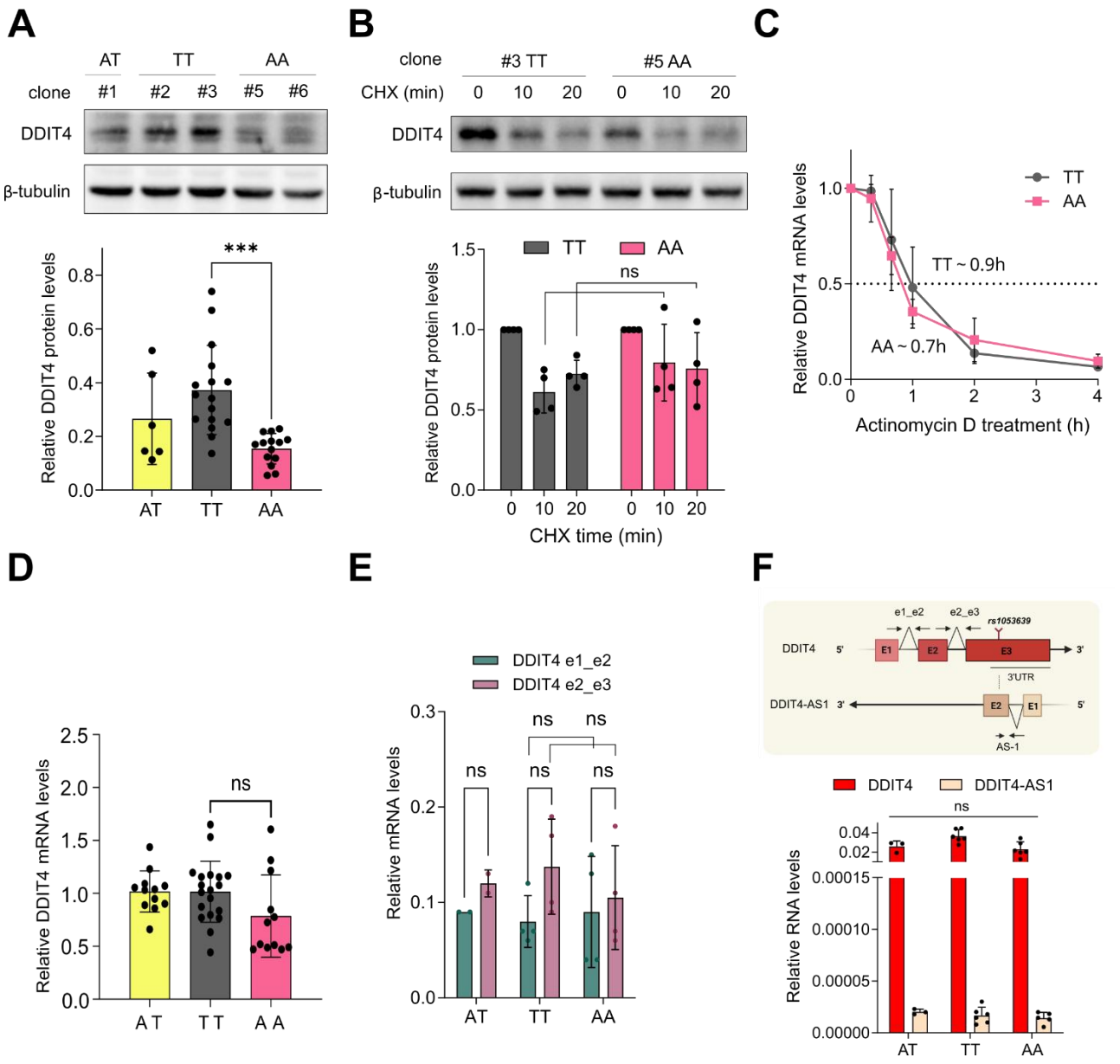

Figure 9. The rs1053639 in the 3'UTR of DDIT4 impacts DDIT4 protein levels.

A) (Top) Western Blot analysis of DDIT4 protein levels across rs1053639 TT and AA HCT116 edited clones. β-tubulin was used as a loading control. (Bottom) Densitometric analysis of DDIT4 protein levels across at least 6 individual blots, considering at least two edited clones per genotype. ***p-value <0.001, ordinary one-way ANOVA. **B)** (Top) Western Blot analysis of DDIT4 protein levels across TT and AA clones treated with 100 µg/ml cycloheximide (CHX) at 10 and 20 minutes. β-tubulin was used as a loading control. (Bottom) Densitometric analysis of DDIT4 protein levels across 2 individual blots, considering two edited clones per genotype. Ns, not significant, two-way ANOVA. **C)** Estimation of DDIT4 mRNA half-life upon inhibition of transcription by Actinomycin D treatment (10 µg/ml) for 0-4 hours. The estimated half-life is expressed in hours and calculated by fitting the decay data in a one-phase decay equation. The curve shows the residual DDIT4 mRNA levels relative to GAPDH mRNA levels at different timepoints and presents results from at least 4 independent replicates. **D)** Steady-state DDIT4 mRNA levels, measured by RT-qPCR and normalized to GAPDH and YWHAZ mRNA levels. Ns, not significant, ordinary one-way

ANOVA. **E)** Relative steady-state DDIT4 mRNA levels measured using primers spanning either the junction between exon 1 and exon 2, or the junction between exon 2 and exon 3. ns, not significant, two-way ANOVA. DDIT4 mRNA levels were normalized to B2M mRNA levels. **F)** (Top) Schematic representation of the relative genomic localization of the sense and antisense DDIT4 transcripts. The region amplified by primers is shown between arrows (Bottom). Relative DDIT4 mRNA levels and DDIT4 antisense 1 (DDIT4-AS1) RNA levels measured by RT-qPCR and normalized to GAPDH mRNA levels. Ns, not significant, ordinary one-way ANOVA.

To investigate whether we could more efficiently uncouple the transcriptional and post-transcriptional events affecting DDIT4 and directly measure the translation efficiency of the two alleles, we cloned either ~ 500 bp (Long) or ~ 109 bp (Short) fragments of DDIT4 3' UTR containing either the reference or the alternative rs1053639 allele downstream of a luciferase reporter plasmid. This design eliminates the variable of DDIT4 transcriptional regulation by removing the control exerted by the DDIT4 promoter; furthermore, the "Long", but not the "Short" construct, contained the rs8316 SNP, which is inherited together with rs1053639 in the most common haplotypes, thereby allowing the discrimination of the contributions of the two variants on the observed phenotypes.

We performed dual-luciferase assays, using the Renilla luciferase as a normalizer of the Firefly luciferase signal first, and then normalizing the Firefly/Renilla ratio to Firefly mRNA levels. Moreover, we performed the assay in both TT and AA homozygous HCT116 clones to exclude the possibility that the observed allele-specific differences in DDIT4 protein levels were due to clonal artifacts or to different global translation efficiencies attributable to different clonal backgrounds, or due to off-target events of the editing process, considering the relatively low number of successfully edited clones.

Overall, we found that rs1053639 and the immediate surroundings are sufficient to show allele-specific differences in reporter activity related to translation efficiency (TE) (**Figure 10**). The magnitude of translation efficiency decreases when comparing the "Long" and "Short" constructs, likely due to the presence of additional regulatory sequences or the influence of rs8316. However, the allele-specific differences remain unchanged, indicating that these additional regulatory layers do not interfere with the effect of rs1053639. The observed differences favored the T allele, reflecting the observed allele-specific DDIT4 protein levels. This phenotype is then unrelated to the control by the DDIT4 promoter and persists irrespective of the clone background.

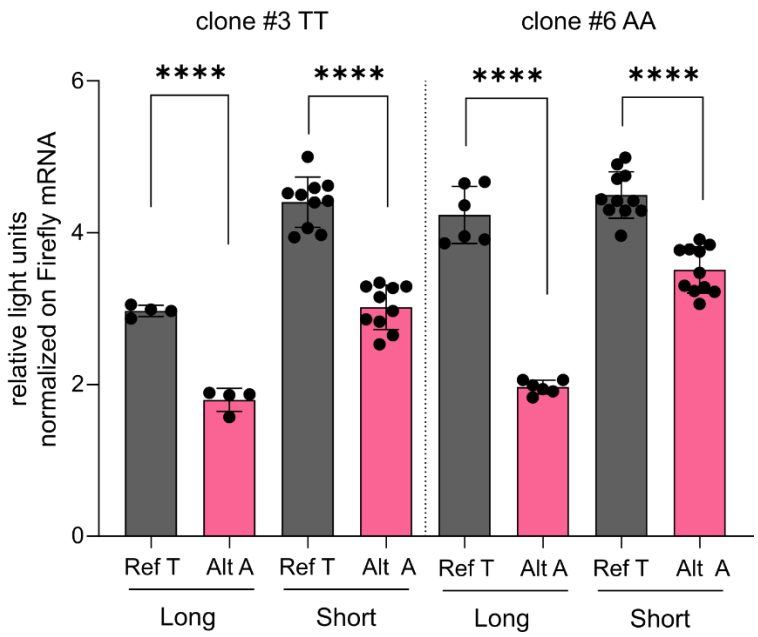

Figure 10. The reference T allele produces significantly higher luciferase signal compared to the alternative A allele.

Luciferase reporter assay of a ~ 500 bp (Long) and a ~ 100 bp (Short) construct encompassing rs1053639 in TT and AA clones. Firefly luminescence was first normalized to Renilla luminescence, then to Firefly mRNA levels. ****p-value < 0.0001, unpaired t-test.

TT homozygous clones exhibit higher DDIT4 protein levels, especially in ER-stress conditions

Next, we challenged the edited clones with the ER stressor thapsigargin (Thastrup et al., 1990). Thapsigargin discharges the intracellular calcium stores by specifically inhibiting the ER calcium-ATPase and was shown to strongly and acutely induce DDIT4 at the transcriptional level via activating PERK, which in turn activates ATF4, which is the most important transcription factor for DDIT4 (Whitney et al., 2009b). We therefore checked the status of the ER stress response upstream of DDIT4 by measuring the protein levels of ATF4 in mock conditions and upon thapsigargin treatment. ATF4 protein levels were comparable across TT and AA homozygous clones in both conditions, suggesting that the ER stress pathway upstream of DDIT4 is unchanged, irrespective of the rs1053639 genotype (**Figure 11A**).

As expected, thapsigargin treatment led to a marked induction of DDIT4 at the transcriptional level, which was comparable among genotypes (**Figure 11B**). However, the allele-specific differences in DDIT4 protein levels were not only maintained but were even amplified upon thapsigargin treatment (**Figure 11C**). This finding further supports the role of post-

transcriptional events in regulating DDIT4 protein levels, which are possibly exacerbated under ER stress conditions.

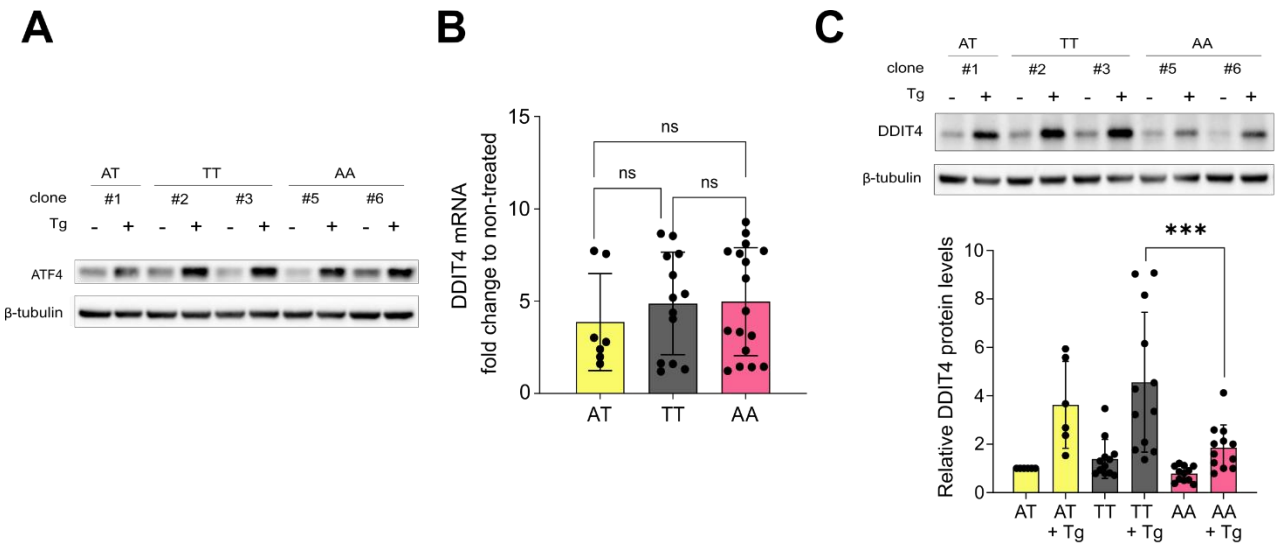

Figure 11. The rs1053639 in the 3'UTR of DDIT4 impacts DDIT4 protein levels, especially in ER-stress conditions.

A) Western Blot analysis of ATF4 protein levels across rs1053639 TT and AA HCT116 edited clones. β-tubulin was used as a loading control. **B)** Fold change of DDIT4 mRNA levels, measured by RT-qPCR and normalized to GAPDH and YWHAZ mRNA levels, upon 100 nM thapsigargin or vehicle for 4 hours. Ns, not significant, ordinary one-way ANOVA. **C)** (Top) Western Blot analysis of DDIT4 protein levels across rs1053639 TT and AA HCT116 edited clones treated with 100 nM thapsigargin or vehicle for 4 hours. β-tubulin was used as a loading control. (Bottom) Densitometric analysis of DDIT4 protein levels across at least 6 individual blots, considering at least two edited clones per genotype. ***p-value <0.001, ordinary one-way ANOVA.

To focus again on the post-transcriptional events affected by rs1053639 and expand the analysis to thapsigargin treatment and other mRNAs, we performed polysomal profiling in TT and AA homozygous clones. Polysomal profiling indeed shows the association of specific mRNAs with ribosomal subunits, monosomes or polysomes, highlighting the translation efficiency of specific mRNAs, irrespective of their mRNA levels.

We interrogated the relative distribution of DDIT4 mRNA across the sucrose gradient fractions obtained upon polysome profiling, along with CDKN1A and RPS26 control mRNAs, using a previously described method (Panda et al., 2017). While no significant shifts arose in the DDIT4, CDKN1A, or RPS26 mRNA distributions in mock condition (**Figure 12 A-C**), we found a significant enrichment, specific for DDIT4 mRNA, in heavier polysomes (fraction 10) in TT clones compared to AA clones when both were challenged with thapsigargin, and a reduction

in subpolysomal fraction 6 and light polysomal fraction 8 in TT compared to AA clones (**Figure 12A**).

At the same time, since DDIT4 is a negative regulator of mTORC1 and might impinge on global protein synthesis, we evaluated the polysomal profiles in mock conditions or upon thapsigargin treatment **(Figure 12D, 12E)** and quantified the relative abundance of signal in polysomes compared to the 80S from polysomal profiling to estimate global protein synthesis rates. This measurement did not highlight significant differences in global protein synthesis across TT and AA clones, although AA clones were slightly more affected by thapsigargin treatment (**Figure 12F**).

Although this result may depotentiate DDIT4 as a global regulator, it also reinforces the observation that the rs1053639 effect on DDIT4 translation efficiency and DDIT4 protein levels is specific to DDIT4 mRNA and is not the result of a globally and indirectly dysregulated context, but the result of a fine and specific regulation by the tranSNP.

The increased association of DDIT4 mRNA with heavy polysomes in TT clones, especially upon thapsigargin treatment, further reinforced the fact that the post-transcriptional effect affecting DDIT4 protein levels may exacerbate upon ER stress induction, and encouraged us to explore possible trans-factors mediating this effect.

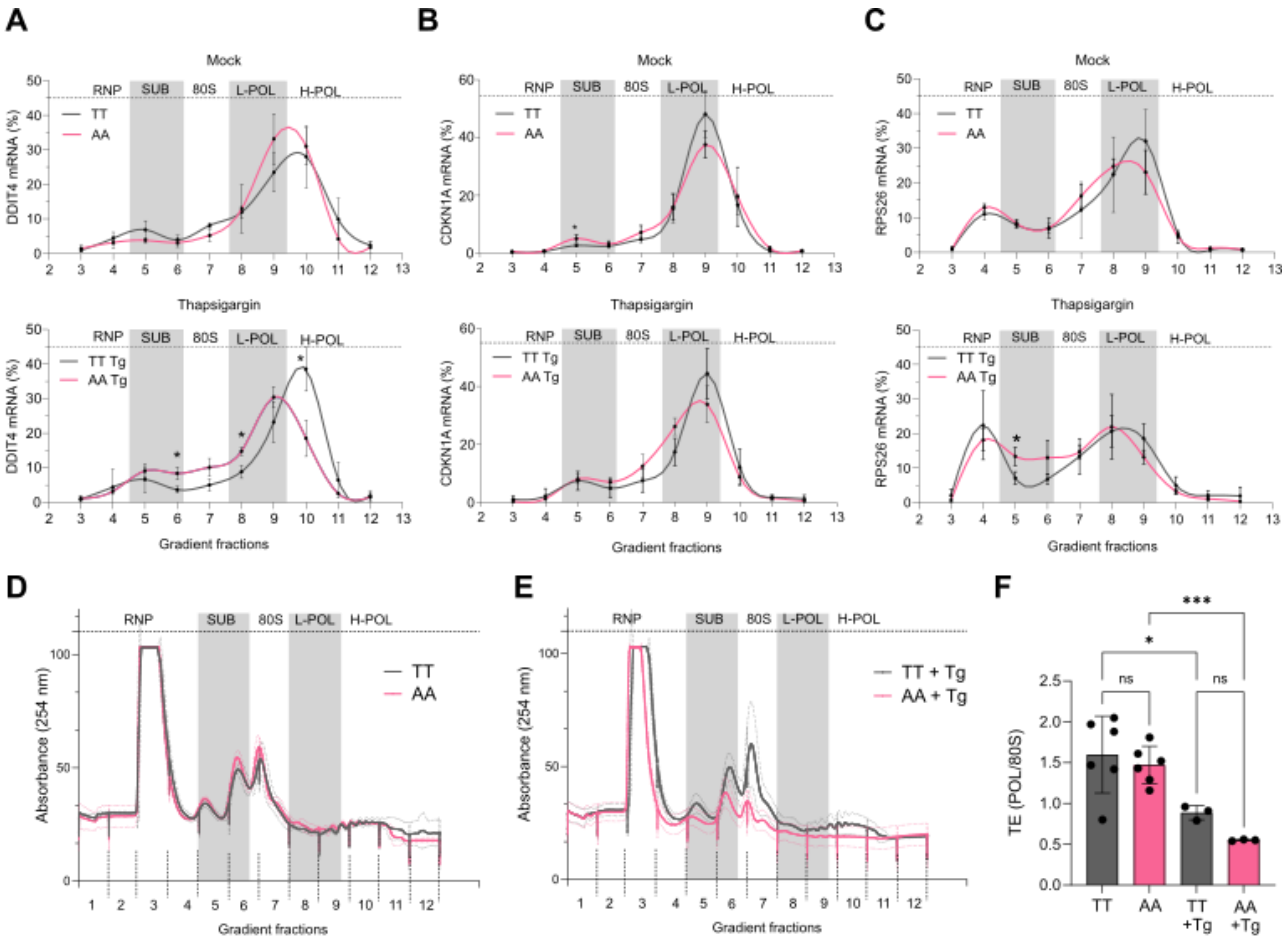

Figure 12. The rs1053639 clones exhibit significant differences in DDIT4 TE, but not in global TE.

A) Distribution of DDIT4 mRNA across polysomal profile fractions in mock conditions (Top) and upon thapsigargin treatment (100 nM, 4 hours) (Bottom), measured by RT-qPCR and expressed as a percentage of distribution over the profile fractions. **B)** Distribution of CDKN1A mRNA across polysomal profile fractions in mock conditions (Top) and upon thapsigargin treatment (100 nM, 4 hours) (Bottom), measured by RT-qPCR and expressed as a percentage of distribution over the profile fractions. **C)** Distribution of RPS26 mRNA across polysomal profile fractions in mock conditions (Top) and upon thapsigargin treatment (100 nM, 4 hours) (Bottom), measured by RT-qPCR and expressed as a percentage of distribution over the profile fractions. Three independent biological experiments were performed. *p-value <0.05, two-way ANOVA. **D)** Polysomal profile of TT and AA clones in mock conditions. At least two clones per genotype were considered. **E)** Polysomal profile of TT and AA clones upon thapsigargin treatment. At least two clones per genotype were considered. **F)** Global TE across TT and AA clones was measured by quantifying the relative abundance of signal in polysomes compared to the 80S from the polysome profiles in 12D and 12E. Ns, not significant, *p-value <0.05, ***p-value <0.001, one-way ANOVA.

The RNA-binding protein RBMX differentially binds to the T/A rs1053639 alleles.

To shed light on potential trans-factors interacting differentially with the rs1053639 alleles, we took advantage of *in silico* predictions for allele-specific binding of RNA-binding proteins (RBPs)

generated by the Laboratory of Computational Genomics (Prof. Alessandro Romanel, University of Trento, ITA) using the TESS software (Schug, 2008) on a list of 552 RBPs. Although binding data were available for 552 RBPs in the TESS software, consensus binding motifs were available only for 53 RBPs. Based on these data, ACO1, RBMX, and YBX1 were predicted to significantly differentially bind to the two rs1053639 alleles.

We decided to focus our attention on RBMX for multiple reasons. First, RBMX exhibited the highest magnitude of allele-specific difference in binding, shifting from poor for one allele (13% of the optimal score) to nearly maximal for the other allele (99% score). The two other candidates showed much lower dynamic ranges of allele-specific binding. Moreover, recent PAR-CLIP data (Liu et al., 2017) highlighted a signal for RBMX binding in the 3'UTR of DDIT4 mRNA in HEK293T cells, and possible functional links between RBMX and DDIT4 already existed as both are recognized components of the DNA damage response and TXNIP-mediated autophagy (Shin et al., 2008b). RBMX is mainly located in the nucleus in normal conditions and was reported to modulate mRNA splicing, modification, degradation, and possibly translation (Heinrich et al., 2009; Liu et al., 2023, 2017; Zuccotti et al., 2020).

To investigate the predicted allele-specific binding *in vitro*, we performed RNA electromobility shift assays (REMSA) using the full-length recombinant RBMX protein and RNA probes corresponding to a portion of the endogenous DDIT4 mRNA sequence containing either the T or the A allele. Moreover, since RBMX is sensitive to structural features of mRNAs (Liu et al., 2017), we set up a collaboration with Dr. Sara Zaccara and Prof. Hashim M. Al-Hashimi (Columbia University, USA) to design RNA probes long enough to preserve the structure of the endogenous RNA to the maximum extent. We used three learning-based methods (EternaFold, CONTRAfold, and Ufold), two thermodynamic-based methods (ViennaRNA and RNAstructure), and one hybrid method (MXFold2) (Sato et al., 2021; Wayment-Steele et al., 2022) to identify the minimum number of nucleotides required to maintain the endogenous RNA secondary structures; based on this, we designed 25-nucleotide-long RNA probes differing only in the base at the tranSNP site, which was located at position 15 out of 25 nucleotides (**Figure 13A, top**). Although the global structure of DDIT4 3'UTR was not significantly impacted by the SNP, significant differences in the local secondary structure were observed when changing the base at the SNP site. We further explored the publicly available AlphaFold 3 tool, which was implemented to generate accurate structural predictions for protein-RNA interactions.

AlphaFold 3 provided several models suggesting that the T allele RNA probe adopts a more favorable spatial conformation for RBMX binding than the A allele RNA probe (**Figure 13A, bottom**). It also predicted that the C-terminal low complexity domain of RBMX binds to DDIT4 mRNA.

Overall, REMSA revealed that RBMX could bind to both RNA probes *in vitro*, but with a possible preference for the T allele, as measured by the apparent dissociation constant (Kd app) (**Figure 13B**).

We thus performed RNA immunoprecipitation (RIP) experiments to evaluate RBMX binding to DDIT4 mRNA within the complexity of a cellular context, specifically in TT and AA homozygous clones. First, we proved that the protocol and antibody used for immunoprecipitating RBMX were effective (**Figure 13C**). We then recovered the RBMX-bound RNAs (and IgG-bound RNAs) and measured the enrichment of DDIT4 mRNA through RT-qPCR across TT and AA clones. RIP experiments confirmed the preferential binding of RBMX to DDIT4 mRNA in TT homozygous clones compared to AA clones (**Figure 13D**).

Overall, we found that the RNA-binding protein RBMX preferentially binds to the T allele of rs1053639 compared to the A allele both *in silico* and *in vitro*.

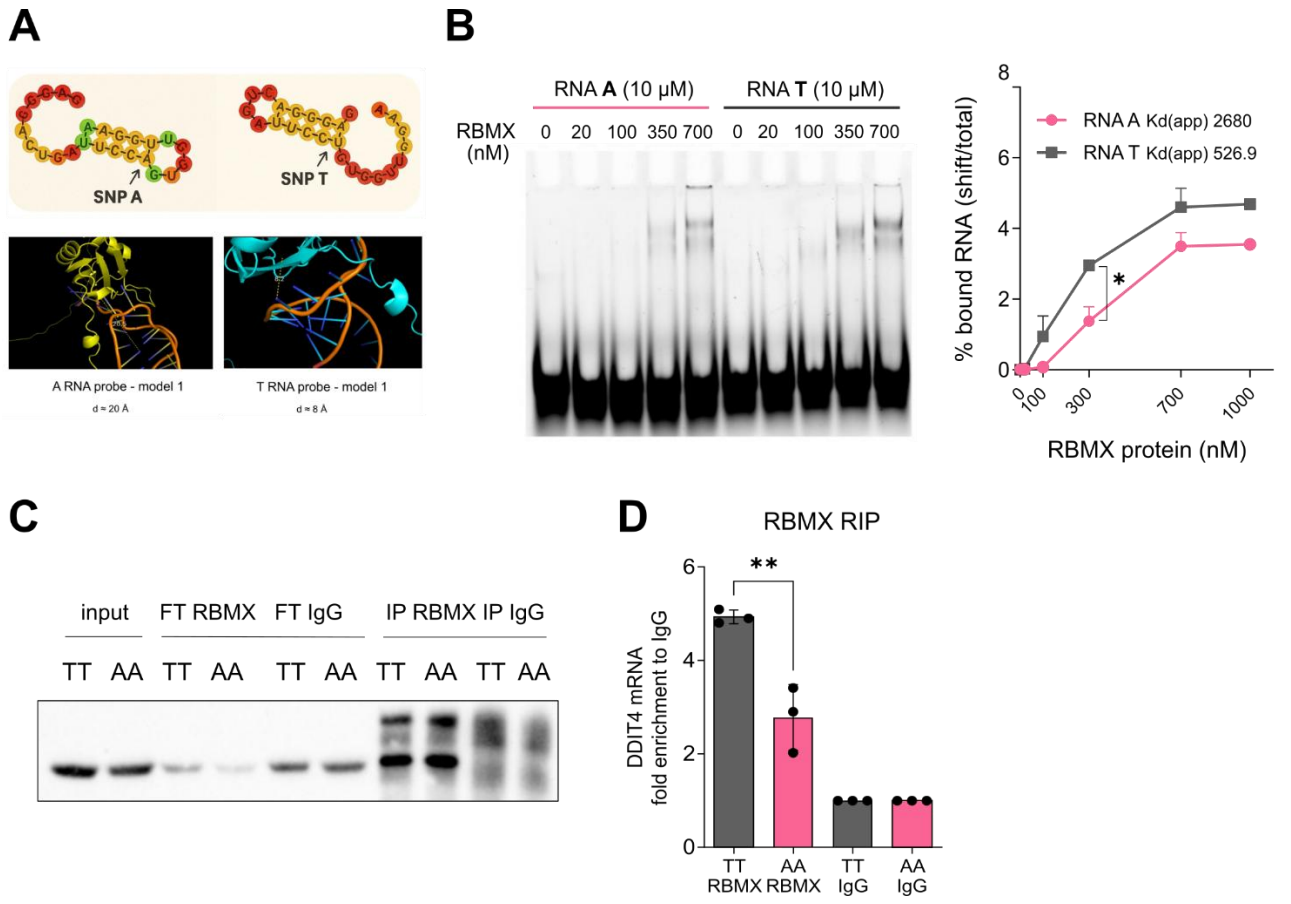

Figure 13. The RNA-binding protein RBMX differentially binds to the T/A rs1053639 alleles *in silico* and *in vitro*. **A)** (Top) REMSA RNA probes were designed based on information from multiple RNA folding prediction tools. (Bottom) AlphaFold3 was used to predict the interactions between the full-length RBMX protein and the RNA probes used for the REMSA. Four models were explored; model 1 is shown as representative. The tool allows the calculation of the distance between a selected RNA nucleotide and a selected protein portion. The distance between the T SNP nucleotide and the RBMX protein was lower than the distance between the A SNP nucleotide and the same protein in all four models. **B)** (Left) REMSA was performed using the full-length recombinant RBMX protein and T or A DDIT4 RNA probes. In the '0' lane, the RNA probe was incubated with the binding buffer and the protein elution buffer. RNA-protein complexes were resolved on a native 6% gel. (Right) Apparent Kd were obtained from the quantification of the shifted bands over the total bands in the REMSA experiments using a nonlinear regression (curve-fit). Error bars plot the standard deviations among biological replicates. *p-value < 0.05, two-way ANOVA with Šídák's test for multiple comparisons. **C)** The endogenous RBMX protein was specifically immunoprecipitated across TT and AA cells with similarly high efficiencies in RIP assays. An IgG control antibody of the same species as the anti-RBMX antibody was used as a control for specificity. FT: flow-through, unbound lysate upon IP. **D)** RBMX RIP-qCPR results expressed as a fold of enrichment relative to the normal IgG for DDIT4 mRNA across TT and AA clones. Three independent biological replicates were performed. **p-value < 0.01, unpaired t-test.

The rs1053639 genotype impacts DDIT4 mRNA localization, but slightly through RBMX

To dive into potential mechanisms by which the allele-specific binding of RBMX could lead to allele-specific differences in DDIT4 protein levels, we evaluated the subcellular localization of RBMX protein in HCT116 cells. While we confirmed the expected, abundant nuclear distribution of RBMX, **Figure 14A** shows that a fraction of RBMX also localizes to the cytoplasm in HCT116, which is consistent with a previous report hypothesizing functions for RBMX outside of the nucleus (Zuccotti et al., 2020).

Considering the dual subcellular localization of RBMX and its validated binding to DDIT4 mRNA in our cellular models, we next evaluated the relative subcellular localization of DDIT4 mRNA across TT and AA clones. Nuclear and cytoplasmic fractions were obtained and verified both at the protein (**Figure 14A**) and RNA level (**Figure 14B**). Notably, DDIT4 mRNA showed higher cytoplasmic localization in the TT clones while being significantly more nuclear in the AA clones (**Figure 14C**).

To shed light on the contribution of RBMX to this phenotype, we confirmed that RBMX protein levels were comparable across TT and AA clones and used siRNAs to deplete them partially (**Figure 14D**). Subcellular fractions were again verified at the RNA level (**Figure 14E**). RBMX

silencing led to a slight increase in nuclear DDIT4 mRNAs in TT but not in AA clones, which is consistent with a stronger effect on the T allele, and with a role for RBMX in retaining mRNAs from the T allele in the cytoplasm (**Figure 14F**).

The allele-specific differences in the subcellular localization of DDIT4 mRNA were only slightly mitigated by RBMX silencing; therefore, the phenotype cannot be strongly ascribed to RBMX. However, we found that the rs1053639 genotype dictated allele-specific differences in DDIT4 mRNA localization, favoring the enrichment of DDIT4 mRNA from the T allele in the cytoplasm, which at least in part mechanistically explains the higher DDIT4 protein levels in TT clones independently from RBMX.

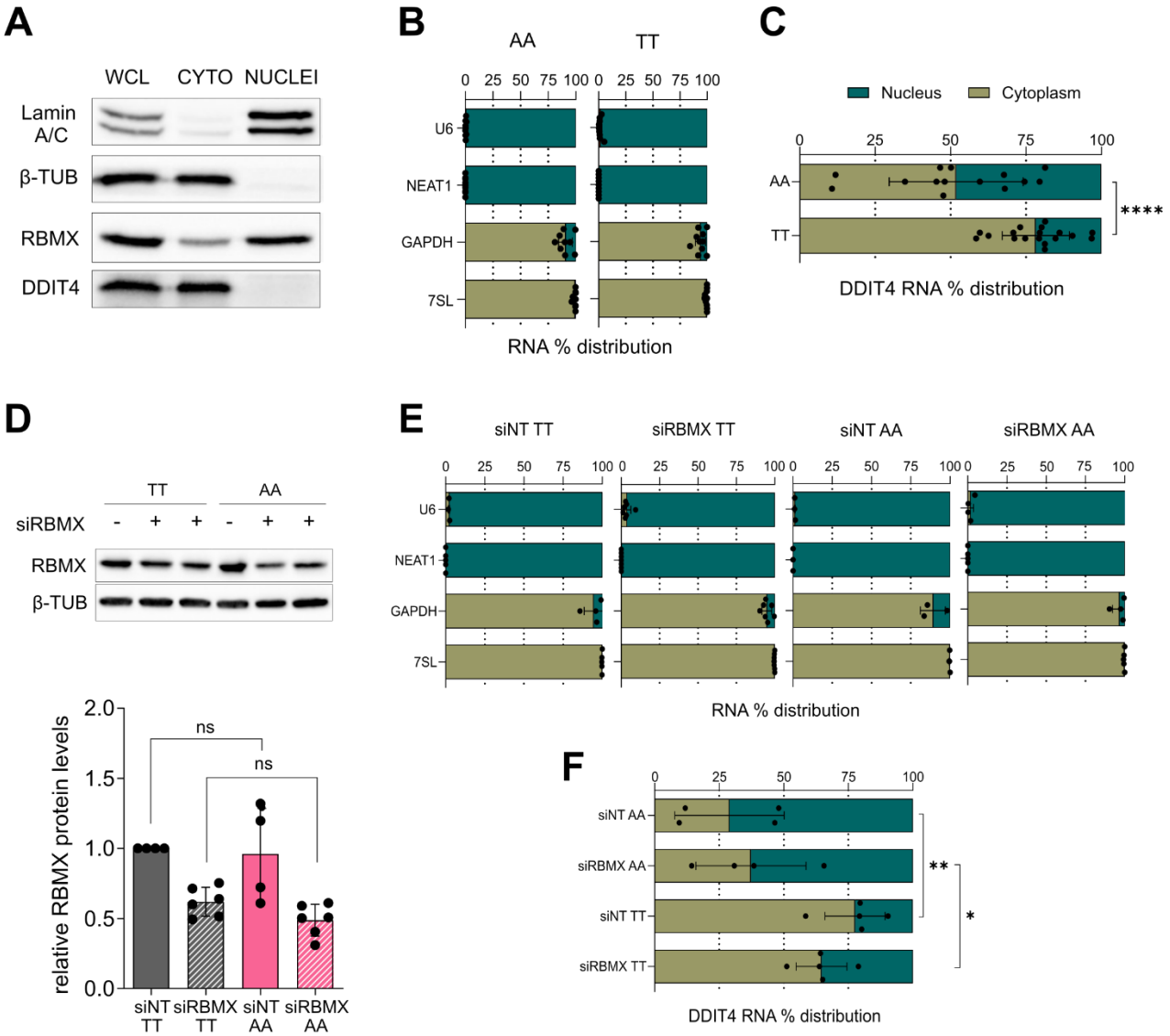

Figure 14. The rs1053639 genotype slightly impacts DDIT4 mRNA localization via RBMX.

A) Cell fractionation was performed in HCT116 cells and validated at the protein level. Lamin A/C and β-Tubulin were used as markers for the nuclear and cytoplasmic fractions, respectively. WCL: whole cell lysate. CYTO: cytoplasm. **B)** Cell fractionation was performed in HCT116 cells and validated at the RNA level. U6 snRNA and NEAT1 were used as markers for the nuclear fraction, 7SL and GAPDH were used as markers for the cytoplasmic fraction. GAPDH mRNA is not completely cytoplasmic, which is consistent with previous reports. Control markers for the AA clones are shown on the left, while markers for the TT clones are shown on the right. **C)** DDIT4 mRNA localization was evaluated in TT and AA clones upon cell fractionation followed by RT-qPCR. Data represent the mean ± SD of at least four independent experiments. The relative expression of the gene in the cytoplasm was calculated as the fold change of the Ct in the cytoplasm compared to the Ct in the nucleus, with nuclear and cytoplasmic RNAs eluted in the same volume of water. ****p-value < 0.0001, unpaired t-test. **D)** TT and AA clones were treated with either a mixture of two siRNAs targeting RBMX or the siRNA control (siNT) for 48 hours. (Top) Representative immunoblot and (Bottom) densitometric analysis to evaluate the efficiency of RBMX depletion. β-Tubulin was used as a loading control. **E)** Cell fractionation was performed in HCT116 cells and validated at the RNA level in control (siNT) and RBMX-depleted samples (siRBMX). U6 snRNA and NEAT1 were used as markers for the nuclear fraction, 7SL and GAPDH were used as markers for the cytoplasmic fraction. **F)** DDIT4 mRNA localization was evaluated in TT and AA cells upon cell fractionation, followed by RT-qPCR in control (siNT) and RBMX-depleted samples (siRBMX). Data represent the mean ± SD of three independent experiments. *p-value <0.05 **p-value <0.01, unpaired t-test.

The rs1053639 alleles are differentially m6A-modified

To explore additional mechanisms by which RBMX could determine allele-specific DDIT4 protein levels, we leveraged the role of RBMX as an m6A reader and the finding that DDIT4 mRNA fate, and primarily stability, is heavily regulated by the m6A modification (Li et al., 2025; Qin et al., 2021; Zhao et al., 2024). We employed the online tool deepSRAMP to predict m6A sites *in silico* based on sequence and genomic position features (Fan et al., 2024). By centering on the SNP site and expanding by 100 nucleotides upstream and downstream, we detected 7 putative m6A sites (**Figure 15A**). Interestingly, two predicted m6A sites were located in close proximity to rs1053639, specifically at positions -9 and +12 relative to the SNP. All the putative m6A sites were conserved when changing the base at the SNP site, but we observed a slight difference in the m6A probability for the m6A site just downstream of rs1053639.

While being aware of this subtle difference of uncertain interpretation, this data prompted us to investigate whether we could quantify the level of m6A at single-nucleotide resolution across TT and AA clones. We employed GLORI (glyoxal and nitrite-mediated deamination of unmethylated adenosines) followed by PCR and Sanger sequencing of DDIT4 fragments of different lengths, but we were not able to obtain any amplicon upon deamination and base

conversion. The SNP-containing portion of DDIT4 3' UTR is indeed extremely GC-rich, and this feature can be exacerbated upon deamination of adenosines (A) into inosines (I) and their conversion into guanosines (G); therefore, one possibility is that the region became inaccessible for amplification by several tested DNA polymerases.

Given these technical limitations, we performed meRIP-qPCR to measure the enrichment of m6A in the TT and AA clones across the same 200-nucleotide region predicted by deepSRAMP. Although we lost single-nucleotide resolution with this technique, meRIP-qPCR showed a significantly higher relative enrichment of m6A in the analysed portion of DDIT4 3'UTR in TT clones compared to AA clones (**Figure 15B**).

To identify possible consequences of the differential modification on the major events regulated by m6A, we used the METTL3 inhibitor STC-15 and perturbed the m6A landscape by impeding its deposition. Upon METTL3 inhibition, DDIT4 mRNA stability increased remarkably, but we could not detect significant allele-specific differences in this phenotype (**Figure 15C**). Similarly, we did not find significant differences in steady-state DDIT4 mRNA levels upon STC-15 treatment (**Figure 15D**). Interestingly, and in the opposite direction compared to what we observed when depleting RBMX, the relative subcellular distribution of DDIT4 mRNA significantly shifted to the cytoplasm upon STC-15 treatment in the TT, but not in the AA clones (**Figure 15E**); the control mRNAs did not display significant changes in subcellular localization upon STC-15 treatment (**Figure 15F**). Interestingly, upon METTL3 inhibition, DDIT4 protein levels were markedly more induced in the TT compared to the AA clones (**Figure 15G**). A similar and possibly higher induction of DDIT4 protein in the TT compared to the AA clones was observed when administering both STC-15 and thapsigargin (**Figure 15H**).

Overall, we found that TT clones exhibited significantly higher levels of m6A modification in the portion of DDIT4 3' UTR in proximity to the rs1053639, and only in TT clones, when inhibiting METTL3, DDIT4 mRNA significantly shifted to the cytoplasm, and DDIT4 protein levels significantly increased.

Despite the allele-specific m6A modification in TT and AA clones, the inhibition of METTL3 by STC-15 did not reduce the allele-specific differences in DDIT4 protein levels, but possibly amplified them, similarly to thapsigargin treatment. These findings call for the need to explore alternative post-transcriptional paths to explain how a 3'UTR tranSNP could result in different protein levels of its own protein.

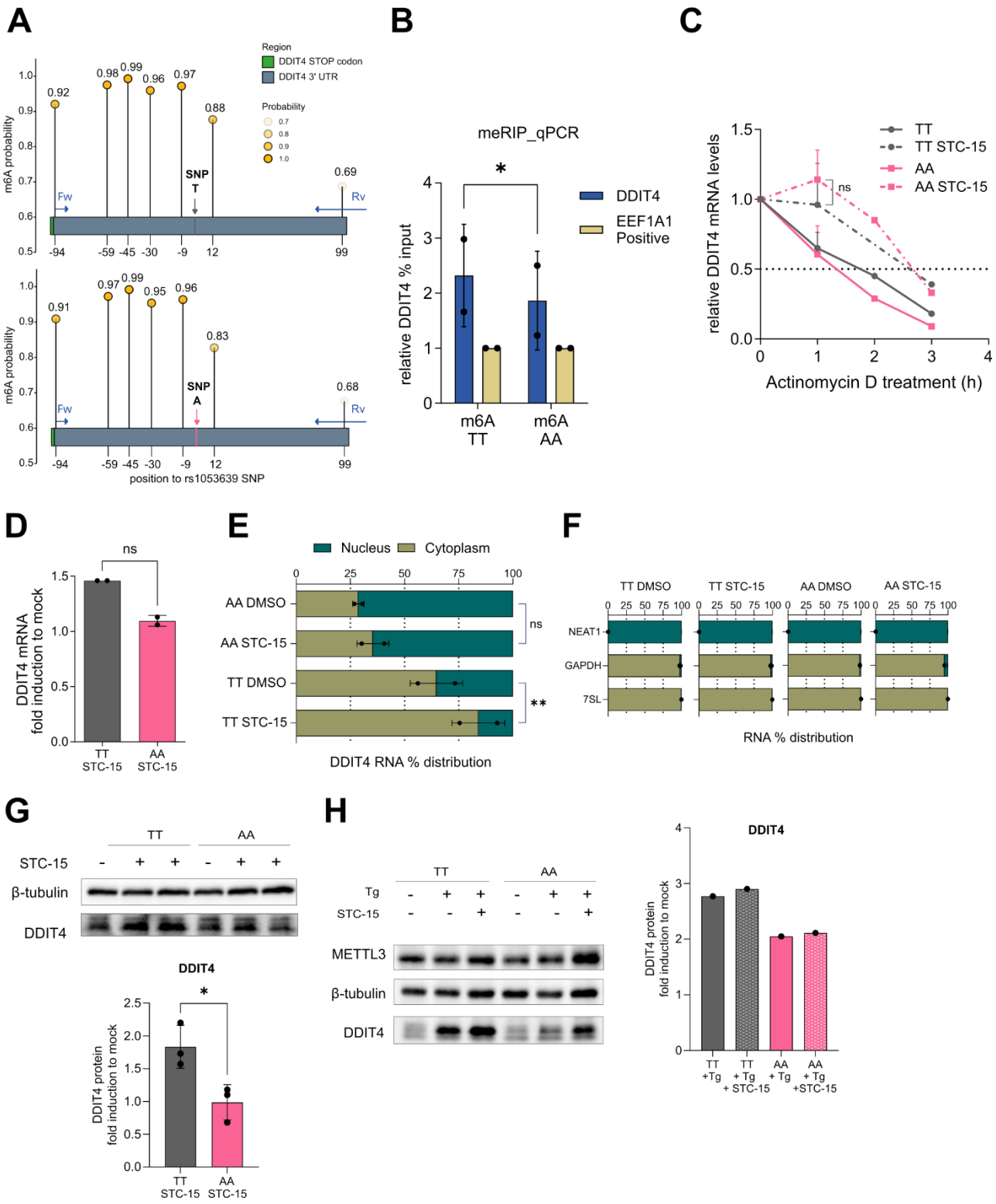

Figure 15. The rs1053639 alleles are differentially m6A-modified in DDIT4 3'UTR, but DDIT4 protein levels do not equalize upon METTL3 inhibition.

A) DeepSRAMP was used to predict the location and accuracy of m6A sites along 200 nt of DDIT4 3'UTR centered on rs1053639. The region covered by meRIP-qPCR primers is also indicated in blue (Fw, Rv). **B)** MeRIP-qPCR was

performed on TT and AA clones, and the enrichment of DDIT4 mRNA compared to the input sample and normalized to the enrichment of a positive control was plotted. Data represent the mean ± SD of two independent experiments. *p-value < 0.05, paired t-test. **C)** The curve shows the residual DDIT4 mRNA levels relative to GAPDH mRNA levels at different timepoints and presents results from two independent replicates. TT and AA clones were treated with Actinomycin D (10 µg/ml) for 0-3 hours after 24 hours of STC-15 (2.5 µM) treatment or vehicle. **D)** Fold induction of DDIT4 mRNA to vehicle upon STC-15 treatment (2.5 µM, 24 hours). The mRNA levels were measured by RT-qPCR and normalized to GAPDH mRNA levels. Ns, not significant, ordinary one-way ANOVA. **E)** DDIT4 mRNA localization was evaluated in TT and AA cells upon cell fractionation, followed by RT-qPCR in vehicle and STC-15-treated samples (2.5 µM, 24 hours). Data represent the mean ± SD of two independent experiments. **p-value <0.01, ns, not significant, paired t-test. **F)** Cell fractionation was performed in HCT116 clones and validated at the RNA level in vehicle and STC-15-treated samples (2.5 µM, 24 hours). U6 snRNA and NEAT1 were used as markers for the nuclear fraction, 7SL and GAPDH were used as markers for the cytoplasmic fraction. **G)** (Top) Western Blot analysis of DDIT4 and METTL3 protein levels across rs1053639 TT and AA HCT116 edited clones treated with either vehicle or STC-15 (2.5 µM, 24 hours). β-tubulin was used as a loading control. (Bottom) Densitometric analysis of DDIT4 and METTL3 protein levels. Results were expressed as a fold change to the vehicle for each clone. **H)** (Top) Western Blot analysis of DDIT4 and METTL3 protein levels across rs1053639 TT and AA HCT116 edited clones treated with either vehicle or thapsigargin (100 nM, 4 hours) or thapsigargin (100 nM, 4 hours) and STC-15 (2.5 µM, 24 hours). β-tubulin was used as a loading control. (Bottom) Densitometric analysis of DDIT4 protein levels. Results were expressed as a fold change to the vehicle for each clone.

The rs1053639 genotype directly impacts DDIT4 mRNA translation via RBMX

To further explore mechanisms by which RBMX could determine allele-specific DDIT4 protein levels, next, we focused our attention on the possible roles of the cytoplasmic fraction of RBMX protein.

Indeed, while we did not detect major changes in DDIT4 mRNA localization by silencing RBMX (**Figure 14F**), we did detect a drop in DDIT4 protein levels specifically in TT clones when silencing RBMX (**Figure 16A**), suggesting that a more direct role for RBMX in DDIT4 translation could also exist. RBMX silencing did not affect DDIT4 mRNA levels (**Appendix Figure 2**). We also observed that by increasing the efficiency of RBMX depletion, DDIT4 protein levels induced by thapsigargin treatment progressively decreased (**Figure 16B**). We found that the induction of DDIT4 by thapsigargin was dominant over the silencing of RBMX in regulating DDIT4 protein levels; yet we observed a reduction of thapsigargin-induced DDIT4 protein levels when RBMX was more effectively depleted (**Figure 16B**).

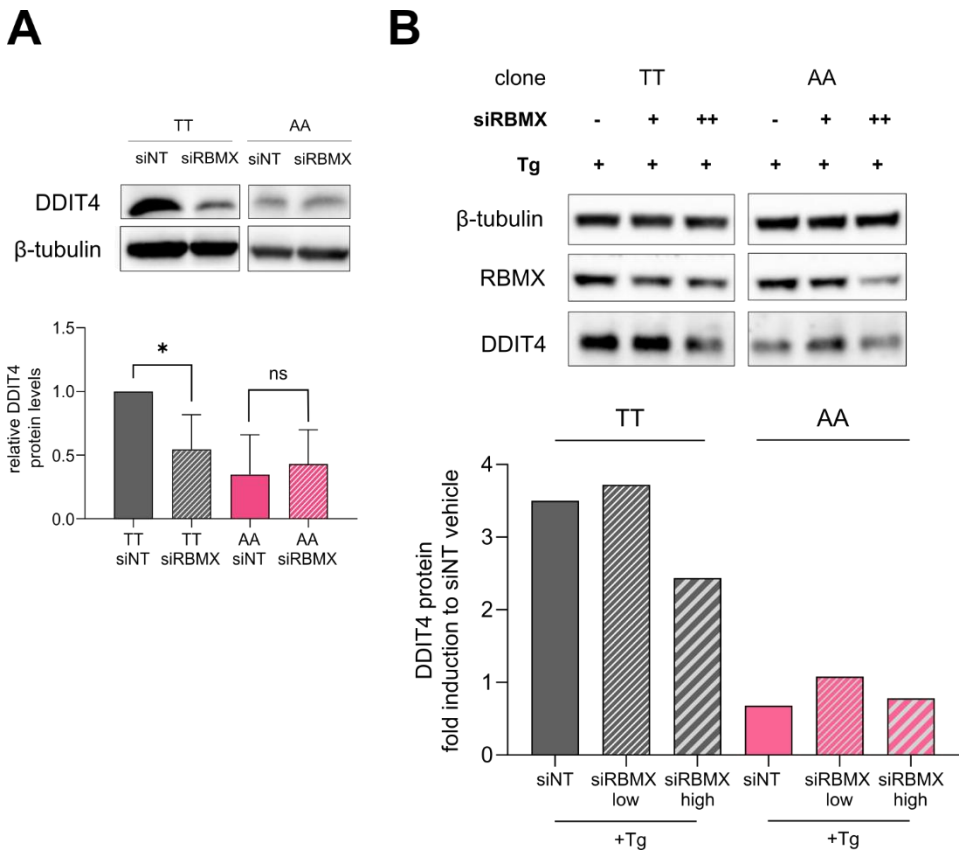

Figure 16. The rs1053639 genotype directly impacts DDIT4 translation via RBMX.

A) (Top) Western Blot analysis of DDIT4 protein levels in control (siNT) and RBMX-depleted (siRBMX) TT and AA clones. β-tubulin was used as a loading control. (Bottom) Densitometric analysis of DDIT4 protein levels from at least three independent experiments. *p-value < 0.05, ns, not significant, unpaired t-test. **B)** (Top) Western Blot analysis of DDIT4 and RBMX protein levels in control (siNT) and RBMX-depleted (siRBMX) TT and AA clones treated either with thapsigargin (100 nM, 4 hours) or vehicle. RBMX was depleted using two different combinations of siRNAs (low/high). β-tubulin was used as a loading control. (Bottom) Densitometric analysis of DDIT4 protein levels.

Looking for more direct mechanisms relating RBMX to translation, as suggested by **Figure 16A**, we found that RBMX co-sedimented with ribosomal subunits and polysomes in HCT116 clones, similarly to the ribosomal protein RPS6 (**Figure 17A, 17B**). When polysomes were affected by thapsigargin treatment, the distribution of both RPS6 and RBMX significantly shifted towards the subpolysomal fractions, highlighting a specific association with ribosome subunits and polysomes beyond the co-sedimentation (**Figure 17A, 17B**). We thus hypothesized that RBXM could directly promote the translation of the mRNAs to which it preferentially binds, such as in this case the DDIT4 mRNA from the T allele, by targeting them to the polysomes, improving their polysomal loading. We also hypothesized that RBMX could significantly move to the cytoplasm

upon ER stress, as described for other RBPs, but we did not find this evidence for RBMX (**Figure 17C**).

Conversely, to understand the consequences of poor RBMX binding, as for the A allele, we performed smiFISH (single-molecule inexpensive fluorescence in situ hybridization) in collaboration with the Laboratory of Cell Biology and Molecular Genetics (Dr. Glenda Paola Grupelli and Prof. Emilio Cusanelli, University of Trento, ITA) to directly visualize patterns of DDIT4 mRNA signal (e.g., aggregation or diffusion) and gather insights on the fate of DDIT4 mRNA. Indeed, the drop in DDIT4 protein levels (**Figure 16A**), with unchanged DDIT4 mRNA localization and levels (**Figure 14F, Appendix Figure 2**) when depleting RBMX in TT clones, suggested that DDIT4 mRNA, even though in the cytoplasm, was not available for translation in the described condition. DDIT4 mRNA produced a diffuse signal in TT clones, while it showed a more punctuated distribution, particularly in the perinuclear region, in AA clones in mock conditions (**Figure 17D**). We quantified this pattern by measuring the number of cytoplasmic spots per cell, which was significantly higher in the AA compared to the TT clones (**Figure 17E**). Upon RBMX depletion, while the number of spots per cell remained unchanged for the AA clones, the TT clones were significantly affected and exhibited a significant increase in the number of spots per cell, which became comparable to that of the AA clones. Interestingly, the number of cytoplasmic spots per cell inversely correlated with DDIT4 protein levels (**Figure 16A, 17E**), both in mock conditions and upon the down- and upregulation of DDIT4 protein levels by RBMX depletion and thapsigargin treatment, respectively.

Since translationally stalled mRNAs are generally deposited in stress granules, we next used markers for stress granules to shed light on the nature of the mRNA cytoplasmic spots and refine our speculative hypothesis according to which, in mock conditions, the preferential binding of RBMX to the T allele would guide DDIT4 mRNA to the polysomes. On the contrary, DDIT4 mRNAs that are less bound by RBMX (e.g., TT upon siRBMX, AA upon siNT or siRBMX) would not be directly targeted to the polysomes and would accumulate in cytoplasmic spots. However, we did not detect a striking overlap between DDIT4 mRNA signal and G3BP1 or TIAR-1 protein signals in mock conditions or ER-stress conditions induced by thapsigargin treatment (**Appendix Figure 3**) to claim the specific association of poorly translated DDIT4 mRNAs with stress granules.

Overall, we showed that RBMX directly contributes to the allele-specific DDIT4 protein levels; we also provided novel evidence that RBMX co-sediments with ribosome subunits and

polysomes, and potentially targets DDIT4 mRNAs for translation into polysomes. Conversely, DDIT4 mRNAs that are poorly bound by RBMX aggregate into cytoplasmic spots, although not overlapping with stress granules.

The 3' UTR tranSNP rs1053639 thus impacts DDIT4 mRNA localization, granularity, and translation via mechanisms encompassing the trans-factor RBMX and m6A, to eventually produce allele-specific DDIT4 protein levels.

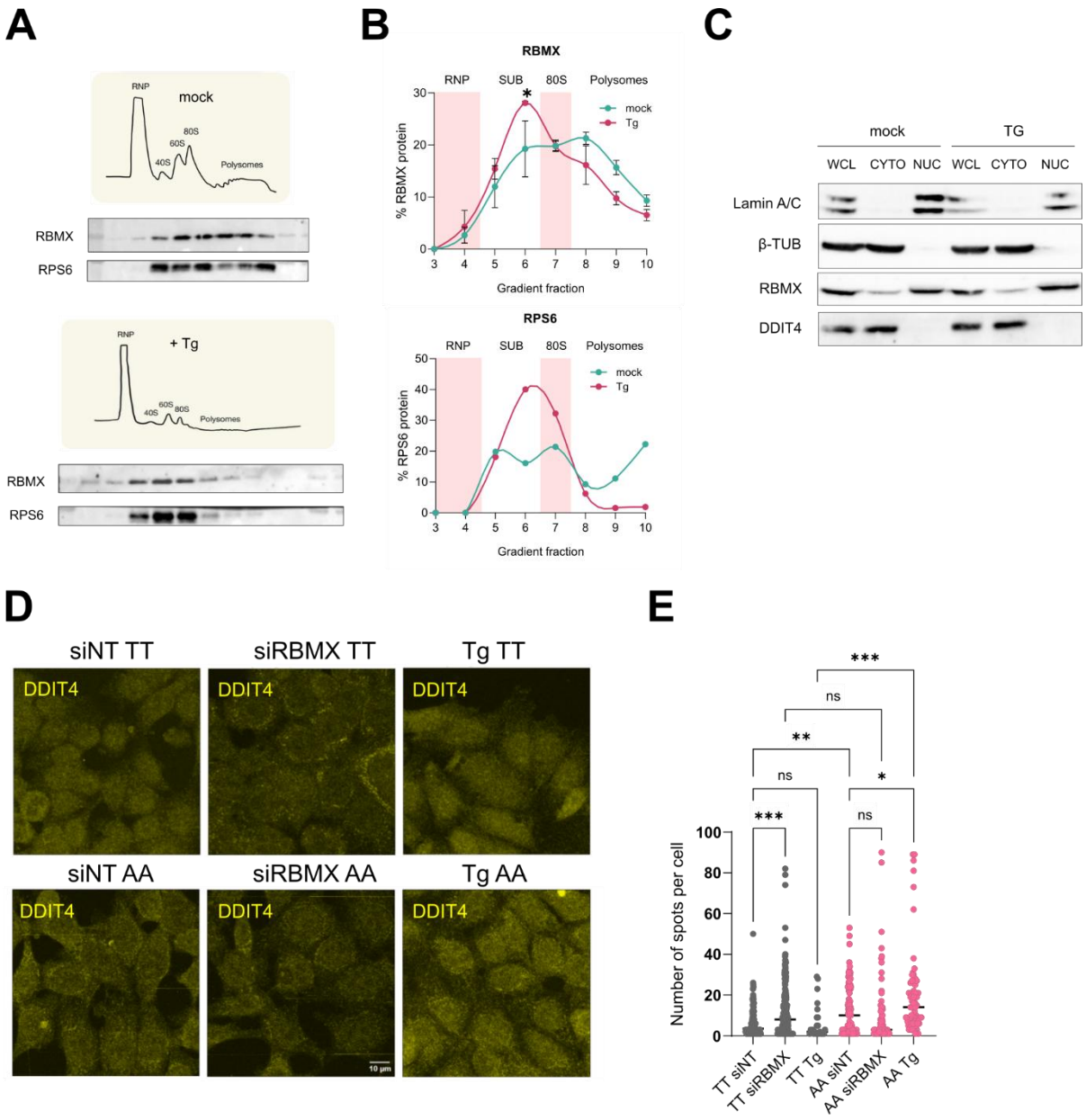

Figure 17. RBMX is associated with polysomes, while poorly translated DDIT4 mRNAs accumulate into cytoplasmic spots.

A) Western Blot analysis of endogenous RBMX and RPS6 protein levels across sucrose-gradient fractions from polysome profiling in HCT116 clones in mock conditions (Top) and under thapsigargin treatment (Bottom). RPS3 is associated with the 40S subunit. **B)** Distribution of RBMX protein (Top) and RPS6 protein (Bottom) across the

polysomal gradient fractions. Fractions 3-4 represent the free RNA, fractions 5-6 represent the ribosomal subunits, fraction 7 represents the 80S subunit, and fractions 8-10 represent the polysomal subunits. *p-value < 0.05, two-way ANOVA. **C)** Cell fractionation was performed in HCT116 cells upon vehicle or thapsigargin treatment (100 nM, 4 hours) and analyzed at the protein level via Western Blot. Lamin A/C and β-Tubulin were used as markers for the nuclear and cytoplasmic fractions, respectively. WCL: whole cell lysate. CYTO: cytoplasm. NUC: nuclei. **D)** Confocal images of smiFISH-IF of TT and AA clones in control (siNT) or RBMX-depleted samples. DDIT4 mRNA is shown in yellow. Scale bar is 10 μm. **E**) At least three fields (15-20 cells per field) for each coverslip and each condition were imaged, and spots were quantified using Cell-Profiler 4.0.7 (Broad Institute, Inc.) and segmented as objects with a typical diameter range of 10 to 30 pixels. The number of DDIT4 mRNA spots per cell was plotted. ns = not significant, ** p< 0.01; *** p<0.001, ordinary one-way ANOVA.

TT clones exhibit enhanced control of the mTOR pathway, but AA outgrow them in co-culture

After proposing possible mechanisms underlying allele-specific DDIT4 protein levels, we asked whether exhibiting different DDIT4 protein levels would be relevant to downstream cellular phenotypes. Since DDIT4 is a well-established inhibitor of mTORC1 (DeYoung et al., 2008), we assessed mTOR pathway activity by measuring the levels of phosphorylated 4EBP1 and S6K (Hay and Sonenberg, 2004), both in mock and thapsigargin treatment conditions, which is when DDIT4 is induced. TT clones significantly reduced the levels of phosphorylated 4EBP1 and S6K, thus mTORC1, in response to thapsigargin treatment. The same markers were not significantly affected in the AA clones (**Figure 18A, 18B, Appendix Figure 1B**). This finding suggested that TT clones may be more responsive to external cues and more adaptive by effectively inhibiting the mTOR pathway in response to acute stress, such as thapsigargin-induced ER stress.

Since mTOR is a major regulator of cell growth and proliferation, we asked whether the TT and AA clones differed in their proliferation rate. Interestingly, although the TT clones had better control of the mTOR pathway than the AA, they did not show any advantage in terms of cell proliferation in the short term (**Figure 18C**) or in terms of global protein synthesis, as already described (**Figure 12F**), which are major phenotypes downstream of the mTOR pathway.

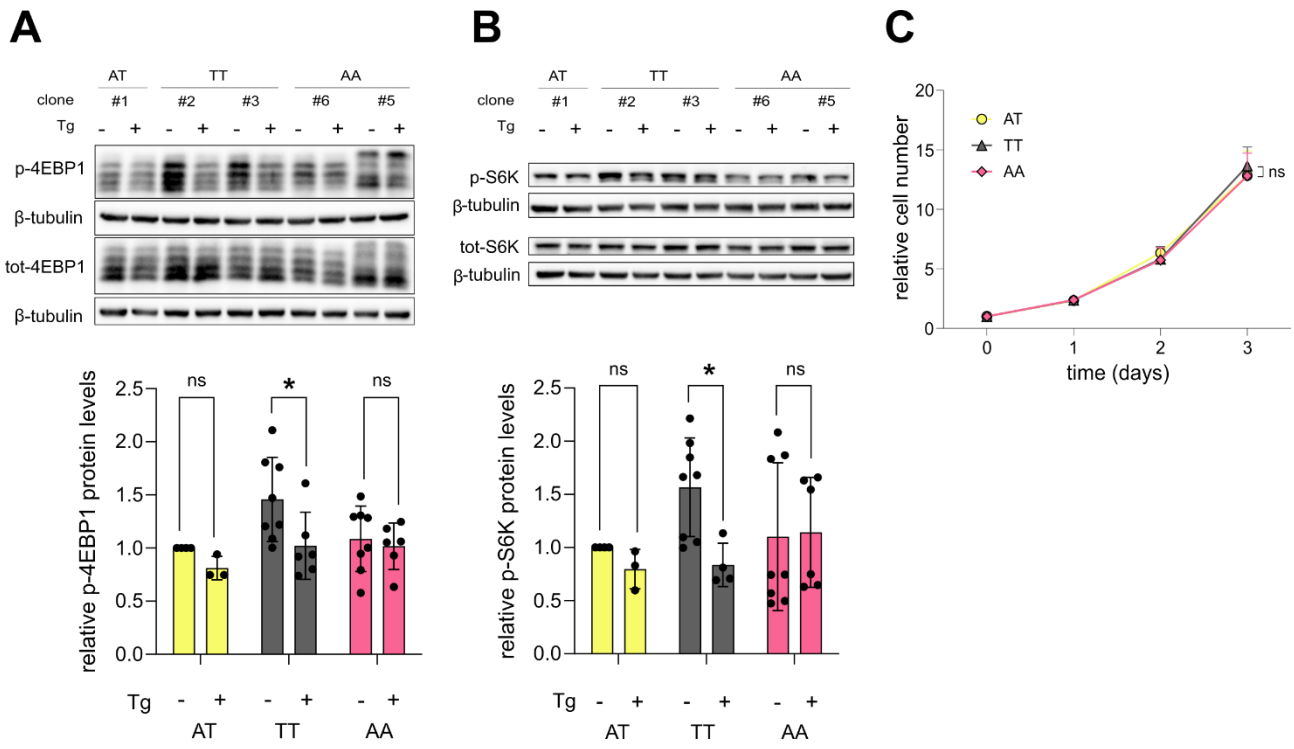

Figure 18. The TT clones exhibit a stronger inhibition of the mTOR pathway upon thapsigargin treatment. **A)** (Top) Western Blot analysis of phosphorylated and total 4EBP1 protein levels across rs1053639 TT and AA HCT116 edited clones treated with vehicle or thapsigargin (100 nM, 4 hours). β-tubulin was used as a loading control. (Bottom) Densitometric analysis of phosphorylated 4EBP1 protein levels normalized to the total 4EBP1 and β-tubulin across at least 3 individual blots, considering at least two edited clones per genotype. *p-value < 0.05, ordinary one-way ANOVA. **B)** (Top) Western Blot analysis of phosphorylated S6K and total S6K protein levels across rs1053639 TT and AA HCT116 edited clones treated with vehicle or thapsigargin (100 nM, 4 hours). β-tubulin was used as a loading control. (Bottom) Densitometric analysis of phosphorylated S6K protein levels normalized to the total S6K and β-tubulin across at least 3 individual blots, considering at least two edited clones per genotype. *p-value < 0.05, ordinary one-way ANOVA. **C)** HCT116 clones were seeded and imaged every 24 hours for 3 days using the Operetta High Content System. The plot shows the cell count at different timepoints relative to the time-zero cell count as the mean of at least 5 replicates ± standard deviation (SD). Ns, not significant. Ordinary two-way ANOVA.

We therefore asked whether other functions of the mTOR pathway were affected in response to different DDIT4 levels or whether mTOR-independent functions of DDIT4 could be implicated as well.

For example, the induction of autophagy is a central function of DDIT4 in cells, and can be both negatively modulated by mTORC1, through the inhibition of ULK1 (Jung et al., 2009), the kinase that initiates the autophagosome, and positively tuned by an mTOR-independent, but DDIT4-dependent, axis involving the direct interaction of DDIT4 and the pro-oxidant protein TXNIP

(Gao et al., 2020; Shin et al., 2008b). Hence, we measured the canonical autophagy readouts both in mock and thapsigargin treatment conditions across TT and AA clones (**Figure 19A-D**). While thapsigargin induces DDIT4 and exacerbates DDIT4-dependent responses, we also found evidence that this treatment leads to the accumulation of mature autophagosomes by blocking the fusion of the autophagosome with the endocytic system (Ganley et al., 2011). While we did not find significant differences in the possibility to activate AMPK-mediated autophagy via ULK1, we found significant allele-specific differences in the levels of LC3-II upon thapsigargin treatment and a trend for p62 protein levels.

However, the direction of the autophagic flux is generally determined by the treatment with chloroquine, an antimalarial agent known to inhibit the autophagic flux by decreasing the autophagosome-lysosome fusion (Mauthe et al., 2018). We thus inhibited autophagy by acute chloroquine treatment and confirmed a prominent dose-dependent accumulation of LC3-II in TT clones compared to AA clones, along with a dose-dependent increase of p62 protein (**Figure 19E-G)**. It is known that changes in p62 levels are often subtle compared to LC3-II flux, because of additional mechanisms of regulation (Klionsky et al., 2012). Conversely, the AA clones showed a moderate accumulation of LC3-II and stable p62 levels. Similarly to thapsigargin, chloroquine was also reported to induce sustained ER stress (Jia et al., 2018), and indeed, DDIT4 protein levels were induced upon chloroquine treatment in our models (**Figure 19H**).

Overall, we found evidence of allele-specific differences in the autophagic flux. The AA clones exhibited a less efficient autophagic flux, whereas the autophagic markers in the TT clones were consistent with a largely functional and active autophagic flux, which is coherent with their stronger ability to inhibit mTORC1 (which negatively regulates autophagy) due to higher DDIT4 protein levels.

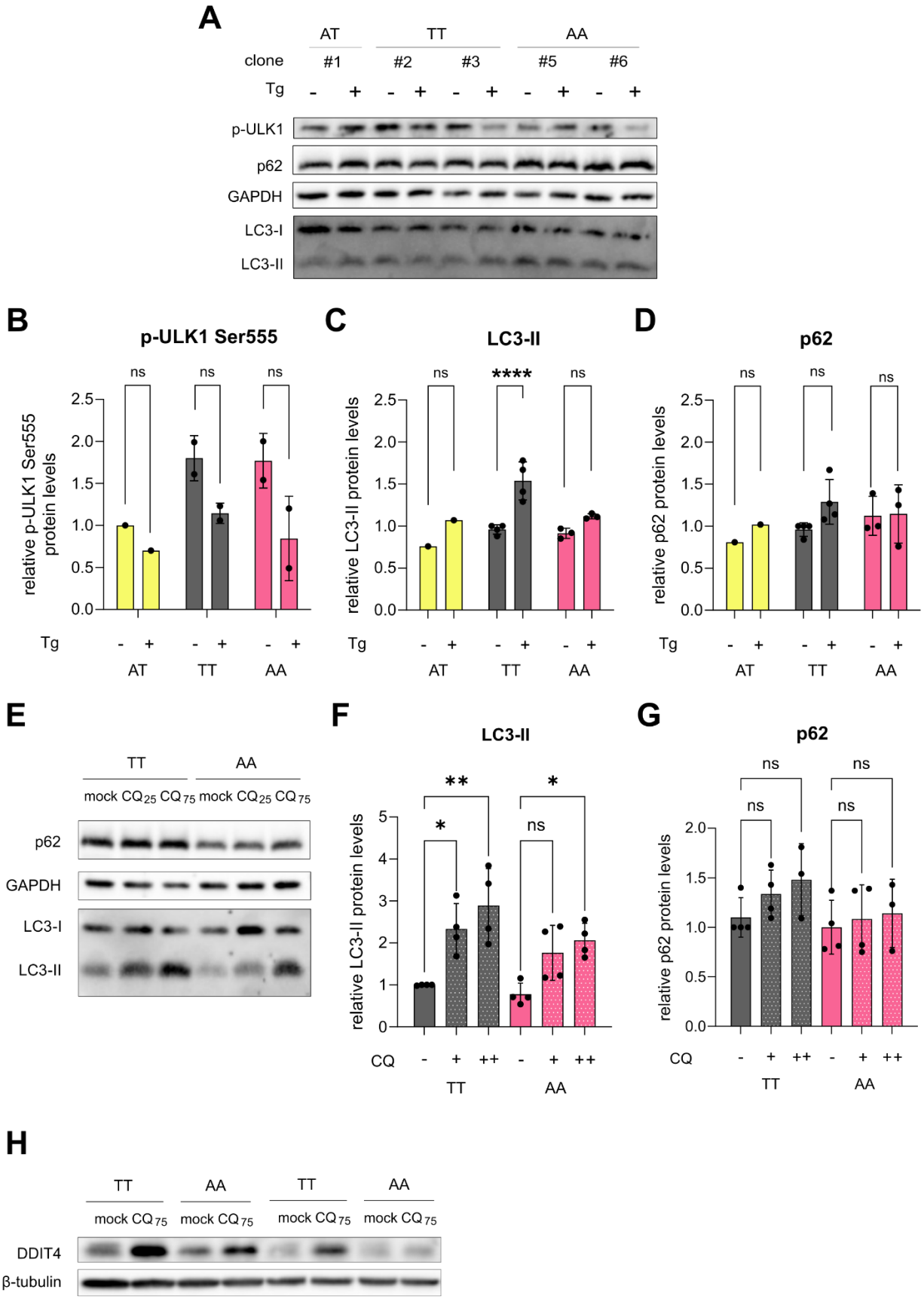
A
AT
TT
AA
clone
#1
#2
#3
#5
#6
Tg
p-ULK1
p62
GAPDH
LC3-I
LC3-II
B
p-ULK1 Ser555
relative p-ULK1 Ser555 protein levels
C
LC3-II
relative LC3-II protein levels
D
p62
relative p62 protein levels
ns
****
E
mock
CQ25
CQ75
F
G
CQ
TT
AA
H
DDIT4
β-tubulin

Figure 19. TT clones exhibit a largely functional and active autophagic flux.

A) Western Blot analysis of phosphorylated ULK-1 (Ser555), LC3-II, and p62 protein levels across rs1053639 TT and AA HCT116 edited clones treated with vehicle or thapsigargin (100 nM, 4 hours). GAPDH was used as a loading control. Densitometric analysis of **B)** phosphorylated ULK-1 (Ser555), **C)** LC3-II, **D)** p62 protein levels normalized to GAPDH across two individual blots, considering two edited clones per genotype. ****p-value < 0.0001, two-way ANOVA. **E)** Western Blot analysis of LC3-II and p62 protein levels across rs1053639 TT and AA HCT116 edited clones treated with either vehicle or chloroquine (CQ; 25 and 75 μM, 6 hours). GAPDH was used as a loading control. Densitometric analysis of **F)** LC3-II **G)** p62 protein levels normalized to GAPDH upon chloroquine treatment. **H)** Western Blot analysis of DDIT4 protein levels across rs1053639 TT and AA HCT116 edited clones treated with either vehicle or chloroquine (CQ; 75 μM, 6 hours). β-tubulin was used as a loading control. Two independent replicates are shown in the same blot.

We subsequently investigated whether cancer cells would benefit from a tighter regulation of mTOR activity and more active autophagy, such as seen in the TT clones, or from a more relaxed response to mTOR and hindered autophagy, such as in the AA clones.

We first generated EGFP-positive TT and AA clones with high clonal purity to effectively distinguish the contribution of each genotype (**Figure 20A**). We then co-cultured EGFP-labelled TT with non-labelled AA clones, and vice versa to control for the effect of the dye on proliferation, for 15 days, with splitting and flow cytometry analysis every 4 days. Cell counts were plotted in **Figure 20B** and converted into relative cellular fitness as recently described (Louro et al., 2024a) in **Figure 20C**. Specifically, cellular competitive fitness (W) was calculated as the natural logarithm of the ratio between the proportion of GFP-positive cells over the proportion of GFP-negative cells at a certain time point, and the proportion of GFP-positive cells over the proportion of GFP-negative cells at time zero.

Notably, while the TT clones showed higher fitness at early time points (3 days), the AA clones showed a growth advantage in prolonged co-culture conditions. We ensured that this result was not influenced by the presence of the fluorescent marker (**Figure 20B**), nor by differences in cell cycle distribution at day 0 or after 7 days of co-culture (**Figure 20D**).

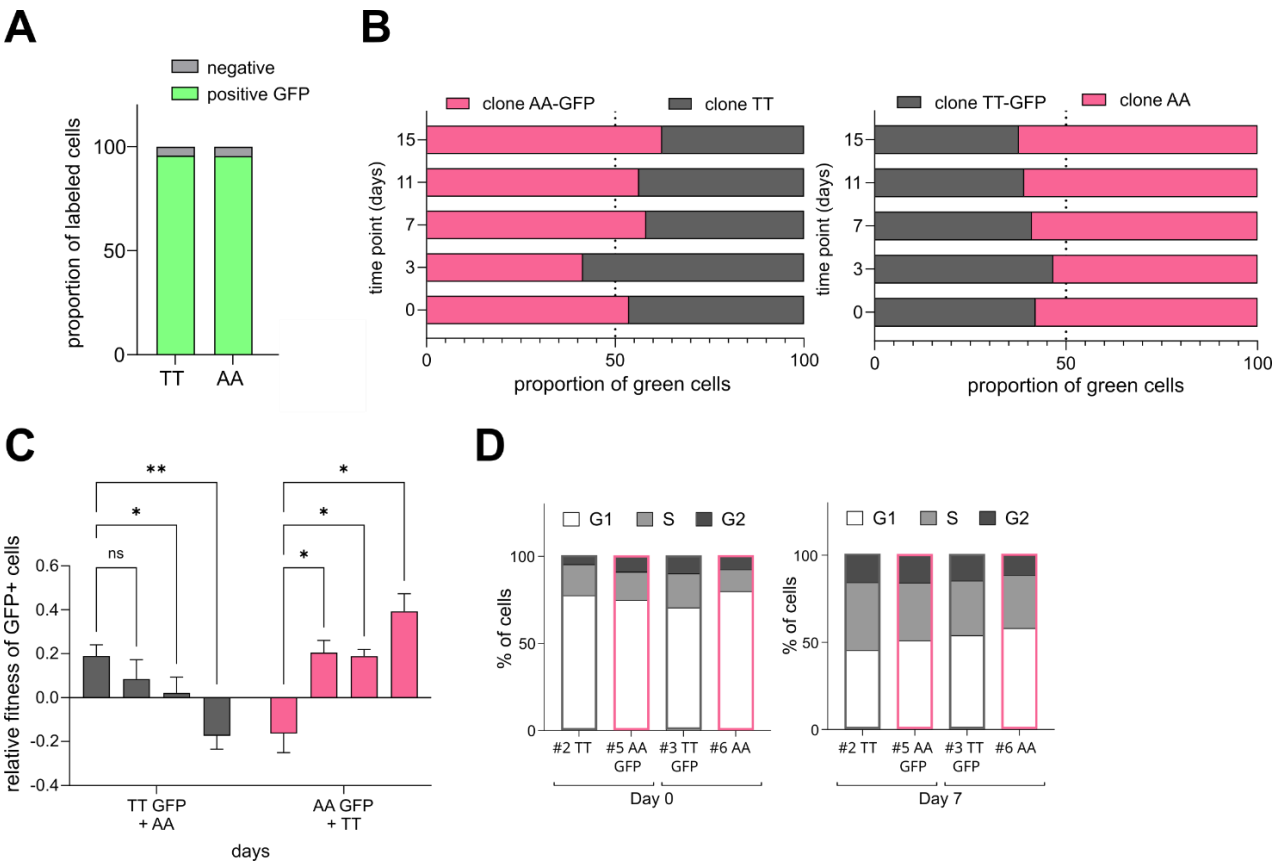

Figure 20. AA clones show higher relative fitness when co-cultured with TT clones for 15 days.

A) TT and AA clones were transduced with lentiviral viruses carrying the EGFP and selected using blasticidin (5 µg/ml, for at least 15 days) to obtain populations with constitutive > 95% EGFP-positive cells. **B)** (Left) EGFP labelled AA clones were mixed 1:1 with unlabeled TT clones and co-cultured for 15 days. (Right) EGFP-labelled TT clones were mixed 1:1 with unlabeled AA clones and co-cultured for 15 days. 10K cells were analyzed by FACS to retrieve cell counts at every time point. **C)** Cell count numbers were converted into a published measure of cellular fitness (W) of EGFP+ cells compared to unlabeled cells using the following formula: pGFP+(t) = NGFP+(t) / (NGFP+(t) + N GFP-(t)), W = ln ((pGFP+(ti) /pGFP-(ti)) / (pGFP+(t0) /pGFP-(t0)). The error bars represent the mean ± SD of at least eight independent experiments (half TT GFP+, half AA GFP+). *p-value < 0.05; **p-value < 0.01, ordinary two-way ANOVA. **D)** FACS analysis of cell cycle for TT and AA clones at day 0 and upon 7 days of co-culture via Hoechst and Propidium Iodide (PI) staining.

AA clones maintain their competitive advantage when xenografted into Zebrafish embryos

To further test the advantage of AA clones in co-culture settings and gain some information on their potential aggressiveness, we developed xenograft experiments in Casper Zebrafish embryos, in collaboration with the Laboratory of Experimental Cancer Biology (Dr. Francesca Lorenzini and Prof. Marina Mione, University of Trento, ITA).

Equal number of cells from EGFP-labelled TT or AA clones were injected into the swim bladder of two-day postfertilization embryos. Cells were then imaged the following day (day 1) and again 48 hours later (day 3) (**Figure 21A**). Results, plotted as the percentage of tumor cells' growth, compared the tumor area from day 1 to day 3 post-injection and showed that, when TT and AA were injected separately *in vivo*, the growth advantage of the AA clones was again apparent after only 3 days (**Figure 21B**).

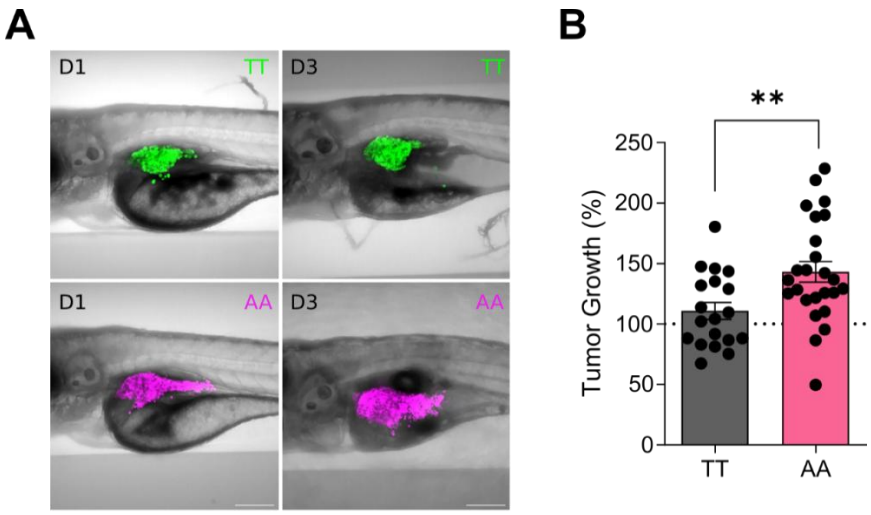

Figure 21. The AA clones grow significantly more than the TT when xenografted in Zebrafish embryos.
A) EGFP-labelled TT or AA clones were xenotransplanted into zebrafish larvae two days post-fertilization. Tumor growth was monitored over three days, with a minimum of 30 larvae per genotype condition. Representative confocal microscopy images were obtained on day 1 and day 3 post-transplantation. TT clones are represented in green, AA clones in violet. **B)** Bar graph showing the percentage of tumor growth relative to day 0 of transplantation. Tumor growth is calculated as the percentage of the tumor (or cell) area on day 3 compared to the tumor area on day 1. Each data point represents an individual larva. **p-value < 0.01. paired t-test.

The rs1053639 tranSNP genotype has prognostic significance in cancer patients

The phenotypic consequences of allele-specific DDIT4 protein levels led us to explore whether the rs1053639 tranSNP genotype might also be relevant in a clinical context, specifically with respect to colorectal cancer prognosis, since HCT116 are colorectal cancer-derived cells. Patients with the AA genotype showed significantly worse prognosis than patients with the AT genotype in the analyzed TCGA COAD cohort for colorectal cancer, considering the disease-free interval endpoint (DFI) (**Figure 22**). We did not consider the association of rs1053639 with additional covariates, such as p53 status or RBMX levels, in this analysis. However, it would be

interesting to predict the potential impact of a tranSNP by combining multiple parameters and generating a comprehensive score.

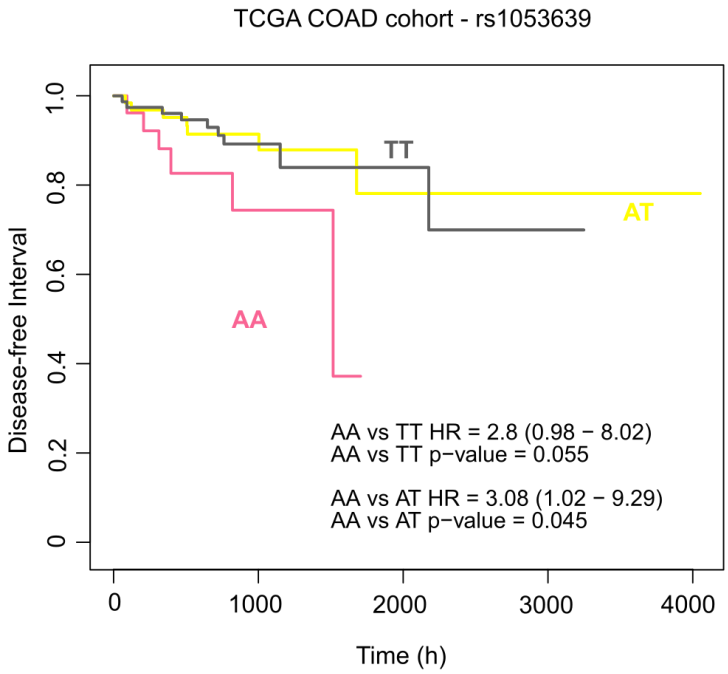

Figure 22. TCGA patients with the AA genotype exhibit a worse prognosis than those with the TT genotype in terms of disease-free interval (DFI).

Kaplan-Meier curve plotting the disease-free interval for rs1053639-stratified TT, AT and AA patients from the COAD TCGA cohort.

The rs1053639 tranSNP genotype affects cell sensitivity to a range of compounds

Guided by the prognostic value of the rs1053639 genotype in terms of DFI, we asked whether the SNP might influence the time between primary treatment and cancer recurrence (DFI) by affecting the ability of cancer cells to survive or proliferate after treatment.

We thus investigated whether the rs1053639 genotype could influence cell sensitivity to a range of compounds. Interestingly, *in silico* pancancer analyses performed by the Laboratory of Bioinformatics and Computational Genomics (Prof. Alessandro Romanel, University of Trento, ITA) using TCGA and RNA-seq data to inform possible germline-somatic interplays highlighted that patients with TT and AA genotypes showed significantly different enrichment in gene expression patterns. In particular, patients with the TT genotype for rs1053639 showed a wider dysregulation of genes related to the Wnt, TGF-β, and MYC pathways, compared to AA patients. Based on this, we tried to include compounds targeting these pathways.

From a preliminary test, we found that the TT clones were significantly more resistant to the METTL3 inhibitors UZH2 and STC-15 (**Figures 23A and 23 B**). We next performed dose-response curves for a set of compounds with broader functions (**Figure 23C-E**). Niclosamide is an FDA-approved anthelmintic that inhibits the STAT3, Wnt, mTORC1, and NF-κB pathways. Nutlin is a well-known p53 activator, and thapsigargin is a potent inducer of ER stress and DDIT4. Preliminary data for additional compounds are shown in the **Appendix Figure 4**. **Appendix Figure 5** instead shows the percentage of PI-positive cells across the above-mentioned treatments. Globally, we found that the TT clones were significantly more resistant to most of the compounds and hypothesized that the higher DDIT4 protein levels could be responsible for this phenotype; indeed, **Figure 11C, 15G,** and our recent report (Hamadou, Alunno et al., 2025b) respectively highlighted that DDIT4 is induced upon STC-15, thapsigargin, and nutlin treatment in an allele-specific manner to higher levels in the TT compared to the AA clones.

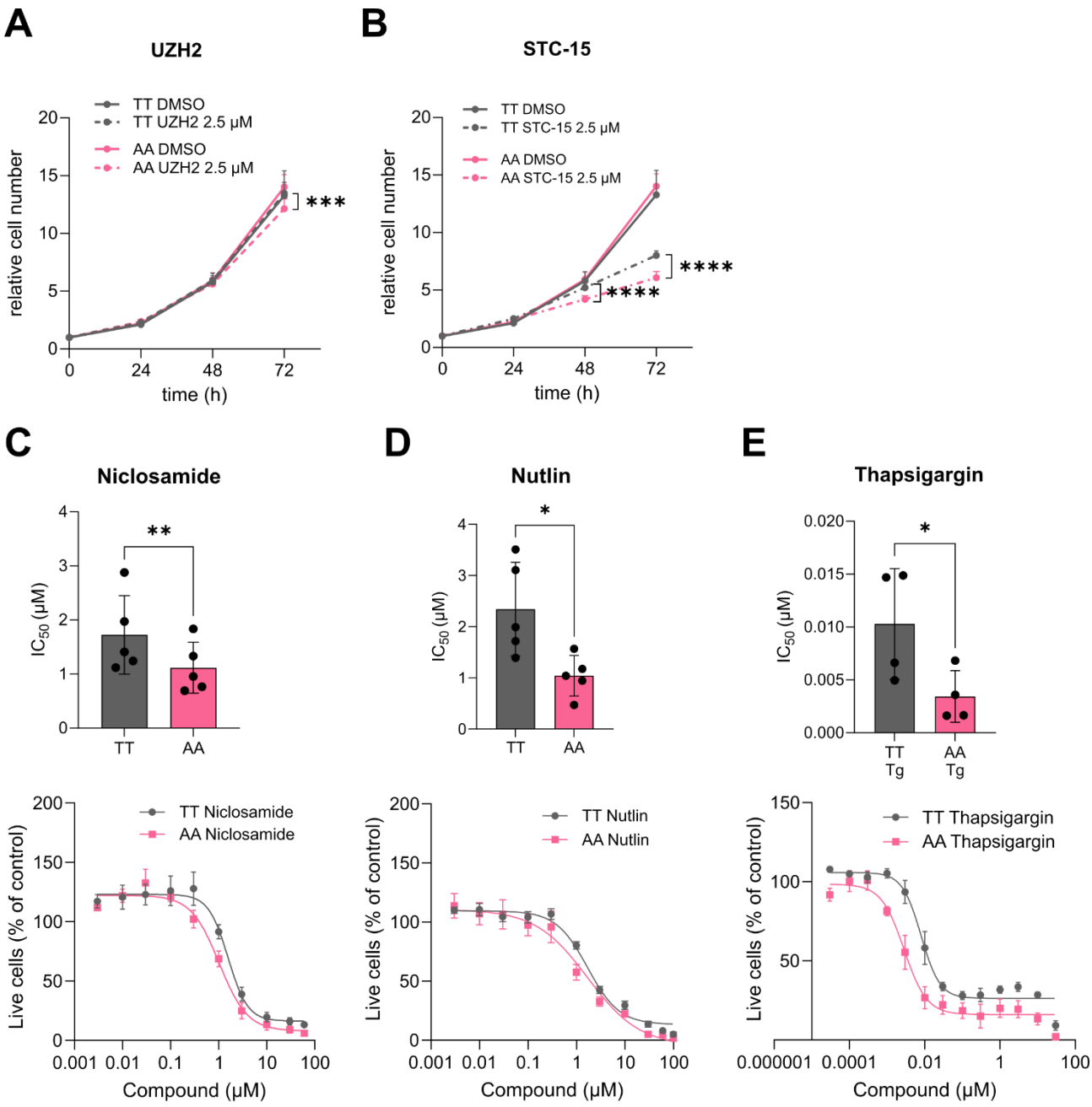

Figure 23. The rs1053639 genotype determines allele-specific sensitivity to multiple compounds.

A) TT and AA clones were treated with 2.5 µM of UZH2 or vehicle, starting 24 hours post-seeding. The cell number was monitored at time zero and every 24 hours for 3 days using the Operetta High Content System. The plot shows the cell count at different time points relative to the time-zero cell count. ***p-value < 0.001, ****p-value < 0.0001. Ordinary two-way ANOVA. **B)** TT and AA clones were treated with 2.5 µM of STC-15 or vehicle, starting 24 hours post-seeding. The cell number was monitored at time zero and every 24 hours for 3 days using the Operetta High Content System. The plot shows the cell count at different time points relative to the time-zero cell count. ***p-value < 0.001, ****p-value < 0.0001. Ordinary two-way ANOVA. **C-E)** Cells were seeded using the automatic VIAFILL dispenser and treated after 24 hours using the Echo Acoustic Liquid Handler with a wide range of concentrations in the nanomolar and micromolar range of either niclosamide, nutlin, thapsigargin, or vehicle for

48 hours. Cells were then incubated with Hoechst and PI (1:2000) for at least 40 minutes at 37 °C, and live imaging was performed using the ImageXpress Micro Confocal High-Content Imaging System. (Top) Bar plot representing IC_{50} values for the respective treatments from at least four independent replicates, considering multiple clones for each genotype. (Bottom) Dose-response curve indicating live cells (Hoechst-positive and PI-negative) normalized to the DMSO control on the y-axis and $\log_{10}$ of the compound concentrations on the x-axis.

The effect of rs1053639 does not appear to be cell line-specific

Given the collective clinical relevance we demonstrated for rs1053639 in colorectal cancer cells and patient data, we asked whether the effect of rs1053639 on DDIT4 translation was conserved across other cancer or non-cancer cell lines, to gain insights into the potential translatability of our findings.

Luciferase reporter assay using the "Long" and "Short" DDIT4 constructs in the lung cancer cell line A549 showed that the higher translation efficiency of the T allele compared to the A allele was maintained as in HCT116 cells (**Figure 24A**). The same result was obtained in the non-cancer RPE-1 cell line (**Figure 24B**). We thus generated a set of AA and AT RPE-1 clones for rs1053639; RPE-1 cells are indeed homozygous for the T allele. Although the editing was sub-optimal in RPE-1 and generated multiple indels around the SNP site, we still detected higher DDIT4 protein levels in the wild type TT compared to the AA edited clones (**Figure 24C**). Also, DDIT4 protein levels were strongly induced by thapsigargin treatment in TT compared to AA clones, as for HCT116 (**Figure 24C**).

Globally, although data is not robust enough to support a general statement, we observed that the effect of rs1053639 was maintained both across another cancer cell line and a non-cancer cell line. This suggests that tranSNPs may cooperate with trans-factors, such as RBMX, but they can also exert at least part of their function independently, stimulating, but at the same time, complicating the idea of predicting the protein output from integrating the SNP genotype and the trans-factor levels, and based on that, predicting patients' outcomes. We attempted to correlate RBMX and DDIT4 protein levels with TCGA survival data; however, the limited availability of RBMX protein data did not allow a robust exploration.

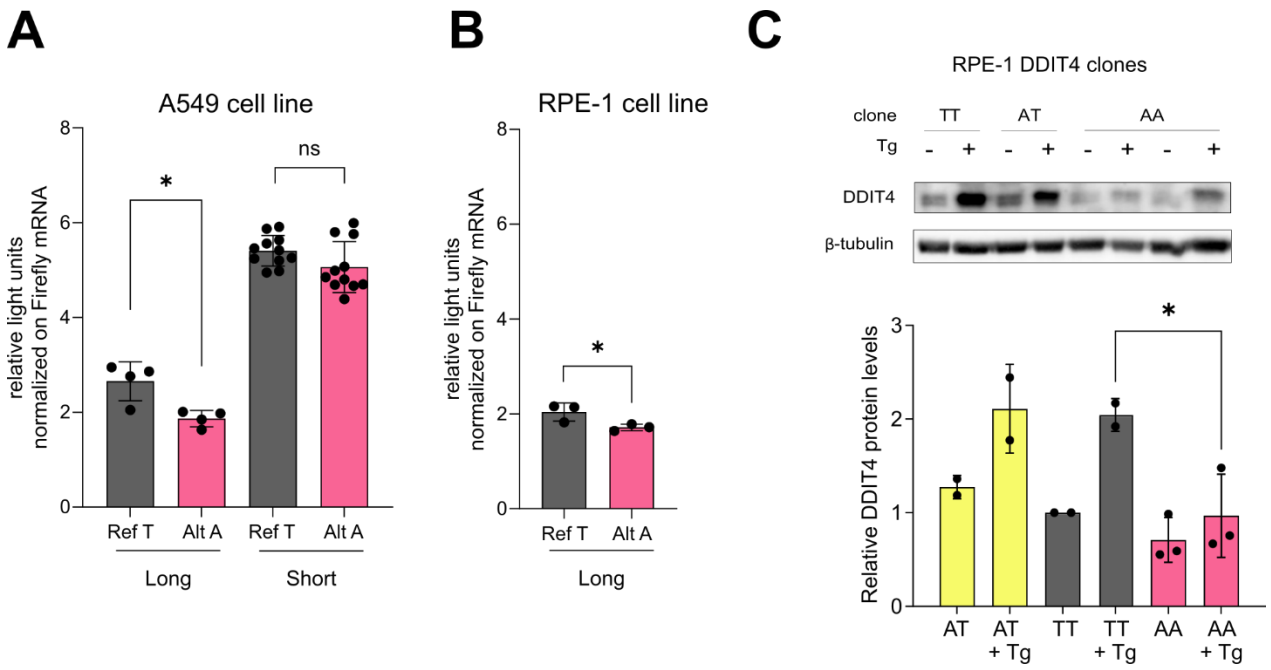

Figure 24. The rs1053639 T allele maintains higher translation efficiency in A549 and RPE-1 cells.

A) Luciferase reporter assay of a ~ 500 bp (Long) and a ~ 100 bp (Short) construct encompassing rs1053639 in wt A549 cells (A/T). Firefly luminescence was first normalized to Renilla luminescence, then to Firefly mRNA levels. *p-value < 0.05, unpaired t-test. **B)** Luciferase reporter assay of a ~ 500 bp (Long) construct encompassing rs1053639 in wt RPE-1 cells (T/T). Firefly luminescence was first normalized to Renilla luminescence, then to Firefly mRNA levels. *p-value < 0.05, unpaired t-test. **C)** (Top) Western Blot analysis of DDIT4 protein levels across rs1053639 TT, AT, and AA RPE-1 edited clones. β-tubulin was used as a loading control. (Bottom) Densitometric analysis of DDIT4 protein levels across two individual blots. *p-value < 0.05, ordinary one-way ANOVA.

TranSNPs can be identified in non-cancer cell lines

To follow up on the potential clinical relevance of tranSNPs, we wondered whether the allelic imbalance leading to the identification of tranSNPs was exclusive to cancer cell lines due to their broad, rewired cellular deregulation or whether it also occurred in non-cancer cell lines. Hence, we attempted to generate a new catalogue of tranSNPs in the hTERT-immortalized retinal pigment epithelial cells (RPE-1). RPE-1 cells were selected as representatives of non-cancer cell lines because of their established use in research, transfection, and editing amenability, as well as their well-described and relatively stable karyotype (Volpe et al., 2025). Starting from exome sequencing data, we identified about 7000 heterozygous analyzable SNPs in RPE-1 cells. We calculated the allelic imbalance across polysome-bound and total cytoplasmic mRNAs for the heterozygous and analyzable SNPs. This dataset was characterized by high coverage (120 million reads), three biological replicates for each fraction, and a

treatment with either 10 μM Nutlin or vehicle for 16 hours. The high coverage allowed the identification of a large number of putative tranSNPs, even along the same mRNA, and allowed a broader exploration of the tranSNP effect by opening the discussion on haplotype and causality, besides possible mechanistic cross-talks. To investigate whether we could improve the tranSNPs identification pipeline, we added a further fraction to this dataset, which is represented by the 80S monosome-bound mRNAs (**Figure 25**). By applying the nominal p-value ≤ 0.05 threshold, we identified 411 tranSNPs in RPE-1 by comparing polysome-bound and total mRNAs (POL-TOT) corresponding to about 5.5% of the analyzable SNPs, 359 tranSNPs by comparing polysome-bound and 80S-bound mRNAs (POL-80S) corresponding to about 6.5% of the analyzable SNPs, and 299 tranSNPs by comparing the 80S-bound and total mRNAs (80S-TOT) corresponding to about 5.4% of the analyzable SNPs, indicating that tranSNPs can be identified in non-cancer settings.

We broadly explored this dataset by selecting both 5' UTR, 3' UTR, and coding (CDS) tranSNPs for experimental validation. To guide the selection, we adopted a conservative approach and applied a further threshold of -2SD > dAF > 2SD to the identified tranSNPs, considering the variance, thus the magnitude of the effect. With this approach, we restricted the tranSNPs to 59 when comparing polysome-bound and total mRNAs (POL-TOT), 89 tranSNPs when comparing polysome-bound and 80S-bound mRNAs (POL-80S), and 52 tranSNPs when comparing the 80S-bound and total mRNAs (80S-TOT).

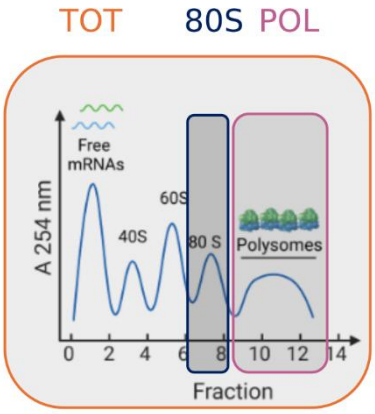

Figure 25. Schematic representation of the tranSNP catalogue strategy in RPE-1 cells.

80S-bound mRNAs were introduced as a separate fraction to compare with total mRNAs and polysome-bound mRNAs.

The use of 80S-bound mRNAs may improve resolution in the identification of tranSNPs

Since the translation status of the 80S monosome is still very debated (Blandy et al., 2025a; Heyer and Moore, 2016), the comparison of polysomal and total mRNAs with the 80S-bound mRNAs holds the potential to contribute to the field by clarifying the potential of the 80S, and to diminish the potential bias originated by the incorporation of polysome-bound mRNAs in total mRNAs, by having a fraction completely free from polysome contamination.

We exploited our new RPE-1 dataset to address this gap by evaluating the allelic imbalance (dAF, delta allelic fraction) of tranSNPs which were significantly imbalanced both in the 80S-TOT and in the POL-80S comparisons.

Most of these tranSNPs displayed complementary allelic imbalance in the 80S-TOT compared to the POL-80S comparison (**Figure 26**). Positive imbalance values in the 80S-TOT comparison indicate that the alternative allele is enriched in the 80S over the TOT, while negative values in the POL-80S comparison place the alternative allele in the 80S over the POL fraction. This systematic observation led us to think that the 80S fraction and the polysomal fraction were opposite to each other.

Furthermore, when we plotted the imbalance values in the TOT-POL comparison (even when statistical significance was not achieved) for the same tranSNPs, we found that TOT-POL values lay in the middle, creating a gradient between the POL-80S and 80S-TOT dAF values, which were instead at the extreme points (**Figure 26**). This further supported the hypothesis that the polysomal and 80S fractions were the furthest apart in terms of dAF, and opened the possibility of the 80S-bound mRNAs being a better proxy for non-translated mRNAs compared to total cytoplasmic mRNAs. The total cytoplasmic mRNAs indeed contain polysomal fractions as well.

Ultimately, data suggested that the comparison between polysome-bound mRNAs and 80S-bound mRNAs could give a higher resolution in tranSNPs identification, thus improving our pipeline.

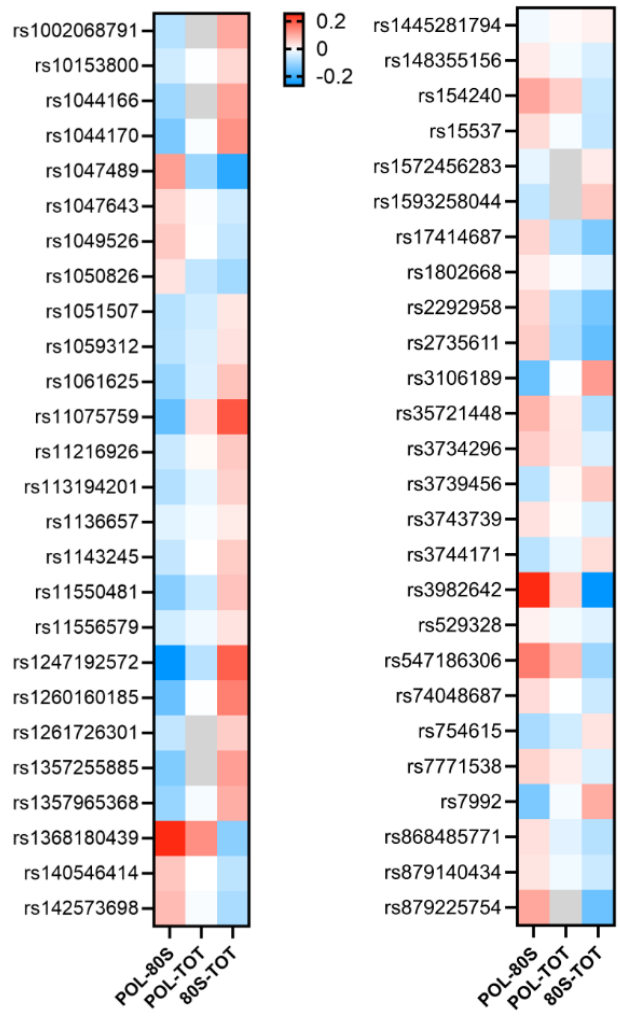

Figure 26. The use of 80S-bound mRNAs may increase the resolution in tranSNPs identification.
Heatmap plotting the delta allelic fraction (dAF) values for significant tranSNPs in the POL-80S and 80S-TOT fractions. The trends of the corresponding POL-TOT values were also plotted.

UTR RPE-1 tranSNPs were validated by luciferase reporter assay

We performed luciferase reporter assays across 5' and 3' UTR tranSNP candidates from all three comparisons. We selected candidates based on the magnitude of imbalance, frequency of the alleles in the population, relevance of the host gene, and concordance of the imbalance with other SNPs *in cis* in the same mRNA. Indeed, the coverage of the RPE-1 dataset enabled the identification of multiple tranSNPs in the same mRNA and the reconstruction of haplotypes. The selected tranSNPs are listed in **Table 1**.

For the 14 candidates, we cloned 109-nucleotide-long fragments of 5' or 3' UTRs containing either the reference or the alternative allele upstream or downstream of a luciferase reporter plasmid. We performed dual luciferase assays, using the Renilla luciferase as a normalizer of

the Firefly luciferase signal first, and then Firefly mRNA levels to normalize the Firefly/Renilla ratios.

SNP Code	Gene Name
rs140546414	ABL1
rs10546414	ARHGAP22
rs12983784	HuR
rs1357255885	PTPN14
rs193226396	CUL3
rs1063181	SPRYD7
rs55899966	TRIB3
rs116895279	ZFP90
rs1404595755; rs796074088; rs1463836962	WASHC1

SNP Code	Gene Name
rs1044631	EML1
rs78686363; rs112437383	UNC119B
rs3737577	S1PR1
rs1061625	TRIM27
rs12984195; rs12984194	POLR1G

Table 1. List of UTR RPE-1 tranSNPs selected for experimental validation.

The list contains the SNP code and the name of the SNP host gene.

Beyond RPE-1 cells, in which this set of tranSNPs was originally identified, we extended the validation to HCT116 cells, as cancer cells are known to have rewired translation machineries (Fernández-Calero et al., 2020) and higher transfection efficiencies. **Figures 27A** and **27B** show that most of the 5' UTR candidates did not exhibit significantly different translation efficiencies in RPE-1 cells, whereas significant differences were observed in HCT116 cells. This is consistent with the fact that oncogenic signaling results in more translationally active cells, which may rely more on the control of the UTRs and other translational features. However, we appreciated significant allele-specific differences among the 3'UTR candidates both in HCT116 and RPE-1 cells (**Figure 27C, 27D**). Notably, we detected a few cases in which the direction of allelic imbalance was opposite in RPE-1 and HCT116 cells, possibly due to the different availability or interaction with trans-factors such as RBPs, miRNAs, or tRNAs.

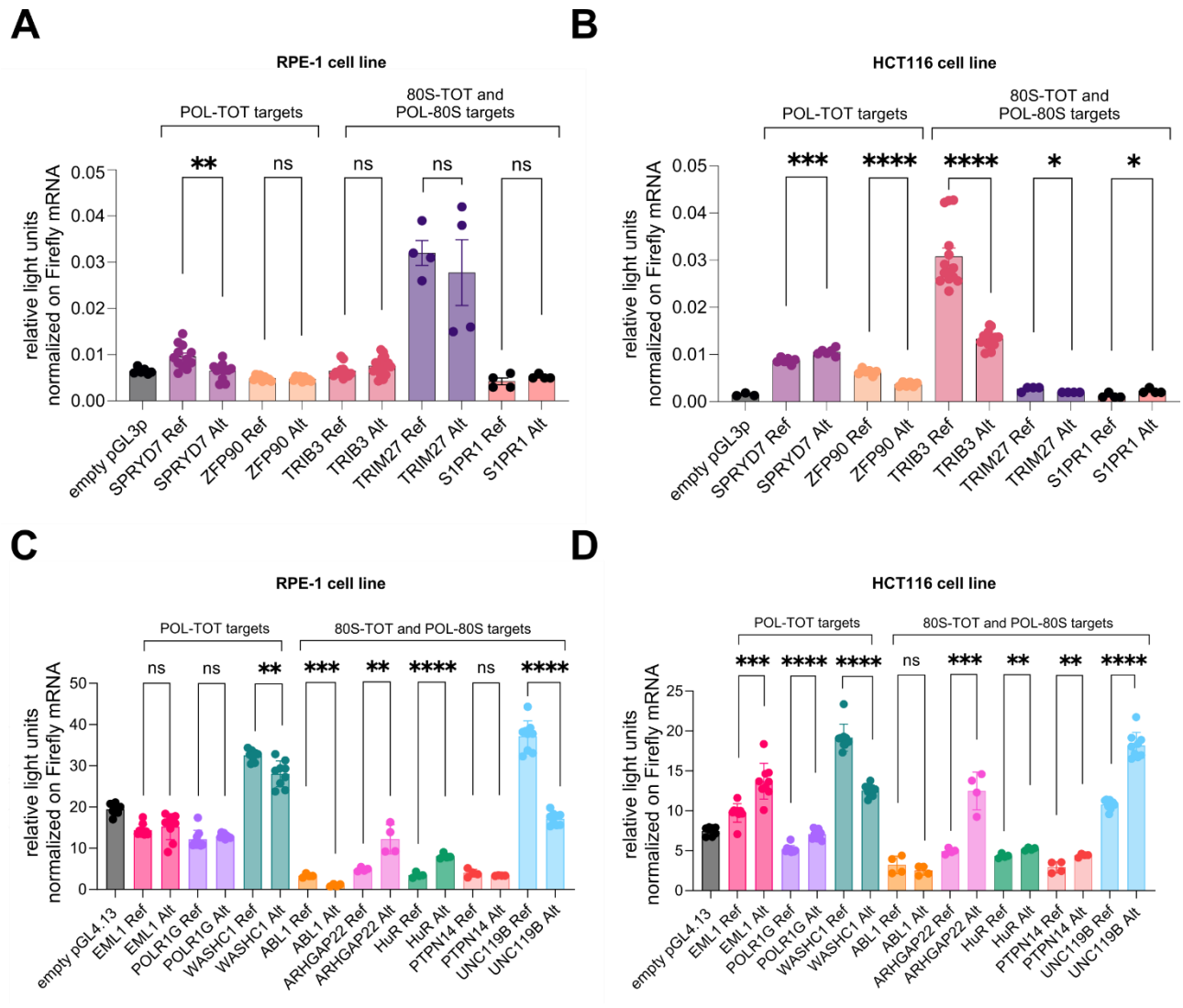

Figure 27. UTR RPE-1 tranSNPs were validated by luciferase reporter assay.

A) Luciferase reporter assay of 5'UTR constructs encompassing candidate tranSNPs in RPE-1 cells. Ns, not significant, **p-value < 0.01, unpaired t-test. **B)** Luciferase reporter assay of 5'UTR constructs encompassing candidate tranSNPs in HCT116 cells. *p-value < 0.05, ***p-value < 0.001, ****p-value < 0.0001, unpaired t-test. **C)** Luciferase reporter assay of 3'UTR constructs encompassing candidate tranSNPs in RPE-1 cells. **p-value < 0.01, ***p-value < 0.001, ****p-value < 0.0001, unpaired t-test. **D)** Luciferase reporter assay of 3'UTR constructs encompassing candidate tranSNPs in HCT116 cells. **p-value < 0.01, ***p-value < 0.001, ****p-value < 0.0001, unpaired t-test.

Coding tranSNPs influence ribosome stalling

We also selected four RPE-1 candidate tranSNPs located in the coding sequence (CDS) (**Table 2**) under the hypothesis that missense or silent changes in the CDS could influence ribosome sliding and stalling on mRNAs, and thus translational pausing (Tsai et al., 2008). We selected candidates based on the magnitude of imbalance, frequency of alleles in the population, host

gene function, and concordance of the imbalance with other tranSNPs in the same mRNA. We also analyzed publicly available RNA-seq data coupled to Ribo-seq data (since ribosome footprints are excluded from the UTRs but not from the CDS) and used them as proxies for total RNA and polysomal RNA, respectively, to independently validate the imbalances observed with our method.

SNP Code	Gene Name
rs2411530; rs373444578	FRG1
rs4656078	GBP3
rs11540407; rs2070162	KRR1
rs1047991	MTPAP

Table 2. List of CDS RPE-1 tranSNPs selected for experimental validation.
The list contains the SNP code and the name of the SNP host gene.

For the 4 candidates, we cloned 109-nucleotide-long fragments of CDS, coding for 33 amino acids and containing either the reference or the alternative SNP allele in ribosome stalling plasmids, which consist of dual fluorescence plasmids characterized by the sequence of interest cloned between a GFP and an mCherry and flanked by two P2A sequences (Kriachkov et al., 2023) (**Figure 28A**). The ribosome stalling plasmids were kindly donated by the Laboratory of Genomic Screening (Dr. Elisa Facen and Prof. Alessandro Provenzani, University of Trento, ITA). Impaired ribosome sliding by the sequence of interest is expected to reduce the mCherry signal, which lies downstream of the cloned sequence and thus the overall mChFP/GFP ratio. The SEC61B sequence, which is known to allow efficient readthrough, was used as a negative control for stalling. A positive control for stalling, containing a sequence coding for a stretch of 17 consecutive lysine residues (polyK), was also used.
The ribosome stalling induced by all the cloned sequences was not severe and comparable to that of the negative control; however, **Figures 28B** and **28C** provided evidence of allele-specific differences in ribosome stalling induced by tranSNPs, with a stronger effect observed in HCT116.

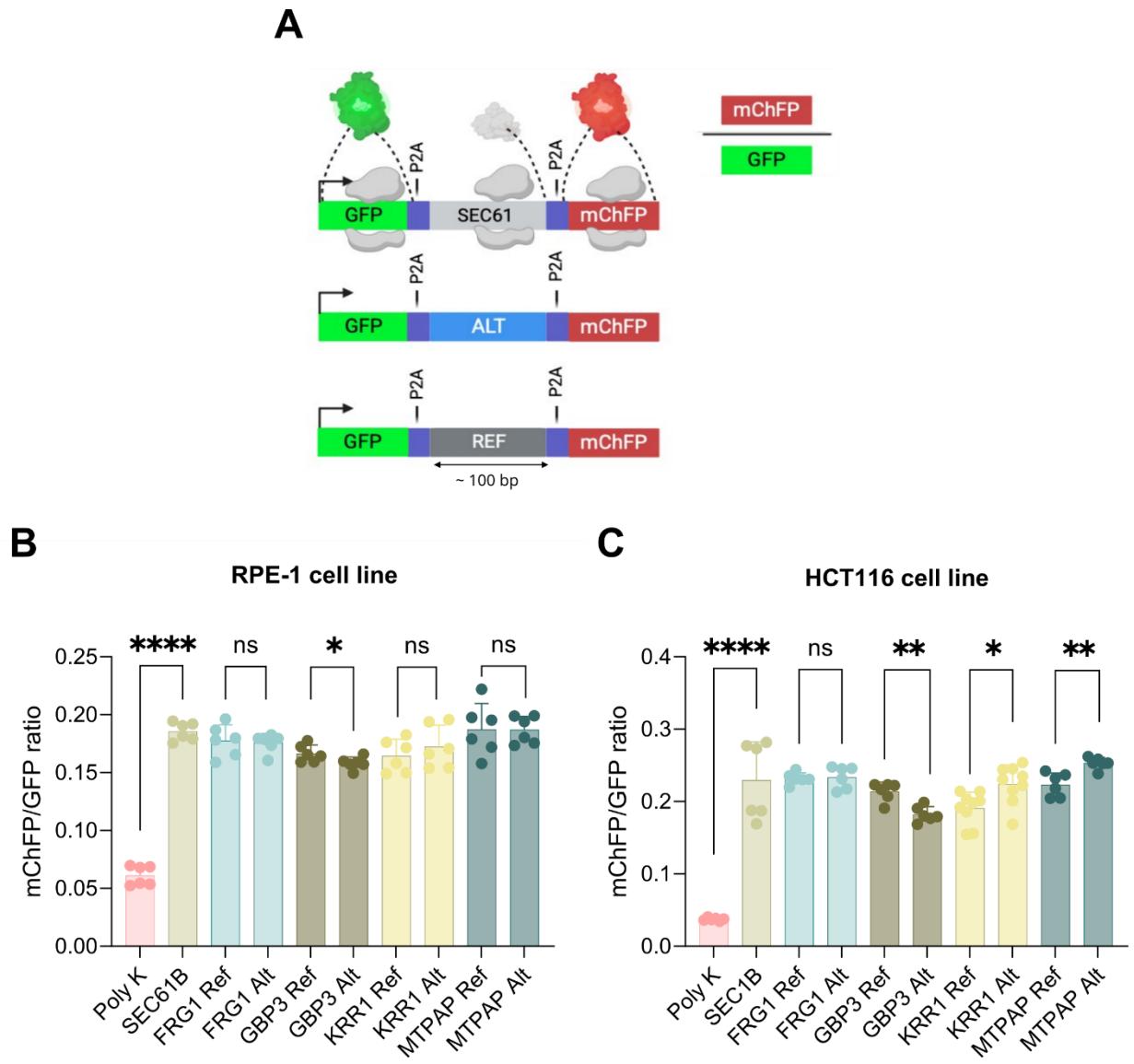

Figure 28. Coding tranSNPs influence ribosome stalling.

A) Schematic representation of the ribosome stalling construct. The cloned sequences of interest (ALT/REF) were flanked by P2A sites to allow ribosome skipping and the cleavage of the three peptides separately from a single mRNA. SEC61B in the ribosome stalling construct was used as a positive control. The ratio between mCherry and GFP signal intensities provides a measure of the efficiency of ribosome scanning on the sequence of interest. mChFP/GFP ratios are reported in **B)** for RPE-1 cells and in **C)** for HCT116 cells. The fluorescence values were obtained using the Operetta High Content System. Data represent the mean ± SD of at least two independent experiments. Ns, not significant, *p-value < 0.05, **p-value < 0.01, ****p-value < 0.0001, unpaired t-test.

Discussion

This study stems from the identification of a novel class of functional SNPs (tranSNPs) by empowering post-transcriptional regulation and sheds light on their mechanistic insights and possible implications in personalized oncology; it provides a comprehensive characterization of tranSNPs through the generation and experimental validation of tranSNPs from the cancer cell line HCT116 and the non-cancer cell line RPE-1. The catalogue generated in HCT116 allowed the description of a specific tranSNP within the cancer-relevant gene DDIT4 and the disclosure of possible mechanisms of action; the catalogue generated in RPE-1 instead provided insights into possible steps to implement the pipeline for tranSNPs identification and demonstrated that tranSNP-mediated regulation is not restricted to cancer cells. Additionally, the study presented preliminary results on instances of cell line specificity among tranSNPs and provided preliminary data on the potential use of the tranSNP genotype as a prognostic marker, supported by evidence of allele-specific vulnerabilities to compounds.

TranSNPs identification pipeline and model generation

Our investigation started with the identification of instances of allelic imbalance between total cytoplasmic mRNAs and polysome-bound mRNAs in the colorectal cancer cell line HCT116. HCT116 cells were particularly suitable for our study since they represent an established model for cancer research, and mostly, because they display a near-diploid genome and are not extremely rearranged or genomically unstable; HCT116 cells are wild type for p53 and harbor the heterozygous KRAS G13D mutation as a major oncogenic driver. However, the calculation of the allelic imbalance through our pipeline should be protected from ploidy issues by the internal normalization between total and polysomal RNA reads in the same cell line.

We established criteria to prioritize candidate tranSNPs for experimental validation and narrowed our analysis to two candidates: rs1053639 (T/A) in DDIT4 3’ UTR and rs137085 (T/C) in POLDIP3 3’ UTR. At this stage, we selected UTR tranSNPs for further validation, reflecting the increasing recognition of the UTRs, which are rich in RBP and miRNA binding sites, as the most important regulatory regions for post-transcriptional control of gene expression. Romo et al., 2024 showed that pathogenic 3' UTR variants annotated in ClinVar are up to 20 times more likely than benign variants to fall in a regulatory site. However, UTRs were neglected for a long time,

given that few experimental and computational tools are available to study the UTRs, and the functional readout of UTR variants is more difficult to detect compared to that of coding variants, since UTRs do not produce proteins differing in the amino acid sequence (Romo et al., 2024; Wieder et al., 2025). However, we think that UTRs might finely and quantitatively modulate the amount of the same protein produced by the two alleles.

The intrinsic structure of the tranSNPs identification pipeline requires the SNPs to be heterozygous, thus limiting the number of tranSNPs potentially identified by our pipeline; however, we thought that the homozygous state would reveal the maximum phenotypic effect. Hence, we exploited CRISPR/Cas9-mediated knock-in to generate homozygous clones at the SNP site and have cellular models to study allele-specific phenotypes.

We encountered cut efficiency limitations for editing rs137085 in POLDIP3, while we successfully obtained homozygous clones for rs1053639 in DDIT4. Editing limitations were possibly due to the poor accessibility of the genomic region because of the elevated GC content and the complex regulatory elements typical of 3' UTR regions. Also, the requirement to edit a very specific genomic location and find a suitable PAM did not allow high flexibility in sgRNA design. The optimal cut occurs 3 nucleotides upstream of the PAM sequence. In the case of DDIT4, rs1053639 coincided with the variable base (N, any base) of the PAM sequence, by being followed by -GG, whereas for POLDIP3, rs137085 was located just downstream of the PAM sequence. While this did not generate mismatches in the sgRNA recognition, the increased distance between the SNP and the cut site may have compromised editing efficiency. We used CRISPR/Cas9-mediated knock-in and administered the Cas9 as a ribonucleoprotein particle (RNP) to reduce the off-target potential; nevertheless, more recently, novel technologies such as base editing and prime editing were developed for improving editing efficiency and precision (Kantor et al., 2020) and it might be interesting to use them to generate precise editing, as for rescuing the editing of single-nucleotide variants.

However, at this stage and to overcome the editing limitations of our method, including possible off-target effects, we considered at least two edited clones for each genotype in most of our analyses. We did not perform a comprehensive analysis of potential off-target sites, nor we sequenced the entire DDIT4 coding sequence beyond the 3' UTR. However, since we observed consistent results across multiple edited clones for each genotype, both in terms of cellular phenotypes and DDIT4 protein levels (**Appendix Figure 1**), we believe that the impact

of potential off-target alterations on the observed allele-specific phenotypes might be limited. **Figure 10** also supports that the clonal background has a negligible impact on the observed phenotypes.

Allele-specific DDIT4 protein levels and RBMX binding

We observed significantly different steady-state DDIT4 protein levels across TT and AA rs1053639 clones. We confirmed that DDIT4 mRNA and protein are short-lived as widely described in the literature (Katiyar et al., 2009; Kimball et al., 2008), but we did not find significant allele-specific differences in protein and mRNA stability and mRNA levels. We also assessed global protein synthesis rates across TT and AA clones to exclude that the higher DDIT4 protein levels in TT clones were the result of a broader increase in translation efficiency, instead of a specific effect on DDIT4 translation. Since the UTRs are extensively bound by regulatory elements such as RBPs and miRNAs (Mayr, 2019) we next interrogated *in silico* predictors for allele-specific binding of RBPs based on their described binding motifs. Such analyses identified RBMX, YBX1, and ACO1 as candidate RBPs differentially binding to the rs1053639 alleles. We focused our attention on RBMX; however, we cannot exclude that beyond RBMX, other RBPs or other regulatory elements, such as miRNAs, may contribute to modulating DDIT4 protein levels. We initially employed RNA electromobility shift assays (REMSA) to dig into the interaction of RBMX with DDIT4 mRNA from the biochemical point of view; however, the limited sensitivity of this technique forced us to use high concentrations of RNA to visualize the RNA-protein complex. At the same time, insufficient protein concentration prevented binding saturation and equilibrium, which is required to calculate the dissociation constant (Kd) (Jarmoskaite et al., 2020). Consequently, we could not obtain a robust quantification, but qualitative, preliminary indications of differential binding. We next attempted to perform RNA immunoprecipitation (RIP) in the heterozygous (T/A) HCT116 cells to measure the relative enrichment of the two alleles in their native context. However, we could not obtain allele-specific primers for PCR or qPCR; we therefore subjected RIP samples to Sanger sequencing, but the approach was not sufficiently sensitive to detect subtle differences. We ultimately confirmed the differential RBMX binding by RIP-qPCR in both cross-linked and non-cross-linked total lysates of TT and AA clones, confirming the preferential binding with the T allele of DDIT4 mRNA.

How a 3' UTR tranSNP in DDIT4 can affect DDIT4 protein output

To gain mechanistic insights on how a SNP in the 3' UTR can affect protein levels, and since RBMX is primarily located in the nucleus, we assessed DDIT4 mRNA localization. We found that DDIT4 mRNA was significantly more enriched in the cytoplasm than in the nucleus in the TT compared to the AA clones. **Allele-specific mRNA localization** may represent one possible mechanism to explain the observed allele-specific protein levels, since translation occurs in the cytoplasm; however, siRNA-mediated depletion of RBMX did not support a key role for RBMX in regulating this phenotype. A possible limitation of our silencing approach is that RBMX is a very abundant and essential RNA-binding protein, and we could not reduce its levels more than 50% in this set of experiments. Furthermore, this subcellular localization mechanism, although intriguing and apparent, cannot fully explain the observed allelic imbalance since the imbalance between polysome-bound mRNAs and total cytoplasmic mRNAs should only provide insights about differences in subcytoplasmic localizations.

We next accounted for the role of RBMX as an m6A reader; we predicted several high-confidence m6A sites in proximity of the SNP position, and measured m6A enrichment across TT and AA clones by meRIP-qPCR; TT clones exhibited significantly higher enrichment of m6A on a SNP-containing fragment of DDIT4 mRNA. Interestingly, the subcellular localization of DDIT4 mRNA in TT clones was significantly affected by the inhibition of the m6A writer METTL3. Unexpectedly, however, this perturbation did not reduce, but rather amplified, the allele-specific differences in DDIT4 mRNA localization and DDIT4 protein levels. Based on the results of these experiments aimed at aligning the m6A levels across TT and AA clones, we interpreted that allele-specific m6A levels are unlikely to be responsible for allele-specific DDIT4 protein levels. Nevertheless, an important limitation of this approach is that the widespread inhibition of METTL3 cannot be considered fully equivalent to the specific modulation of selected m6A sites around the SNP, which are slightly differentially m6A-modified among the TT and AA clones according to meRIP-qCPR. Moreover, the global removal of m6A by STC-15 was strongly associated with the activation of the innate interferon (IFN) immune response in response to the m6A-naked mRNAs accumulating as double-stranded RNAs (dsRNAs) (Guirguis et al., 2023). This data is strongly accepted and claimed since STC-15 is currently evaluated in clinical trials and has even been administered in combination with PD-1 inhibitors for its ability to trigger the IFN response and transform the tumor microenvironment (TME) from

immunosuppressive to immunostimulatory. Hence, more targeted experiments would be necessary to claim that **allele-specific m6A levels**, and not allele-specific response to stress or activation of the innate immunity pathway, are responsible for the observed phenotypes attributed to METTL3 inhibition and ultimately allele-specific DDIT4 protein levels. However, there are no documented links between DDIT4 and the activation or regulation of the innate immune response to date.

Although we were still unable to envision the contribution of the allele-specific RBMX binding on DDIT4 protein levels via mRNA localization or modification, we strikingly observed that depleting RBMX resulted in significantly reduced DDIT4 protein levels in TT clones, which dropped to comparable levels to the AA clones in a sort of "rescue" experiment, whereas the levels in AA clones were unaffected. This observation suggested a possible **direct role for RBMX on mRNA translation**, consistent with the differences in subcytoplasmic localizations or polysomal loading directly suggested by our tranSNP-identifying pipeline. Interestingly, we found that RBMX, although predominantly nuclear, can associate with ribosomes and polysomes similarly to a ribosomal protein. To date, the roles of RBMX have been primarily related to transcription and splicing. Siachisumo et al., 2024b described that RBMX can maintain the correct splicing, especially of a class of ultra-long exons, through cryptic splice site repression. The last exon of DDIT4 is an ultra-long exon (>1 kbp), and we found a possible AG-rich RBMX binding site at a cryptic splice site, but **Figure 9E** eliminates the possibility of splicing-related allele-specific RBMX regulation. Only Zuccotti et al., 2020 suggested a possible role for RBMX in translation, although with an artificial construct, and by mining RAPIDASH data to uncover ribosome-associated proteins (RAP), RBMX scored high as a RAP candidate (Susanto et al., 2024); we thus provided novel evidence supporting a role in translation for the cytoplasmic RBMX in the endogenous context. We proposed that RBMX contributes to the allele-specific regulation of DDIT4 protein levels by directly guiding to the polysomes the mRNA derived from the allele which it preferentially binds, increasing its polysomal targeting, loading, translation efficiency, and ultimately protein levels; it is indeed established that RNA-binding proteins determine the fate of their target mRNAs from the moment in which the mRNAs leave the RNA polymerase machinery to when they reach the polysomes, and hnRNP proteins, such as RBMX (also known as hnRNP G) are believed to be among the first factors to bind the nascent transcripts (Neriec and Percipalle, 2018). Similar

mechanisms have been described for other RBPs, including HuR, Staufen, and FMRP, whose association with polysomes has been correlated with either increased mRNA translation or targeting into translationally silenced complexes, as in the case of FMRP (Bergalet et al., 2011; Gallouzi et al., 2000; Kurosaki et al., 2025). It is also possible that RBMX cooperates with other RBPs, forming complexes to target mRNAs to specific subcellular or subcytoplasmic locations. Interestingly, Zuccotti et al., 2020 performed a gene ontology enrichment analysis of protein interactors of RBMX retrieved by STRING and other public databases. RBM3, FXR2, KHDRBS1, CIRBP, and AUF1 were reported among the RBMX interactors, concluding that RBMX is associated with positive regulators of translation. Interestingly, most of the listed RBMX interactors are prevalently nuclear RBPs known to migrate to the cytoplasm to regulate translation, particularly under stress conditions. RBM3, a translation regulatory protein, was reported to migrate to the cytoplasm to bind the 60S subunit, especially during cold stress (Dresios et al., 2005). The association of HuR with polysomes has also been reported to be dynamic, depending on cellular conditions and stimuli. Hence, we cannot exclude that in stress conditions, RBMX could migrate to the cytoplasm to a greater extent and increase the targeting of T allele DDIT4 mRNAs to the polysomes, thus amplifying the effect that we already observed on translation. However, thapsigargin treatment (100 nM, for 4 hours) was insufficient to induce a massive translocation of RBMX to the cytoplasm and was also dominant over RBMX depletion in modulating DDIT4 protein levels.

Conversely, we suggested that when RBMX was poorly bound, DDIT4 mRNA was not directly targeted to the polysomes, since we observed its accumulation into cytoplasmic spots correlating with lower DDIT4 protein levels. The subcytoplasmic location of translation is important to control protein output (Horste et al., 2023) and motivated us to further investigate the nature of DDIT4 mRNA spots. Transcriptome-wide studies of stress granules (SGs) did not detect a strong association of DDIT4 mRNA with SGs: about 7% of DDIT4 mRNA molecules were associated with SGs induced by sodium arsenite in U2OS cells (Khong et al., 2017; Matheny et al., 2021, 2019). Also, subcytoplasmic maps developed by Horste et al., 2023 in HEK293 proposed that DDIT4 mRNA was equally distributed among TIS granules (enriched in the RBP TIS11B and where generally low-abundance proteins are translated), the endoplasmic reticulum (ER), and the soluble part of the cytoplasm. We also experimentally interrogated co-localization of DDIT4 mRNA with the self-aggregating RBP TIAR-1, which is predominantly

nuclear and moves to the cytoplasm upon stress to transiently inhibit translation by promoting the formation of translationally silent stress granules (Mazan-Mamczarz et al., 2006). However, we did not detect co-localization, at least under ER stress, with either TIAR-1 or G3BP1. Given the perinuclear localization of DDIT4 mRNA and the localization of TIS granules close to the ER, it would be interesting to test their colocalization with DDIT4 mRNA as well. Although the applied stress might have been too mild (100 nM thapsigargin, for 4 hours) to observe the typical G3BP1 granules, we still observed the DDIT4 mRNA spots, which suggested that DDIT4 mRNA localizes to a granule type that is distinct from the classical SGs. Notably, Neriec and Percipalle, 2018 reported that upon nuclear export, translationally repressed complexes of mRNAs bound to RBPs (ribonucleoparticles; RNPs) assembled into larger granules, named cytoplasmic transport granules, to be transported to specific cellular locations for storage or for translation; transport granules were proposed to generate from the homo-dimerization of RNA-bound hnRNPs and actin polymerization and contain only one type of mRNA and a specific set of RBPs (Sinnamon et al., 2012), which might correspond to the cytoplasmic DDIT4 spots we observed.

RBMX modulation may be beneficial to cancer patients based on the rs1053639 genotype

The evidence that allele-specific DDIT4 protein levels are at least in part regulated by the trans-factor RBMX poses RBMX as a potential actionable target for cancer patients stratified for the rs1053639 genotype. Indeed, based on our data, modulating RBMX levels could be relevant in TT patients, whereas the same approach is unlikely to be effective in AA patients, who appear insensitive to RBMX-dependent regulation.

Up to date, there is no evidence of pharmacological targeting of RBMX in the cancer field (https://depmap.org); drugging RNA-binding proteins in general is not very common because RBPs often lack defined, druggable pockets. Moreover, RBPs are often pleiotropic and part of big complexes that regulate complex protein-RNA interactions, making it difficult to achieve specific, targeted effects (Bertoldo et al., 2023).

However, RBMX is aberrantly expressed in multiple tumor types, such as esophageal cancer and metastatic bladder cancer, and is associated with tumor invasion, metastasis, and prognosis (Sheng et al., 2024; Tuersun et al., 2023a; Yan et al., 2021a). RBMX expression was found significantly higher in osteosarcoma and esophageal cancer tissues compared to the adjacent normal tissues, and the overall survival of esophageal cancer patients with high RBMX expression was significantly lower than that of patients with low RBMX expression (Tuersun et

al., 2023b). In the same tumor, RBMX underwent copy number amplification, mutation, and deep deletion, indicating that both its amount and function are perturbed in cancer. Furthermore, RBMX expression was positively correlated with the levels of follicular helper T cells, eosinophils, and initial B cells. Two additional and independent studies proposed a role for RBMX in mediating the immunosuppressive tumor microenvironment by reducing immune cell infiltration and proposed that inhibiting RBMX may help tumors to respond to immunotherapy (Qiu et al., 2025; Sheng et al., 2024). When RBMX was depleted, the recruitment and proportion of CD8+ T cells significantly increased via the downregulation of H2-K1 and upregulation of THBS1; co-culture experiments confirmed that RBMX depletion significantly enhanced the cytotoxic activity of CD8+ T cells. Instead, other studies in metastatic bladder cancer patients showed that RBMX expression negatively correlated with tumor stage, histological grade, and poor prognosis (Yan et al., 2021b).

Allele-specific DDIT4 protein levels determine allele-specific cancer-related phenotypes

Since DDIT4 is a recognized inhibitor of mTORC1 (Foltyn et al., 2019), which is a central hub of cancer metabolism, we expected differences in the ability of rs1053639 clones to support specific cancer-related functions, such as proliferation, or to cope with changing environmental conditions. Indeed, the mTOR protein can form two complexes, mTORC1 and mTORC2, which are composed of discrete protein binding partners and different functions; while mTORC1 promotes cell growth, proliferation and biosynthesis in response to nutrients, mTORC2 regulates cell survival, metabolism, and cytoskeletal organization mainly in response to growth factors (Jhanwar-Uniyal et al., 2019; Montero et al., 2012).

We expected lower activity of mTORC1 in TT clones in basal conditions, as TT clones exhibit significantly higher protein levels of the mTORC1 inhibitor DDIT4, but we observed the opposite phenotype. This result might be ascribed to cell adaptation through feedback loops that compensate for chronically higher DDIT4 protein levels or to basal DDIT4 levels. Indeed, we then confirmed that upon acute DDIT4 induction by thapsigargin treatment, TT clones inhibited mTORC1 more effectively than the AA clones, as expected (**Figure 18 A, 18B, Appendix Figure 1B**).

Similarly, we did not observe significant differences in the proliferation rate of TT and AA clones for up to 3 days in basal conditions, but we did observe allele-specific differences in the

percentage of live cells upon thapsigargin treatment, which might indicate different abilities to cope with cellular stress.

We thought that longer time points and more stressful conditions may engage the mTOR pathway more strongly, revealing differences in proliferation; indeed, there is evidence that during mouse embryonic development, cells can sense the fitness of the neighboring cells and trigger p53 to repress mTOR in the less fit to be eliminated, thus outcompeting them (Bowling et al., 2018). Thus, we co-cultured TT and AA EGFP-labelled clones to introduce an extra trigger, and for a period of 15 days. Interestingly, we found fluctuations in the cellular fitness of the clones, eventually favoring the AA clones, which are consistent with fluctuating DDIT4 and mTORC1 levels. We attempted to assess DDIT4 protein levels and mTORC1 activation markers at various time points during the co-culture by FACS sorting, but insufficient material was recovered to perform the subsequent Western Blot analyses.

Further insights into cell competition were obtained by injecting TT and AA clones separately into Zebrafish larvae and evaluating their interactions with multiple host cell types for 3 days, assuming that the extra triggers of the *in vivo* setting would accelerate the process of cell competition and require a shorter time point; this set of experiments confirmed the higher proliferative potential of AA clones under prolonged stress conditions, or in the presence of additional cell types.

Overall, these findings are also consistent with the observed allele-specific differences in the autophagic flux, which favored the TT clones. An increased autophagic flux is indeed likely a consequence of higher DDIT4 protein levels and more effective mTORC1 inhibition, but mTOR-independent autophagy has also been described. The RNA-binding protein RBM33 modulates DDIT4 mRNA stability via m6A to eventually impact DDIT4/TXNIP-based autophagy (Yu et al., 2023); RBMX also directly affects TXNIP transcription (Shin et al., 2008b), suggesting that RBMX binding to DDIT4 mRNA might be part of an upstream signaling pathway aimed at ultimately regulating autophagy. Despite the activation route, autophagy can represent an advantage by clearing damaged organelles and protecting TT clones from oxidative stress, genomic instability, and chronic inflammation in the short term (Sun et al., 2013). However, the double-edged role of autophagy may be the cause for the AA clones outcompeting the TT clones when co-cultured for 15 days. It has been described that while moderate autophagy can support survival, excessive autophagy can lead to cell death and limit tumor growth (Maiuri et al., 2007). Also, autophagy inherently demands energy supply (Mandic et al., 2024; Mijaljica et al., 2011;

Plomp et al., 1989), and the TT clones may end up with poor resources for growth and for autophagy itself in the long term, whereas the AA clones, which cannot effectively inhibit mTOR, may become metabolically advantaged and have the possibility to outcompete. Additionally, recent studies highlighted the role of autophagy in regulating metabolism within the tumor microenvironment, proposing that cells with active autophagy can release metabolites or signaling molecules that the defective ones can exploit (Lahiri et al., 2019; P. Zhang et al., 2023).

Germline variants may shape the trajectory of cancer evolution and inform patient stratification

Our phenotypic data collectively demonstrated that the germline rs1053639 variant influenced the rewiring of the mTOR pathway and relevant cancer-related phenotypes. While we acknowledge that cancer evolution trajectories do not generally stem from one single mutation or polymorphism but from the cooperation between multiple genetic and environmental events, we definitely think that rs1053639 can contribute to shaping cancer evolution trajectories by modulating key somatic regulatory pathways, such as mTOR and the cellular stress response.

Pan-cancer analyses using TCGA data did not highlight a differential representation of TT or AA patients in the cancer population compared to the non-cancer population; however, given the double-edged role of DDIT4 in cancer, it would be more accurate to consider each cancer type separately, which was not possible due to the small sample size. The same analyses highlighted that tumors from patients with the TT genotype showed a wide dysregulation of genes related to the Wnt, TGF-β, and MYC pathways, while such alterations were less prevalent in AA patients. Based on our experimental findings, particularly the co-culture and the *in vivo* assays, we propose that the genetic background of AA patients may be intrinsically more permissive to tumor-related events and therefore may not require extensive rewiring of major signaling pathways.

This germline-somatic interplay led us to hypothesize that TT and AA clones may display differential vulnerability to compounds based on their different evolutionary trajectory related to mTOR and stress response. We selected a list of FDA-approved and investigational compounds to test this hypothesis. We first assessed the sensitivity to niclosamide, which is a negative modulator of mTORC1, NF-kB, STAT3, and Wnt signaling approved by the FDA as an anthelmintic drug to treat parasitic infections (Chen et al., 2018). Notably, as mTORC1 has been

reported to inhibit DDIT4 through a negative feedback loop, STAT3 has also been described as a transcriptional repressor of DDIT4 (Garcia-Segura and Malagelada, 2023; Katiyar et al., 2009); therefore, this treatment may strongly derepress DDIT4 expression. Given the enrichment of Wnt pathway dysregulation in TT patients, we further tested XAV939, a tankyrase (TNKS1/2) inhibitor that stabilizes axin and promotes β-catenin degradation (Huang et al., 2009), and WNT-C59, which is a potent inhibitor of porcupine (PORCN), a membrane-bound O-acyltransferase required for palmitoylation, secretion, and the biological activity of Wnt (Motono et al., 2016). However, we could not appreciate allele-specific differences in sensitivity due to the extremely low potency of the compounds in our cellular models. We next tested everolimus, which is an allosteric inhibitor of mTOR used as an immunosuppressant to prevent the rejection of organ transplants, but also approved to treat advanced breast cancer, neuroendocrine tumors, and advanced renal cell carcinoma (Hasskarl, 2018). We also tested the TGF-β inhibitor A-83-01, which is a potent inhibitor of TGF-β type I receptor ALK5 kinase (Tojo et al., 2005), but its potency was very limited across our cellular models. To target the MYC pathway, we employed the peptide Omomyc, a selective MYC inhibitor. Omomyc forms a heterodimer with MAX, hindering MYC binding to E-box sequences on DNA and thereby reducing its full activation and transcription of genes involved in cell growth and proliferation (Savino et al., 2011). In addition, we tested the susceptibility to Nutlin, which inhibits MDM2 to stabilize the tumor suppressor p53 (Tovar et al., 2006; Vassilev et al., 2004), and the autophagy inhibitor chloroquine (CQ). TT clones were significantly more resistant to the tested compounds than the AA clones. Interestingly, recent data proposed that cells resistant to PI3K inhibitors can be resensitized through the constitutive activation of mTORC1, which suppresses the induction of autophagy, leading to energy stress, a critical depletion of aspartate, and cell death (Gremke et al., 2025). The constitutive activation of mTORC1 is a feature of the AA clones and is associated with their lower DDIT4 protein levels. Hence, DDIT4-dependent mTORC1 rewiring in AA clones may reflect their increased sensitivity to most of the tested treatments.

Overall, these findings, together with the prognostic value of rs1053639 in terms of DFI, suggest that stratification of cancer patients based on rs1053639 genotype may help guide therapeutic decision-making by identifying treatments to which patients are more likely to respond, while sparing them from ineffective interventions and posing rs1053639 as an interesting cancer

biomarker for targeted therapy and prognosis, but not for cancer risk; indeed, the rs1053639 did not appear as a hit in any GWAS study to date.

Exploring the cell line specificity of tranSNPs

We began interrogating the cell line specificity of rs1053639 by assessing the translation efficiency of the two alleles in another cancer and a non-cancer cell line using the luciferase reporter assay. Interestingly, in both cases, we confirmed higher translation efficiency for the T allele. By interrogating the Cancer Cell Line Encyclopedia (CCLE)/DepMap and CLISGen (Cell Lines SNP Genotypes), we found examples of cancer cell lines with the AA genotype for rs1053639 that nevertheless exhibited high DDIT4 protein levels (OSRC2 renal cell carcinoma and C32 melanoma cell lines), but they also exhibited high DDIT4 protein levels. Notably, the cell lines harboring higher DDIT4 protein levels and lower DDIT4 mRNA levels were predominantly homozygous for the T allele (769P renal cell carcinoma, WM793 melanoma, and SW620 colorectal adenocarcinoma cell lines).

It is therefore possible, and not surprising, that the trans-factor levels play a synergistic role with the tranSNP genotype in eventually determining protein levels. While we mostly studied epithelial cell lines (HCT116, RPE-1, A549), different tissues may exhibit different levels or types of trans-factors and therefore opposite translational potential of the T allele. A larger and integrated study would be needed to generalize the cell line specificity of rs1053639 and other tranSNPs and elucidate the dependency of genetic variants on trans-factors.

In this regard, the online tool RegVar (https://regvar.omic.tech) integrates the sequence, epigenetic, and evolutionary information of SNPs across 17 human tissues to give tissue-specific predictions of regulatory probabilities. Interestingly, the highest regulatory score for rs1053639 was detected in the sigmoid colon (0.37), followed by 0.28 in the lung and 0.27 in the pancreas and whole blood. The lowest value was 0.056 in the anterior cortex. It would be interesting to generate a score-based platform incorporating the allelic imbalance, the levels of the predicted trans-factors insisting on that site, luciferase data, and survival data, to predict the protein output of the alleles. However, the combinatorial complexity of the number of potential trans-factors and their interactions makes such predictions challenging. We are currently producing a fourth catalogue of tranSNPs in the pancreatic adenocarcinoma cell line Mia-PaCa-2 to shed more light on the context-dependent properties of tranSNPs.

Notably, we did not find tranSNPs in common across all three of our available catalogues, likely because of the requirements for heterozygosity, the analyzability thresholds in the different datasets, and the absence of common functional ontologies among tranSNPs. We only found one tranSNP host gene shared among the HCT116 and RPE-1 tranSNPs, which is KRR1, which is involved in ribosomal RNA (rRNA) processing in Saccharomyces cerevisiae and is the first precursor of the small eukaryotic ribosomal subunit (Gromadka and Rytka, 2000; Singh et al., 2021).

The use of 80S-bound mRNAs may improve the resolution in tranSNPs identification

Our RPE-1 dataset provided evidence that the 80S-bound mRNAs may represent the less-translated fraction in RPE-1 and may improve resolution in tranSNPs identification. However, luciferase reporter assays performed in RPE-1 and HCT116 to validate UTR tranSNPs from the RPE-1 dataset revealed that this observation may be cell-line specific. Indeed, the tranSNPs identified through the comparison with the 80S were not necessarily better validated in HCT116 compared to the ones identified through the comparison with the total cytoplasmic mRNA.
This is not surprising as the translational potential of the 80S monosome is still very debated in the field, and recent evidence suggested that it can be highly tissue-dependent, at least in Drosophila melanogaster (Blandy et al., 2025b), complicating the use of 80S-bound mRNAs as a proxy for untranslated mRNAs and opposed to the polysome-bound mRNAs in an absolute sense in any cell line. Interestingly, 80S monosomes appeared to be translationally active in the head and embryo, where translation regulation needs fine regulation (with extensive use of TOP mRNAs, upstream ORFs), whereas they appeared to be inactive in the testis and ovary, where polysomes were the major source of protein synthesis. This observation may help predict the translational potential of the 80S based on the translational regulation demand.

Interpreting the ribosome stalling assay

We acknowledge that performing the ribosome stalling assay on a restricted portion of the entire CDS may not be fully representative; however, this approach allows us to focus more specifically on the effect of the SNP itself. Moreover, recent data from our laboratory showed that comparable results were obtained when cloning either a SNP-containing fragment of 33 amino acids or the entire CDS of the EIF4H protein in the same ribosome stalling plasmid (Hamadou, Alunno, Peroni et al., 2025a).

Nonetheless, a critical aspect of the ribosome stalling assay, as well as of the principle underlying our tranSNPs-identifying pipeline, is the distinction between translationally active and inactive mRNAs within polysome-bound fractions. Indeed, while engagement with polysomes is generally considered a proxy for active translation, the number of ribosomes per mRNA does not necessarily reflect translation efficiency, as it may also reflect ribosome aggregation due to stalling. To overcome this ambiguity, it would be ideal to separately analyze the individual fractions originated upon polysome profiling, although it may be difficult to extract sufficient mRNA for RNA-seq. As an alternative, polysome fractions could be subdivided into light and heavy polysomes, considering the light as a proxy for the actively translating mRNAs and the heavy as potentially stalled ones. Based on this notion, the result of the ribosome stalling assay cannot be interpreted univocally and must be carefully evaluated.
In parallel to the investigation of ribosome stalling as a mechanism of action for missense and silent coding tranSNPs, we hypothesize that silent tranSNPs may cause different protein levels by codon usage, which is the preferential use of one codon codifying for the same amino acid, and ends up regulating the speed of translation elongation (Liu, 2020).

Conclusions and Future Perspectives

Overall, this study provides a comprehensive characterization of a novel class of functional SNPs, named tranSNPs, identified in the same laboratory by leveraging the renewed awareness of post-transcriptional events in regulating gene expression. Through our investigation, we proposed novel strategies to improve the tranSNP-identifying pipeline, we explored the cancer-type specificity of tranSNPs, and the possibility of identifying tranSNPs in non-cancer settings. Beyond the global investigation of the phenomenon, we focused on the rs1053639 tranSNP in the 3' UTR of DDIT4 to gather mechanistic insights. We uncovered mechanistic links related to mRNA localization, modification, and polysome loading mediated at least in part by the allele-specific binding of the RNA-binding protein RBMX to the rs1053639 T/A alleles. All mechanisms converged on higher protein output from the T allele compared to the A allele, which ultimately influenced downstream phenotypes such as mTORC1 inhibition, autophagy, and proliferation during *in vitro* co-culture and *in vivo* xenotransplants in Zebrafish embryos. We also identified allele-specific sensitivities to FDA-approved and investigational compounds, and prognostic relevance for disease-free interval in a TCGA cohort for the rs1053639. When further explored, the rs1053639 and tranSNPs in general could become an original source of SNPs to be used as biomarkers for prognosis or for informed targeted therapy.

Since DDIT4 lies at the intersection of major cellular pathways, many avenues can still be explored when studying rs1053639.

Firstly, it would be interesting to exploit novel genome editing technologies to **implement the generation of edited homozygous cellular models,** such as prime editing, base editing, or designing alternative allele-specific sgRNAs to minimize re-cutting during CRISPR/Cas9-mediated knock-in.

From a mechanistic point of view and given the role of RBMX and the allele-specific susceptibility to nutlin treatment, it would be interesting to study how rs1053639 affects the **DNA damage response** (DDR) and whether TT and AA clones exhibit different levels of genomic instability. Indeed, both RBMX and DDIT4 operate at the interface of the DDR, and their interaction, beyond the regulation of autophagy, may serve to regulate the response to DNA damage as well. It would also be interesting to study whether the **RBMX binding affinity** changes upon DDIT4-modulating treatments.

Also, **pull-down** of labelled DDIT4 T or A mRNA probes with cellular lysates coupled to mass spectrometry experiments may discover novel allele-specific interactors, which may point to additional mechanisms such as alternative polyadenylation, miRNA binding, alterations of uORFs, or RNA secondary structures.

Moreover, it would be valuable to better characterize the contribution of **thapsigargin** treatment to post-transcriptional regulation independently of its transcriptional effects, since polysome profiling and western blot data clearly showed an effect on polysomal distribution irrespective of the mRNA levels, and an amplification of the differences from mock to thapsigargin-treated DDIT4 protein levels.

From a phenotypic point of view, it would be interesting to perform additional assays to zoom in on the apparently higher aggressiveness of the AA clones, which overgrew *in vitro* and *in vivo* under certain conditions. **Clonogenic assays**, tests of resistance to **contact inhibition**, and **longer timepoints in the in vivo experiments** could help study their metastatic potential.

Other stressors, such as hypoxia or nutrient deprivation, may also be used to induce DDIT4 and study additional cellular phenotypes.

Finally, from a clinical point of view, it would be useful to strengthen **clinical collaborations** and generate a local cohort of colorectal cancer samples of sufficient sample size to ensure statistical power. This would allow robust correlations between DDIT4 protein levels and prognosis first, and possibly also with RBMX protein levels.

Materials and Methods

Cell culture

The human colorectal cancer cell line HCT116 was purchased from the Biological Resource Center ICLC Cell bank. Cells were cultured in standard Roswell Park Memorial Institute (RPMI) 1640 medium (GIBCO) supplemented with 10% fetal bovine serum (FBS), 100 units/ml penicillin, 100 mg/ml streptomycin antibiotic mix (GIBCO), and 1% L-Glutamine (GIBCO). The human lung cancer cell line A549 was cultured in Dulbecco's Modified Eagle Medium and Ham's F12 (DMEM/F12) supplemented with 10% fetal bovine serum (FBS), 100 units/ml penicillin, 100 mg/ml streptomycin antibiotic mix (GIBCO), and 1% L-Glutamine (GIBCO). The human non-cancer cell line of retinal pigmental epithelia RPE-1 was cultured in Dulbecco's Modified Eagle Medium and Ham's F12 (DMEM/F12) supplemented with 10% fetal bovine serum (FBS), 100 units/ml penicillin, 100 mg/ml streptomycin antibiotic mix (GIBCO), and 1% L-Glutamine (GIBCO). The cells were maintained in a humidified atmosphere at 37°C and 5% CO2. Cells were split twice a week.

RNA extraction

RNA was extracted using TRIzol™ Reagent (Invitrogen) or NucleoSpin® RNA (Macherey-Nagel) according to the manufacturer's instructions and depending on the downstream analyses. Total RNA was extracted using the NucleoSpin® RNA, whereas cytoplasmic RNA was extracted using TRIzol™. RNA purity and concentration were assessed by NanoDrop™ Spectrophotometer (Thermo Fisher Scientific).

cDNA and RT-qPCR

RNA was retrotranscribed using the RevertAid First Strand cDNA Synthesis Kit (Thermo Fisher Scientific) and random hexamer primers according to the manufacturer's instructions. One µg of RNA was retrotranscribed for most applications; exceptions will be discussed on a case-by-case basis. The cDNA was diluted 1:8 in water, equivalent to a final concentration of 6.25 ng/µl. RT-qPCR was performed using the PowerUp SYBR mix (Applied Biosystems) in 10 µl, using 12.5 ng of cDNA as input and 0.4 µM of each primer. Primers were designed using Primer Blast (NCBI) and are listed in **Table 5**. The QuantStudio5 instrument was used to amplify the cDNA and measure gene expression. Technical triplicates were performed, and average Cq values were normalized to housekeeping genes (dCt) and to controls (ddCt) when possible.

Protein extraction and Western Blot

Adherent cells were detached with trypsin and centrifuged at 300 *g* for 5 minutes. The pellet was washed once with PBS 1X. Total protein extraction was performed using RIPA lysis buffer 1X (50 mM Tris-HCl, pH 8, 150 mM NaCl, 1% Igepal, 0.5% Sodium Deoxycholate, 0.1% Sodium Dodecyl Sulfate) supplemented with cOmplete™ Mini protease inhibitors (Roche) and phosphatase inhibitors cocktail I (MedChemExpress).

RIPA buffer was added to the cell pellet, and the samples were thoroughly vortexed every 10 minutes for 30 minutes while kept on ice. After the extraction, samples were centrifuged at 14000 rpm for 15 minutes at 4°C to remove cellular debris. Supernatants were transferred to new tubes, and the protein content was quantified using the Pierce™ BCA Protein Assay Kit (Thermo Fisher Scientific). For each sample, equal amounts of protein (20-30 µg) were loaded on SDS-PAGE gels. Before western blotting, the lysates were denatured by boiling at 95°C for 10 min in 1X Laemmli Sample Buffer supplemented with DTT (Bio-Rad). Samples were loaded on SDS-PAGE gels, run at 120 V for about 2 hours, and electrophoretically transferred to a nitrocellulose membrane (Cytiva Amersham™) at 350 mA for 1.5 hours. Membranes were blocked in 5% non-fat dry milk prepared in PBS 1X-Tween 0.1 % (PBST) for 1 hour and then incubated for the appropriate primary antibody overnight at 4°C, or at room temperature for 1 hour. **Table 7** lists the antibodies used in this study. Membranes were recovered and washed three times for 5 minutes each with PBST. Membranes were then incubated with peroxidase-conjugated secondary antibodies (1:10000 dilution) for 1 hour at room temperature. Membranes were washed three more times for 5 minutes each with PBST. Signal was then detected by using Amersham ECL Select Western Blotting Detection Reagent (GE Healthcare Life Sciences) and BioRad ChemiDoc™ XRS+ Imaging System. Image processing and densitometric quantification of the bands were performed using the Image Lab software.

mRNA Stability assay

3 x 10^5 cells were seeded in a 6-well plate format. After 24 hours, cells from the first timepoint (t0) well were collected by trypsinization, washed with PBS 1X, resuspended in 500 µl of TRIzol™ (Invitrogen), and frozen at -80°C. Simultaneously, cells in the remaining wells were treated with 10 µg/ml of Actinomycin D to block *de novo* transcription. After 20 minutes, 40 minutes, 1 hour, 2 hours, and 4 hours from the treatment, cells were pelleted from the corresponding timepoint wells and resuspended in TRIzol™. Once all the pellets were recovered and frozen, they were thawed at room temperature for 15 minutes, and RNA was extracted following the TRIzol® manufacturer's instructions. RNA was quantified, and 1 µg of timepoint t0 RNA from each cell line was retro-transcribed. For the timepoints following t0, RNA was retro-transcribed volumetrically to the reference t0 for each cell line, and 12.5 ng were amplified via RT-qPCR. Primers are listed in **Table 5**. GAPDH, whose levels do not quickly fluctuate over time, was used as a housekeeping control. The mRNA abundance (remaining levels) at every time point was then calculated relative to the start of transcription inhibition (t0) for each cell line (2^-ddCt). The mRNA decay rate was calculated by a nonlinear regression curve fitting using the one-phase decay function (GraphPad Prism 10).

Cycloheximide chase assay

6 x 10^5 cells were seeded in a 6-well plate format. After 24 hours, cells from the first timepoint (t0) well were collected by trypsinization. The cell pellet was resuspended in 50 µl of RIPA lysis buffer 1X supplemented with cOmplete™ Mini protease inhibitors (Roche). Simultaneously, the media was aspirated from the remaining wells and replaced with 100 µg/ml of cycloheximide (CHX, Cayman Chemical) in 2 ml of fresh media to prevent further protein synthesis. CHX indeed inhibits eukaryotic translation elongation by binding to the 60S ribosomal subunit's E-

site and preventing the release of deacetylated tRNA. After 10 minutes, 20 minutes, 30 minutes, and 1 hour from the treatment, cells were pelleted from the corresponding timepoint wells and resuspended in RIPA buffer 1X as well. Once all the pellets were harvested, proteins were extracted, quantified (see Protein Extraction Section), and Western Blot was performed on 35 µg of timepoint t0 protein extract. For the following timepoints, the protein amounts were loaded volumetrically to the reference t0 for each cell line. β-tubulin protein was used as a control, being a stable protein over time and treatments. Normalized protein abundance was calculated relative to the start of translation inhibition (t0) for each cell line.

Polysome profiling

Cells were grown in 150 mm dishes to 70-80% confluence and incubated for 10 min with 50 µg/ml (HCT116) or 100 µg/ml cycloheximide (RPE-1) at 37°C to block protein synthesis and immobilize ribosomes on mRNAs. Cells were then rinsed with ice-cold PBS 1X containing 50 µg/ml (or 100 µg/ml) cycloheximide, scraped, and pelleted. The cell pellet was lysed with 600 µl of ice-cold lysis buffer (20 mM Tris-HCl pH 7.5, 100 mM KCl, 5 mM MgCl2, 0.5 % NP-40, 0.2 U/µl RNasin® Ribonuclease Inhibitor (Promega), cOmplete™ Mini Protease Inhibitor Cocktail 1X (Roche), 100 µg/ml cycloheximide) by incubation on ice for 10 minutes and centrifugation at 12000 g at 4 °C for 10 min to remove cellular debris and nuclei. The cytoplasmic lysate was then loaded on a 15-50% linear sucrose gradient dissolved in salt buffer (100 mM NaCl, 20 mM Tris-HCl, pH 7.5, and 5 mM MgCl2) and processed by ultracentrifugation in a Beckman SW41 rotor at 40000 rpm for 1 hour and 40 minutes at 4°C. The gradient was then fractionated in 1 ml fractions, and the absorbance was measured at 254 nm by the Teledyne Isco model 160 gradient analyzer equipped with a UA-6 UV/VIS detector. RNA was extracted from the fractions using TRIzol® based on the manufacturer's instructions. Proteins were extracted from the fractions by adding Laemmli Sample Buffer supplemented with DTT (Bio-Rad) and boiling the samples at 95°C for 10 min before loading them on SDS-PAGE gels.

CRISPR/Cas9-mediated knock in

Edited HCT116 clones at the rs1053639 or rs137085 site were attempted by exploiting a CRISPR-Cas9 mediated knock-in with the Cas9 delivered as a ribonucleoparticle (RNP), as previously described (Ghetti et al., 2021). We designed single gRNAs (sequences are reported in **Table 3**) in close proximity to the tranSNP site to cut both alleles at the same time and maximize the efficiency of Homology-directed Repair (HDR). The same protocol with a few modifications (*i.e.,* not providing the donor DNA as a template for repair and not inhibiting DNAPKcs) was used beforehand to test the cutting efficiency of the sgRNAs. For both protocols, the sgRNA was prepared by mixing 1:1 the gene-specific portion Alt-R® CRISPR-Cas9 crRNA (IDT) and the common scaffold AltR® CRISPR-Cas9 tracrRNA (IDT). The mixture was heated at 95°C for 5 minutes and allowed to cool down at room temperature for 5 minutes for optimal annealing. 3 µl of sgRNA were further incubated with 120 pmol of recombinant Cas9 for 20 minutes at room temperature to generate the ribonucleoprotein (RNP). In parallel, cells were harvested by trypsinization, and 2.5×10^5 cells per condition were electroporated in the 4D-Nucleofector System (Lonza) using the SE Cell Line 4D-Nucleofector Kit S (Lonza). The electroporation mixture combined 20 µl of cell suspension, 1.2 µl of Alt-R® Cas9

Electroporation Enhancer (IDT), 5 µl of RNP complex, and PBS to a final volume of 30 µl. Additionally, 1.2 µl of Ultramer® DNA Oligonucleotide (100 µM, IDT) was added in the case of knock-in generation to provide a template donor DNA for HDR. Electroporated cells were recovered from the strip and seeded in a 12-well plate format either untreated or, in the case of knock-in generation, treated with 1 µM of NU7441 DNA-PKcs inhibitor for 48 hours to favor HDR occurrence. The medium, both with and without the drug, was changed after 24 hours. The cells were kept in culture up to full recovery and expanded until 2.5×10^5 cells could be harvested for DNA extraction and Sanger sequencing. DNA was extracted by adding 20 µl of the QuickExtract™ DNA Extraction Solution (Lucigen) to the cell pellet. After vortexing, the sample was incubated at 65°C for 15 minutes and 98°C for 10 minutes. 1 µl of this DNA was used for the PCR amplification using the GoTaq® Green Master Mix (Promega) in 25 µl of reaction. PCR primers (shown in **Table 5**) were specifically designed to produce 300-700 bp long amplicons and to have the SNP of interest asymmetrically located 100-200 bp from one or the other end of the amplicon, to have optimal sequencing interpretation. The PCR product was then purified using the MinElute PCR Purification Kit (QIAGEN). 75 ng of purified PCR products were sequenced using the Mix2Seq Kit and Sanger sequencing service provided by Eurofins. The TIDE software (Brinkman and van Steensel, 2019) was employed to identify and quantify insertions and deletions (indels) in the bulk edited population. The Synthego ICE software (Synthego Performance Analysis, ICE Analysis. 2019. v3.0) was employed to assess the knock-in efficiency in the edited bulk population. A limiting dilution assay was performed on the knock-in edited bulk population by seeding 1 cell/well in a 96-well plate format to eventually obtain clones. The media was changed once a week for 3-4 weeks, then potential clones were expanded to 24-well plates, and at the same time, pellets were harvested for DNA extraction and sequencing. The efficiency of clone production was about 1 in 3 seeded cells; 85 clones were screened by sequencing.

REMSA (RNA electromobility shift assay)

The full-length recombinant RBMX protein was purchased from Origene (TP710403). FAM-labelled fluorescent RNA probes (GAGGGACUGAUUCCU/AGUGGUUGGAA-3'FAM) for the T and A alleles were purchased from Metabion. The binding reaction was set up in 10 µl of binding buffer (10 mM HEPES, 50 mM KCl, 1 mM EDTA, 0.05% NP-40, 10% Glycerol, 0.5 mM DTT, pH 11.5). 10 U of RNasin (1 µl) were also added to each reaction and incubated for 30 minutes at RT in the dark. Upon incubation, 1 µl of 6X Orange Dye was added to each reaction to facilitate sample visualization. The RNA-protein complex was resolved by running the binding reaction on a 6% TBE polyacrylamide native (non-denaturing) gel at 80V for 1 hour in TBE 1X at RT. The gel was pre-run in cold TBE 0.5X at 100V for 30 minutes and imaged using the SYBR filter in the ChemiDocTM XRS imaging system (Bio-Rad).

RNA immunoprecipitation-qPCR (RIP-qPCR)

8×10^6 cells were seeded in 150 mm cell culture dishes (Sarstedt) and harvested by scraping after 48 hours. Cells were lysed in 800 µl of HNTG lysis buffer (20 mM HEPES, pH 7.9, 150 mM NaCl, 1% Triton-X 100, 10% glycerol, 1 mM MgCl2, 1 mM EGTA, 100 U/mL RNasin (Promega), 1X protease inhibitors (Roche)) for 30 minutes on ice. The lysate was obtained by centrifugation

at 15000 rpm, 4°C for 10 minutes, and the protein amount was quantified. Meantime, 20 µl of Protein A Dynabeads (Invitrogen) per condition were washed twice with 500 µl of IPP500 buffer (20 mM HEPES pH 7.4, 500 mM NaCl, 1.5 mM MgCl2, 0.5 mM DTT, 0.05% NP40) and incubated with either 0.22 µg of anti-RBMX/hnRNP G antibody or 0.22 µg of anti-Normal Rabbit IgG antibody in 100 µl of IPP500 buffer for 1h 30 at room temperature on a rotating wheel. After antibody conjugation, beads were further washed once with 900 µl of IPP500 buffer and twice with 900 µl of IPP150 1x buffer (20 mM HEPES pH 7.4, 150 mM NaCl, 1.5 mM MgCl2, 0.5 mM DTT, 0.05% NP40) and once with 1X PBS. Nonspecific binding was blocked by incubating the beads with 300 µl of 10 mg/ml Bovine Serum Albumin (BSA) for 30 minutes at room temperature on a rotating wheel. Beads were further washed three times with 800 µl of IPP150 1X buffer and incubated with 1 mg of the protein lysate in IPP150 1X buffer and 1X protease inhibitors in a final volume of 400 µl O/N at 4°C on a rotating wheel. Before the incubation with the beads, 10% of the lysate in IPP150 1X buffer was isolated as protein input for Western Blot analysis, and 1% was isolated as RNA input for qPCR analysis. After O/N incubation, the flow-through (unbound lysate) was collected for Western Blot analysis, the beads were washed four times with 800 µl of IPP150 1X buffer, and 10% of the last wash was also collected for Western Blot analysis upon elution in 1X Laemmli Sample Buffer. Samples were heated at 98°C for 10 minutes to detach the proteins from the beads. Conversely, elution both for RIP samples (beads) and RNA inputs was performed by incubation with 5 µl of >600 U/ml proteinase K solution (Qiagen) and 150 µl of Proteinase K buffer (20 mM Tris-HCl, pH 7.4, 10 mM MgCl2, 0.2% Tween-20) at 55°C for 30 minutes in a heat block shaking at 700 rpm. The output RNA was extracted with TRIzol® reagent (Invitrogen) according to the manufacturer's instructions. The whole amount of eluted RNA was retrotranscribed using the RevertAid First Strand cDNA Synthesis Kit (Thermo Scientific), and 1 µl of undiluted cDNA was used in the following RT-qPCR analysis in a final volume of 10 µl with the qPCRBIO SyGreen Mix (PCR Biosystems) and the QuantStudio 5 Real-Time PCR System (Applied Biosystems®) instrument. Primers are listed in **Table 5**.

Gene silencing

24 hours post-seeding, cells were transfected with a single or a mixture of siRNAs targeting RBMX (IDT) at a final concentration of 40 nM for 72 hours. Control cells were transfected with the same concentration of a non-targeting siRNA (IDT, 51-01-14-04) for 72 hours. The siRNAs were diluted in Opti-MEM™ Reduced Serum Medium (Thermo Fisher Scientific), and INTERFERin (Polyplus) was used as a transfection reagent according to the manufacturer's instructions. The transfection reaction was incubated at room temperature for 10 minutes before being added dropwise to the cells. The sequences of siRNAs used in this study are listed in **Table 6**.

Cell fractionation

Cell fractionation was performed using a 0.1% Igepal buffer in PBS 1X as described in the publicly available REAP fractionation protocol (Suzuki et al., 2010), coupled with an RNA extraction protocol to improve the extraction of the RNA from the nuclei (Gagnon et al., 2014). Cells were seeded in 10-cm dishes and, once confluent, were detached by trypsinization, washed with PBS 1X, and lysed in 900 µl of ice-cold 0.1% Igepal buffer in PBS 1X buffer for 2

minutes; 300 µl of this lysate were removed as whole cell lysate (WCL). The lysate was then fractionated by centrifugation at 12000 rpm for 40 seconds at room temperature. 300 µl of the supernatant were isolated as a cytoplasmic fraction (CYTO). The pellet was washed with 1 ml of 0.1% Igepal buffer and centrifuged at 12000 rpm for 40 seconds at room temperature to obtain the nuclear fraction (NUC). 50 µl out of 300 µl were isolated from each fraction for Western Blot analyses upon further lysis by RIPA buffer 1X (see Protein Extraction Section). The remaining 250 µl were used for TRIzol-based RNA extraction. To implement RNA extraction, the CYTO and NUC fractions were resuspended in 1 ml of TRIzol; lower volumes of TRIzol did not successfully extract RNA under our conditions. RNA was incubated for 10 minutes in TRIzol at room temperature, then 10 µl of EDTA 0.5 M were added before incubation at 65°C for 5 min, 600 rpm (or until the pellet was completely dissolved). Subsequently, chloroform was added to follow the conventional TRIzol protocol.
Nuclear and cytoplasmic RNA were eluted in the same volume of water (80 µl), quantified, and 1 µg per fraction was retro-transcribed and analysed via RT-qPCR. Primers are listed in **Table 5**.

MeRIP-qPCR

6 x 10^6 cells were seeded in 150 mm cell culture dishes (Sarstedt) and harvested by scraping after 48 hours. The pellet was resuspended in 500 µl of TRIzol ® reagent (Invitrogen), and RNA was precipitated overnight in isopropanol. The next day, 25 µl per sample of protein G Dynabeads (Invitrogen) were washed with binding buffer (100 mM Tris-HCl, pH 7.4, 50 mM NaCl, 0.5% NP-40) and conjugated with 5 µg of anti-m6A antibody or 5 µg of anti-Normal Rabbit IgG antibody for 1 hour and 30 minutes at room temperature on a rotating wheel. Upon conjugation, beads were washed three times with binding buffer. The beads were further incubated with 2 µg of RNA in 500 µl of binding buffer supplemented with RNase inhibitors (Promega) overnight at 4°C on a rotating wheel. The 1% input sample was harvested at this stage and incubated under the same conditions as the IP samples. The next day, the flow-through (unbound lysate) was harvested in new tubes, and the samples were washed twice with binding buffer, twice with high salt buffer (50 mM Tris-HCl pH 7.4, 150 mM NaCl, 0.5% NP-40), and twice with low salt buffer (50 mM Tris-HCl pH 7.4, 50 mM NaCl, 0.5% NP-40). RNA-m6A complexes from the input and IP samples were released from the beads by incubation with 5 µl of >600 U/ml proteinase K solution (Qiagen) and 150 µl of Proteinase K buffer (20 mM Tris-HCl, pH 7.4, 10 mM MgCl2, 0.2% Tween-20) at 55°C for 30 minutes in a heat block shaking at 700 rpm. The output RNA was extracted with TRIzol® reagent (Invitrogen) according to the manufacturer's instructions. The whole amount of eluted RNA was retrotranscribed using the RevertAid First Strand cDNA Synthesis Kit (Thermo Scientific), and 1 µl of undiluted cDNA was used in the following RT-qPCR analysis in a final volume of 10 µl with the qPCRBIO SyGreen Mix (PCR Biosystems) and the QuantStudio 5 Real-Time PCR System (Applied Biosystems®) instrument. Primers are listed in **Table 5**. A sequence around the stop codon of human EEF1A1 was used as a positive control, as in the Magna MeRIP™ m6A Kit (Millipore).

Single-molecule inexpensive Fluorescence *In Situ* Hybridization (smi-FISH)

The smiFISH protocol was adapted from Querido et al., 2020. 50000 cells per well were seeded in 12-well plates on 22 × 22 mm glass coverslips (Prestige) previously stripped with 1 M HCl,

sterilized, and stored in 100% ethanol. Cells were fixed in 4% paraformaldehyde (PFA) (Electron Microscopy Science) for 20 min at room temperature and then washed twice with PBS 1X. Permeabilization was performed in 0.5% Triton X-100, PBS 1X for 5 min at room temperature. Once permeabilized, samples were incubated at room temperature in a solution containing SSC 1X and 15% formamide, for 40 min and placed cell-side down on a 50-µl drop of hybridization buffer containing the probe [SSC 1X, 15% formamide, bovine serum albumin (BSA) (4.5 mg/ml), 10.6% dextran sulfate, 2 mM Vanadyl Ribonucleoside Complex (VRC), yeast tRNA (0.4 mg/ml), 1 µl of probe mix] in an air-tight hybridization chamber protected from light overnight at 37°C. The probe mix preparation is described in the next paragraph. The following day, coverslips were washed twice with prewarmed SSC 1X solution containing 15% formamide for 30 min at 37°C. After that, coverslips were rinsed twice with PBS 1X, cells were stained with DAPI (1 ng/µl) (4',6-diamidino-2-phenylindole) in PBS 1X, for 12 min at room temperature, and washed with PBS 1X. Samples were mounted on precleaned glass slides using ProLong Diamond Antifade Mountant (Thermo Fisher Scientific).

Probe preparation was performed as described by Querido et al., 2020. For DDIT4 detection, 3 primary probes targeting the DDIT4 sequence were used and prepared as a 20 µM equimolar mixture in milliQ water. Sequences of the probes are shown in Table S4. Primary probes were mixed with 50 pmol of fluorescently labeled secondary probes in NEB3 1X solution [100 mM NaCl, 50 mM Tris-HCl (pH 8), 10 mM MgCl2] in a final volume of 10 µl. Primary probes were annealed with secondary probes in a PCR thermocycler (85°C for 3 min, 65°C for 3 min, 25°C for 5 min. As described in the previous paragraph, the probe mix (1 µl) was used for the smiFISH hybridization buffer preparation.

For smiFISH/IF experiments, the smiFISH technique was performed first, using the protocol described in the smiFISH paragraph, and followed by the immunofluorescence protocol as described hereafter. After the overnight probe hybridization, cells were washed twice in prewarmed SSC 1X, 15% formamide solution. After two rinses in PBS 1X, cells were incubated in blocking solution (PBS 1X, 2% BSA, 0.1% Triton X-100) for 3 hours and incubated for 1 hour at room temperature with the primary antibody diluted in blocking solution. For RBMX detection, we used the antibody in Table S7 at a 1:200 dilution. Cells were then washed five times for 6 min with PBS 1X, 0.1% Triton X-100, and incubated with the appropriate fluorescent secondary antibody for 1 hour [goat anti-rabbit Alexa Fluor 488 (AF488), from Thermo Fisher Scientific, catalog no. A-11034, 1:1500 dilution; donkey anti-mouse AF647, from Thermo Fisher Scientific, catalog no. A-31571, 1:1000 dilution]. After incubation, cells were washed five times for 6 min with PBS 1X, 0.1% Triton X-100, and stained with DAPI (1 ng/µl) in PBS 1X for 12 min. After two washes with PBS 1X, coverslips were mounted on glass slides using ProLong Diamond Antifade Reagent (Thermo Fisher Scientific).

Images were acquired using a confocal laser scanning Leica TCS SP8 inverted microscope (Leica Camera AG) with a plan apochromatic 63×/1.40 oil immersion objective and 2× zoom. Normal photomultipliers (PMTs) were used to detect DDIT4 smiFISH signal, RBMX, b-tubulin, G3BP1, TIAR-1, and DAPI signals. Optimal acquisition parameters, including a nanometer range of excitation, gain, offset, and laser power, were optimized for the visualization of each fluorophore at the beginning of the acquisition and maintained throughout each experiment. Z-stack images were acquired in each experiment with a 0.3-µm step and 2048 × 2048-pixel size resolution using Leica Application Suite X (LAS X) imaging software.

Images were analyzed using CellProfiler 4.0.7 (Broad Institute, Inc.). Briefly, cell nuclei were identified as the primary object using the DAPI signal. For each object, the cellular region was defined by propagating from the nucleus, applying a low segmentation threshold to the smoothed smiFISH signal. The cytoplasm was defined as a tertiary object by subtracting the nuclear masks from the cellular regions. DDIT4 smiFISH signal spots were segmented as objects with a typical diameter range of 10 to 30 pixels. Subsequently, objects were localized based on their position relative to the nuclear or cytoplasmic regions. Since the majority of the spots exhibited a perinuclear localization, the nuclear regions were reduced by 5% to prevent misleading classification. Morphological features and intensity values for both DDIT4 smiFISH and RBMX signals were calculated at the object level.

Cell proliferation

2500 cells per well were seeded into 96-well plates (Corning). The cell number was followed by the high content fluorescent microscope Operetta (PerkinElmer) in digital phase contrast every 24 hours for 96 hours. The cell number was normalized to the cell number measured 24 hours post-seeding (time-zero).

Cell transduction

Cells were seeded and, when at most 70-80% confluent, were transduced with lentiviral particles and polybrene at MOI (multiplicity of infection) of 0.5 (1 viral particle every 2 cells) to express GFP constitutively. 24 hours post-transduction, the medium was changed, and cells were treated with 5 µg/ml blasticidin for at least 15 days, to reach at least 95% of GFP+ cells.

Competition assay and FACS analyses

Competition assay: For competition growth assays, GFP-labelled HCT116 clones and non-fluorescent HCT116 clones of different genotypes were mixed at a 1:1 ratio and seeded into duplicate wells. Cells were cultured in standard conditions for 15 days and detached using trypsin and analysed every 4 days. The cell number (expressed as percentage of EGFP-positive cells) at every time point was assessed using the FACSymphony™ Aria A1 (BD Biosciencies); 10K cells per sample were analysed. Analysis of flow cytometry data was performed using FlowJo software (FlowJo, LLC) in collaboration with Dr. Vincenza Vigorito (CIBIO, University of Trento). Results were expressed either as the percentage of GPF+ cells, computing the raw numbers from the FACS analysis, or as relative cellular fitness, calculated as described in a recent report (Louro et al., 2024b) using the following formula.

Cellular fitness of the EGFP-positive clone relative to the EGFP-negative competitor clone:
pGFP+(t) = NGFP+(t) / (NGFP+(t) + N GFP-(t)), W = ln ((pGFP+(ti) /pGFP-(ti)) 400 / (pGFP+(t0) /pGFP-(t0))

Cell cycle analysis: On separate samples, cells were collected and washed once with PBS 1X before fixation in 70% cold ethanol and stored for at least 4 hours at −20°C. Fixed cells were then washed twice in PBS 1X and permeabilized. The cell cycle was analysed by staining the cells with the fluorescent dye 7-aminoactinomycin D (7-AAD) to quantify the DNA content for

cell cycle phase distribution (G0/G1, S, G2/M). The 7-AAD was incubated for about 30 minutes at room temperature. Analysis of flow cytometry data was performed using FlowJo software (FlowJo, LLC) in collaboration with Dr. Alessandro Mattè (CIBIO, University of Trento).

Xenotransplantation in Zebrafish larvae

Animal rearing: Zebrafish (Danio rerio) strains were raised and maintained in the Model Organism Facility (MOF) at the Department CIBIO, University of Trento, under standard conditions (Kimmel et al., 1995). The transgenic zebrafish line Casper (White et al., 2008) was used to acquire live images in transparent larvae. All zebrafish studies were performed according to European and Italian law, D.Lgs. 26/2014, authorization 11/2023-PR to MM.
Larvae preparation: Embryos were initially maintained at 28 °C at a maximum density of 50 embryos per Petri dish in fish water supplemented with 0.0002% methylene blue (Sigma, Burlington, MA, USA) as an antifungal agent. After 24 h, embryos were placed in fish water without methylene blue. *Xenotransplantation of human cancer cell lines:* the protocol of the xenotransplantation procedure was adapted from (Lorenzini et al., 2025; Marines et al., 2023). GFP labelled HCT116 clones (edited AA and TT for rs1053639) were harvested from a 100 mm Petri dish on the day of xenotransplantation and resuspended in 70 µl of PBS. 0.5 µL of cell suspension containing 200-400 cells was transplanted in the swim bladder of 2 dpf zebrafish larvae anesthetized in 0.16 mg/ml PBS/Tricaine (MS-222) under a Nikon SMZ800 stereomicroscope, using a micromanipulator (Marzhouser Wetzkar MM 33 links) and the manual microinjector (CellTram® 4r Air Eppendorf). Transplanted embryos were maintained at 33°C in fish water. Larvae were selected for a good transplantation profile using a Leica MZ 10F fluorescence stereomicroscope.
Live-imaging and image analysis: each larval xenograft was imaged one day post-transplantation (D1) and 3 days post-transplantation (D3) using Leica TCS SP8 laser scanning confocal system (CD7) (Objectives: 10x/1). Images were acquired in z-stack mode with a z-step interval of 7 µm to a range of 170-230 µm, depending on the tumor size. The 488/633 nm lasers were used with appropriate filters to acquire images of green fluorescent cancer cells. Image analysis was performed using Fiji software. To study tumor growth of cancer cells in vivo, the maximum projection of every image was created, and a threshold was applied for each larva on day 1 (D1) and day 3 (D3) to generate a mask of the tumor area. The area on D3 was normalized to the area of D1 to assess the percentage of tumor growth for each larva.

Compound screening

1000 GFP-labelled cells per well were seeded in 50 µl of medium in 384-well transparent SpectraPlates™ (Revvity) using the VIAFILL™ (INTEGRA Biosciences) bulk reagent dispenser. After 24 hours, cells were treated with multiple concentrations (100 µM – 1 nM) of compounds using the Echo 650® Series Acoustic Liquid Handler (Beckman Coulter) with the collaboration of the High Throughput Screening facility at CIBIO (University of Trento). On the same day, cells from a few wells were stained with Hoechst and Propidium Iodide (PI) and imaged to produce the time-zero measurement: 5 µl of a Hoechst and PI mixture (1:1000 each in RPMI medium) were added to the cells, plates were centrifuged at 300 g for 30 seconds and cells were imaged using the ImageXpress® Micro Confocal System (Molecular Devices). Images from the blue

(Hoechst; staining nuclei, total cells), far red (PI; staining dead cells), and green (staining total cells) channels were acquired. After 48 hours from the treatment, cells were stained with Hoechst and PI and imaged as just described for the time-zero measurement. Image analysis was performed using KNIME, and data were shown as poc when normalized to the vehicle control, or as npi when normalized to the time-zero and DMSO according to the GR (growth rate) formula from Gupta et al., 2020; Hafner et al., 2016.

The following compounds were administered: Nutlin (Cayman Chemical), Everolimus (HTS CIBIO Facility), Niclosamide (HTS CIBIO Facility), Thapsigargin (HTS CIBIO Facility), XAV939, Omomyc (Basso Lab, CIBIO). All compounds were dissolved in DMSO except for Omomyc, which was dissolved in a dedicated vehicle (20 mM Sodium Acetate, 200 mM Sorbitol, 0.02% (w/v) Polysorbate (in Tween 20), pH 5.5).

Cloning

Forward and reverse primers containing the restriction sites and the sequence of interest (insert) were designed (sequences are reported in **Table 8**), resuspended to a final concentration of 100 µM, and simultaneously annealed and phosphorylated by mixing 1:1 (8.5 µl each) in a final volume of 20 µl with 2 µl of 10X DNA ligase buffer (Thermo Fisher Scientific) and 0.5 µl of PNK kinase (New England Biolabs). Annealed inserts were diluted 1:500 in water.
Meantime, backbone plasmids (about 1 µg) were double-digested using restriction enzymes for 3 hours at 37°C using 0.5 µl of each enzyme in a final volume of 20 µl. The digestion product was purified from gel using the Promega Gel Extraction and PCR Clean-Up Kit and quantified using the NanoDrop™ Spectrophotometer (Thermo Fisher Scientific).
About 50 ng of digested backbone were incubated with 1-2 µl of annealed insert (or water in the insert negative sample) and 2 µl of DNA T4 Ligase (Thermo Fisher Scientific) in a final volume of 20 µl for 2 to 3 hours at 22°C. The ligation product was entirely transformed into competent DH5α E. Coli bacteria (see Bacteria Transformation Section), and all bacteria were plated onto Ampicillin Liquid Broth (LB) Agar plates and incubated overnight at 37°C. Single colonies were picked and cultured in 5 mL of liquid LB supplemented with Ampicillin overnight at 37°C in a shaking incubator. Plasmid DNA was extracted using the PureYield™ Plasmid Miniprep System (Promega), quantified, and the correct insertion was verified via diagnostic digestion and Sanger sequencing.

Competent cells preparation

Competent DH5α E. coli bacteria were streaked on LB plates without antibiotics. Single colonies were inoculated in 20 ml of liquid LB without antibiotics overnight at 37°C in a shaking incubator. 15 ml of liquid culture were diluted in 200 ml of liquid LB and placed for 2 hours at 37°C in a shaking incubator. Cells were spun down for 5 minutes at 4°C at 4000 rpm. Cell pellets were resuspended in 7.5 ml of LB PEG and 2.5 ml of glycerol 40% and aliquoted on dry ice before storage at -80°C.

Bacterial Transformation

100 µl of KCM buffer were added to each DNA tube (and one water tube as a negative control) and incubated for 2 minutes. Competent DH5α E. coli bacteria were slowly thawed on ice, 100 µl per DNA tube were added, and incubated for 10 minutes on ice. Samples were then heat shocked by incubation at 42°C for 1 minute, and quick movement to the ice for 2 minutes. 800 µl of LB without antibiotics were added to each sample for the pre-growth, and samples were incubated at 37°C in shaking for at least 1 hour. Samples were pelleted for 2 minutes at 3000-4000 g, aspirated, resuspended in 80 µl of LB, and streaked on Ampicillin LB Agar plates to grow overnight at 37°C upside down. Single colonies were then picked from the plates and inoculated in liquid cultures for downstream applications.

Luciferase reporter assay

5000 cells were seeded in a 96-well plate format in 100 µl of medium.
After 24 hours, cells were transfected with 75 ng of DNA from the cloned constructs on Firefly backbone plasmids (pGL3 promoter for 5'UTR targets and linker pGL4.13 for 3'UTR targets, see **Table 6**; a "linker" was added to the pGL4 plasmid to generate an EcoRI and an NdeI restriction site around the XbaI site), and 25 ng of DNA from the Renilla luciferase plasmid. Plasmid DNA was diluted in Opti-MEM™ Reduced Serum Medium (Thermo Fisher Scientific), and FuGENE® HD (Promega) was used as a transfection reagent in a 4:1 ratio. The transfection reaction was assembled in a 5 µl of volume and incubated at room temperature for 15 minutes before being added dropwise to the cells.
After 48 hours from the transfection, cells were washed with 150 µl of PBS 1X and lysed using 50 µl per well of Passive Lysis Buffer 1X (PLB) in shaking at 500 rpm for 15 minutes. PLB and the following reagents were part of the Dual-Luciferase® Reporter™ Assay System. 10 µl of lysate were then transferred into white 384-well plates. 10 µl of Luciferase Assay Reagent (LAR), which is the Firefly Luciferase substrate, were added to each well. Upon brief shaking, the Firefly luciferase signal was detected using the Varioskan™ LUX Multimode Microplate Reader (Thermo Fisher Scientific). Three readings were performed. STOP&Glo reagent was then diluted 1:50 in the provided buffer, and 10 µl were added to each well. Upon brief shaking, the Renilla luciferase signal was detected using the same instrument; three more readings were performed. Data were analyzed by calculating the ratio between the Firefly and the Renilla luminescence signals for each well. The remaining, untransferred 40 µl of lysate were collected, and RNA was extracted using TRIzol™ (Invitrogen). RNA was then quantified, retrotranscribed, and Firefly mRNA was amplified via RT-qPCR (as in the cDNA and RT-qPCR Section).

Ribosome stalling assay

109-nucleotide long sequences (coding for 33 amino acids) comprising either the alternative or the reference version of the CDS tranSNPs indicated in **Table 2** were cloned in dual reporter ribosome stalling plasmid constructs (Kriachkov et al., 2023) upstream of an mCherry and downstream of a GFP sequence, separated by P2A sequences which induce the ribosomes to

skip the formation of peptide bonds without interrupting translation, allowing the translation of separate peptides from a single mRNA (Lin et al., 2013).
Cells were seeded in a 96-well plate format and, after 24 hours, transfected with 100 ng of the above-mentioned ribosome stalling plasmids using the FuGene transfection reagent (Promega) in a 4:1 ratio. A known staller sequence (coding for 17 consecutive lysines, polyK) cloned in the same plasmid was used as a positive control. A SEC61B sequence (106 amino acids), which is known to allow read-through, was cloned into the same plasmid and used as a negative control. GFP and mCherry signals, and digital phase contrast were detected after 24-, 36-, and 48-hours post-transfection using the Operetta High Content Imaging System (Perkin Elmer). GFP and mCherry intensities were used to calculate mChFP/GFP ratios, which were used as proxies for ribosome stalling. Low mChFP/GFP ratios indicated that stalling events occurred.

Tables

Tables 1 and 2 are embedded in the main text to improve text comprehension.

Table 3. Summary table for the sequences of the crRNA and donor DNA sequences.

Sequence Type	Sequence (5'->3')
DDIT4 crRNA	GTGGTTGGAAAACTGAGGCA
POLDIP3 crRNA	AGAGGAAGTTCTCCAGAGTT
DDIT4 Ultramer® DNA Donor	TTTGGGGTGGAGACTAGAGGCAGGAGCTGAGGGACTGATTCCWGTGGTTGG AAAACTGAGGCAGCCACCTAAGGTGGAGGTGGGG

Table 4. Summary table of the genotypes of selected rs1053639 edited clones.

Clone code	SNP status	Sequence Notes
#1	AT	-
#2	TT	-
#3	TT	GTG deletion starting at +1 from the SNP
#5	AA	GTG deletion starting at +1 from the SNP
#6	AA	GTG deletion starting at +1 from the SNP
#7	AA	9-nt deletion starting at +3 from the SNP
#10	AA	1-nt deletion starting at -1 from the SNP and a 2-nt deletion at +1 from the SNP
#11	TT	1-nt deletion starting at +3 from the SNP
#12	TT	2-nt deletion starting at +4 from the SNP
#13	TT	1-nt deletion starting at +3 from the SNP

Table 5. Table of primers used in this study for RT-qPCR, RIP, and meRIP.

Gene Name	Forward Primer Sequence (5'->3')	Reverse Primer Sequence (5'->3')
18S	GTAACCCGTTGAACCCCATT	CCATCCAATCGGTAGTAGCG
7SL	ATCGGGTGTCCGCACTAAGTT	CAGCACGGGAGTTTTGACCT
B2M	AGGCTATCCAGCGTACTCCA	ATGGATGAAACCCAGACACA
CDKN1A	CTGGAGACTCTCAGGGTCGAAA	GATTAGGGCTTCCTCTTGGAGAA
DDIT4 CDS (e1_e2)	CTAGCTGCGGCTTCTACGC	CCAAAGGCTAGGCATGGTGA
DDIT4 e2_e3	CGGAGGAAGACACGGCT	TGCATCAGGTTGGCACACAA
DDIT4 3'UTR	ACTTCAACCTGAGGGGGCCGACA	CTAAGCCTTTGTTTCATGCT
DDIT4 TIDE	CCAAGATCCAGGGGCTGTTT	GTGCCTCTTCCTTCACCCTG
DDIT4-AS1	CTACAACAGGTCATAACAAAAAT	ATGAAACAAAGGCTTAGGG
circDDIT4	CTCAGAGTGCCGGAGCGTAG	GAGTGCCATCTGGGTCTTCC
GAPDH	CCACTCCTCCACCTTTGAC	ACCCTGTTGCTGTAGCCA
meRIP positive	CGGTCTCAGAACTGTTTGTTTC	AAACCAAAGTGGTCCACAAA

NEAT1	GGGGCGGATCGGTGTTGCTT	CCCGGTTCCATCTGCTCGCC
RPS26	CCTAAGGATTCTCCCGGTGT	GCACGACCATTGTTCCTTCT
U6 snRNA	CTCGCTTCGGCAGCACATATACT	ACGCTTCACGAATTTGCGTGTC
YWHAZ	CAACACATCCTATCAGACTGGG	AATGTATCAAGTTCAGCAATGGC

Table 6. Sequences of siRNAs used in this study.

Name	Sequence (5'->3')
siRBMX 13.1	AUCAAGAGGAUAUAGCGAUAGAGAT
siRBMX 13.2	AUGUUCUCAGUACGAAAAACCUGAA
siRBMX Shashi	CAAAUCAAGAGGAUAUAGCGAUAUU

Table 7. Table of antibodies used in this study.

Protein Name	Antibody Code	Host Specie	Source
ATF4	sc-390063	Mouse	SantaCruz
β-tubulin	sc-5274	Mouse	SantaCruz
DDIT4	67059-1-Ig	Mouse	Proteintech
DDIT4 IHC	10638-1-AP	Rabbit	Proteintech
GAPDH	sc-32233	Mouse	SantaCruz
G3BP1	E9G1M	Rabbit	Cell Signaling
Lamin-A/C	ab40567	Mouse	Abcam
p-4EBP1 Thr 37/46	236B4	Rabbit	Cell Signaling
p53 (DO-1)	sc-126	Mouse	SantaCruz
p-RPS6 Ser 240/244	GTX133942	Rabbit	Genetex
p-S6K Thr 421/Ser 424	GTX635621	Rabbit	Genetex
RBMX	D7C2V	Rabbit	Cell Signaling
RPL21	sc-393663	Mouse	SantaCruz
tot-4EBP1	9452	Rabbit	Cell Signaling
tot-RPS6	GTX113542	Rabbit	Genetex
tot-S6K	GTX107562	Rabbit	Genetex

Table 8. Sequences of primers used for molecular cloning.

Gene Name	Forward Primer Sequence (5'->3')	Reverse Primer Sequence (5'->3')
DDIT4	aattcGACGACTGAACTTTTGGGGT GGAGACTAGAGGCAGGAGCTGAG GGACTGATTCCWGTGGTTGGAAA ACTGAGGCAGCCACCTAAGGTGG AGGTGGGGGAATAGTGTTTCca	tatgGAAACACTATTCCCCCACCTCCACCT TAGGTGGCTGCCTCAGTTTTCCAACCAC WGGAATCAGTCCCTCAGCTCCTGCCTCT AGTCTCCACCCCAAAAGTTCAGTCGTCg

FRG1	ggccgcGCCGAGTACTCCTAYGTGAA GTCTACCAAGCTCGTGCTCAAGGG AACCAAGACGAAGAGTAAGAAGAA AAAGAGCAAAGAKAAGAAAAGAAA AAGAGAAGAAGATGAAg	gatccTTCATCTTCTTCTCTTTTTCTTTTCTTMT CTTTGCTCTTTTTCTTCTTACTCTTCGTCTTGG TTCCCTTGAGCACGAGCTTGGTAGACTTCA CRTAGGAGTACTCGGCgc
GBP3	ggccgcCTGAAGCTAACGCAAGGTAC CAGTCAAAAAGATAAAAATTTTAATC TGCCCCRACTCTGTATCCGGAAGTT CTTCCCAAAGAAAAAATGTTTTGTCT TCGATCTGCCCg	gatccGGGCAGATCGAAGACAAAACATTTTTT CTTTGGGAAGAACTTCCGGATACAGAGTYG GGGCAGATTAAAATTTTTATCTTTTTGACTGG TACCTTGCGTTAGCTTCAGgc
KRR1	ggccgcTATATCATCATTAGGGCCAGA GATCTGATAAAACTGYTAGCAAGGA GTGTTTCATTTGAACAGGCAGTACR AATTCTTCAGGATGATGTTGCATGTG ACATCATTAAAg	gatccTTTAATGATGTCACATGCAACATCATCC TGAAGAATTYGTACTGCCTGTTCAAATGAAA CACTCCTTGCTARCAGTTTTATCAGATCTCT GGCCCTAATGATGATATAgc
MTPAP	ggccgcTTCAGATCACGTTTCTTCAAT CTGAAGTTGAAAAACCAGACTTCTG AACGGTCAYGCGTACGGTCAAGTAA TCAGTTGCCACGTTCAAACAAGCA GCTTTTTGAATTAg	gatccTAATTCAAAAAGCTGCTTGTTTGAACGT GGCAACTGATTACTTGACCGTACGCRTGAC CGTTCAGAAGTCTGGTTTTTCAACTTCAGAT TGAAGAAACGTGATCTGAAgc
ABL1	aattcCTCCTGGACCTTGACAGAGCA GCTAACTCCGAGAGCAGTGGGCAG GTGGCCRCCCCTGAGGCTTCACG CCGGGAGAAGCCACCTTCCCACC CCTTCATACCGCCTCGTca	tatgACGAGGCGGTATGAAGGGGTGGGAAG GTGGCTTCTCCCGGCGTGAAGCCTCAGGG GYGGCCACCTGCCCACTGCTCTCGGAGTT AGCTGCTCTGTCAAGGTCCAGGAGg
ARGHAP22	aattcGGAATGGCAGAGCTCACTTCT GTACCACRTCTGCTGGTCTCCAGC CTTGTATGGAGTTAGAAGCGTCTGTA TCTCTGGAGCAGCCAGGCGCTCTG GAGCCAGCTGGAGca	tatgCTCCAGCTGGCTCCAGAGCGCCTGGC TGCTCCAGAGATACAGACGCTTCTAACTCC ATACAAGGCTGGAGACCAGCAGAYGTGGTA CAGAAGTGAGCTCTGCCATTCCg
HuR	aattcAGAGGCTTTGATTGAATTCCCT TTTGACCCGTGTGTAACTTCCTCTG GTAGTTRGACCCCAGGCAGCTCCG AATTTGTGAACCTGCTTCCTGATGAA TTCTCCCTTGTca	tatgACAAGGGAGAATTCATCAGGAAGCAGG TTCACAAATTCGGAGCTGCCTGGGGTCYAA CTACCAGAGGAAGTTACACACGGGTCAAAA GGGAATTCAATCAAAGCCTCTg
PTNP14	aattcCACCCGGCTAATTTTTATATTTT TAGTAGAGACGGGGTTTTGCCATGT TGGCCRGACTGGTCTCAAACCTCT GACCTCGTGATGACCCCCCTCGGC CTCCCAAAGTGCca	tatgGCACTTTGGGAGGCCGAGGGGGGTCA TCACGAGGTCAGAGGTTTGAGACCAGTCTG GCCAACATGGCAAAACCCCGTCTCTACTAA AAATATAAAAATTAGCCGGGTGg
CUL3	agcttAGCCGAGCCGGACGTGAGGG GGACCCCGCGGAGCCGCCGCGC CAGCGCAGCCCCCCAGCCGCATC GGAGTCGCCAGAGTCCGAGCCGC CGCCGCCGCCGCCGCCCCCC Gc	catggCGGGGGCGGCGGCGGCGGCGG GCGGCTCGGACTCTGGCGACTCCGATGCG GCTGGGGGGCTGCGCTGGCGCGGCGGCT CCGCGGGGTCCCCCTCACGTCCGGCTCG GCTa

SPRYD7	agcttATAGACAAGTCCGGACCTCGG GCGGGGGCAGGAGACGGAGCTGA GCGGCGGGGGGCAGTGTCGCCTC GGTCTAGGGACGGCGGCGGAGTC GGTGGTCCCTGCGCGc	catggCGCGCAGGGACCACCGACTCCGCC GCCGTCCCTAGACCGAGGCGACACTGCC CCCCGCCGCTCAGCTCCGTCTCCTGCCC CCGCCCGAGGTCCGGACTTGTCTATa
TRIB3	agcttGACCGGGGGCCGGGCGCGC ACGAGACTCGCAGCGGAAGTGGA GGCGGCTCCGCGCGCGTCCGCTG CTAGGACCCGGGCAGGGCTGGAG CTGGGCTGGGATCCCGAGCTCGGc	catggCCGAGCTCGGGATCCCAGCCCAGCT CCAGCCCTGCCCGGGTCCTAGCAGCGGA CGCGCGCGGAGCCGCCTCCACTTCCGCT GCGAGTCTCGTGCGCGCCCGGCCCCCGG TCa
ZFP90	agcttTCGGCGGGGGCGGGAGGAG CTGCCCGAGGCTCTGGGTGGGCC GGAGGTCGCGAAATCCGGAGCCC CCCAGAGGCGCTCCTGCCCCGGA GCCGGGCCCTGGCGAGGCAGGAc	catggTCCTGCCTCGCCAGGGCCCGGCTCC GGGGCAGGAGCGCCTCTGGGGGGCTCCG GATTTCGCGACCTCCGGCCCACCCAGAGC CTCGGGCAGCTCCTCCCGCCCCCGCCGA a
WASHC1	aattcCAGCCAGGACAAGCTGCTCA GACCTGCTTCCCTGGGAGGGGGTG ACGGAACCAGCAGTGTGTGGAGAC CAGCTTCAAGGAGCGGAAGGCTG GCTTGAGGCCca	tatgGGCCTCAAGCCAGCCTTCCGCTCCTTG AAGCTGGTCTCCACACACTGCTGGTTCCGT CACCCCCTCCCAGGGAAGCAGGTCTGAG CAGCTTGTCCTGGCTGg
EML1	aattcTTTGTATTTTATGACCAAGTAGA CCAAGTCAGAAAGATCTCTCTCGAG CGTACCATAAACCTGCAGAGAGAA GTCTCGAAAGGCTCCACCAGGTAC CAAGGca	tatgCCTTGGTACCTGGTGGAGCCTTTCGAG ACTTCTCTCTGCAGGTTTATGGTACGCTCGA GAGAGATCTTTCTGACTTGGTCTACTTGGTC ATAAAATACAAAg
UNC119B	aattcGCGCGCCAAAGGAGCTGCCA AACAGTGCTGTGTTTTCTTCCCCAG TATTTTTTCTTCCCTTTTTTTCCTGCC CCGTAGGTTGCAGAGGTACTATAGT AAAGca	tatgCTTTACTATAGTACCTCTGCAACCTACG GGGCAGGAAAAAAAGGGAAGAAAAAATAC TGGGGAAGAAAACACAGCACTGTTTGGCA GCTCCTTTGGCGCGCg
S1PR1	agcttTCACTCATCGAACCACCCCTG AAGCCAGTGAAGGCTCTCTCGCCT CGCCCTCTAGCGTTCGTCTGGAGTA GCGCCACCCCGGCTTCCTGGGGA CACAGGKTTGGCACCc	catggGGTGCCAAMCCTGTGTCCCCAGGAA GCCGGGGTGGCGCTACTCCAGACGAACG CTAGAGGGCGAGGCGAGAGAGCCTTCACT GGCTTCAGGGGTGGTTCGATGAGTGAa
TRIM27	agcttCGCCCGGTGCCTCTCAGGAA CAGCGAACCGGAGAGAGCGCCGG AGAGTTGGGCTCAGTGCRGAGCTC GGCGCCGGGGCCCATGCCCGTGC GCCCCCGCAGGCCGGCGCc	catggGCGCCGGCCTGCGGGGGCGCACGG GCATGGGCCCCGGCGCCGAGCTCYGCAC TGAGCCCAACTCTCCGGCGCTCTCTCCGG TTCGCTGTTCCTGAGAGGCACCGGGCGa
POLR1G	aattcCAGTGCTGGGATTATAGGTGTG AGCCACTGCGCCTGGCTAAGTTATT ATTATTTTTTTGAGACAGTCTCCTGGT GTCACCCAGGCTGGAGTGCAGTGG TGTca	tatgACACCACTGCACTCCAGCCTGGGTGA CACCAGGAGACTGTCTCAAAAAAATAATAAT AACTTAGCCAGGCGCAGTGGCTCACACCT ATAATCCCAGCACTGg

A = adenine

C = cytosine

G = guanine
T = thymine
R = G or A (purine)
Y = T or C (pyrimidine)
K = G or T (cheto)
M = A or C (amino)
S = G or C (strong)
W = A or T (weak)
B = G or T or C (except A)
D = G or A or T (except C)
H = A or C or T (except G)
V = G or C or A (except T)
N = A or G or C or T (any)

Appendix

Appendix Figure 1. Appendix to main Figures 9 and 18.

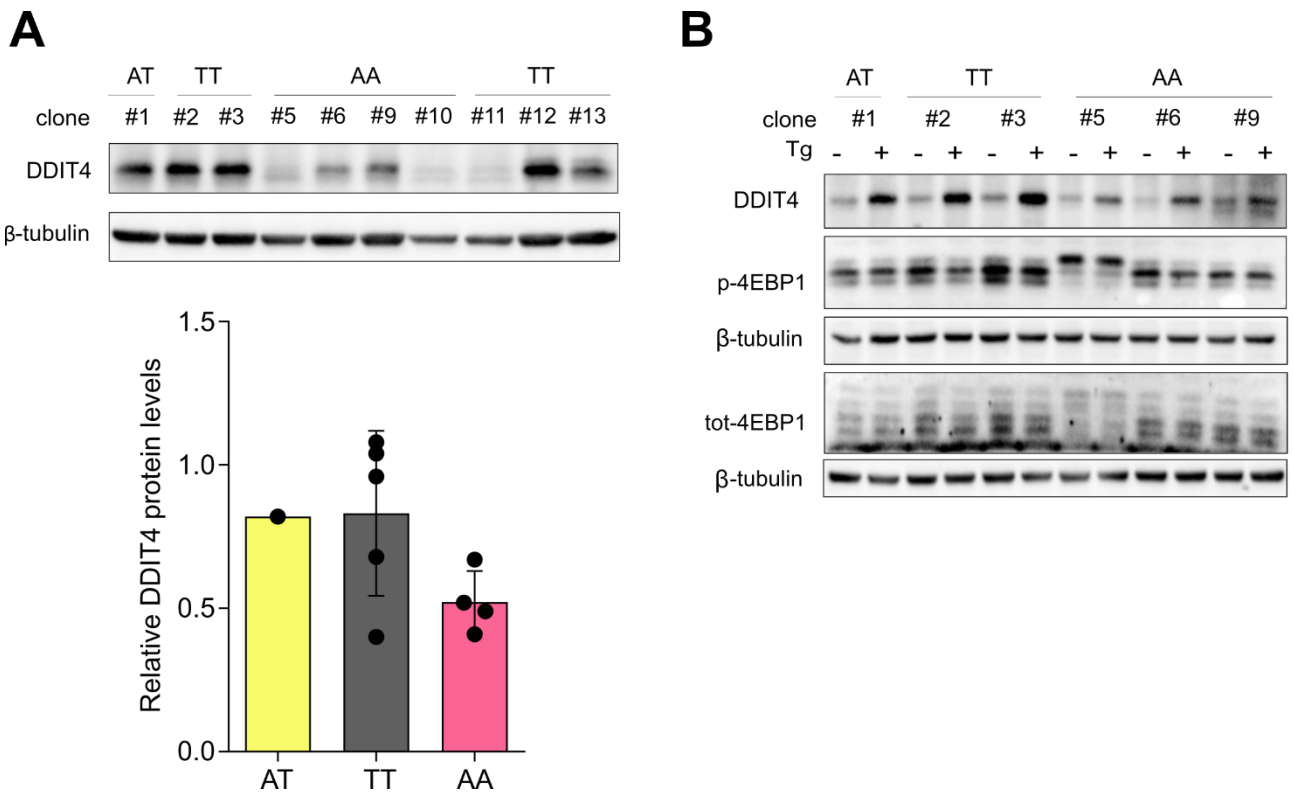

Appendix Figure 1. Multiple HCT116 TT and AA clones were considered to overcome editing limitations in the study.

A) Western Blot analysis (Top) and quantification (Bottom) of DDIT4 protein levels across all the available rs1053639 TT and AA HCT116 edited clones. β-tubulin was used as a loading control. SNP genotypes are shown in detail in Table 4. **B)** Western Blot analysis of DDIT4 and phosphorilated-4EBP1 protein levels across multiple rs1053639 TT and AA HCT116 edited clones. β-tubulin was used as a loading control. The blot shows that the differential phosphorylation of phospho-4EBP1 for clone 5 is not a feature of the AA genotype, but it is specific to clone 5 only and may be due to the different number of residue which is phosphorylated.

Appendix Figure 2. Appendix to main Figure 16.

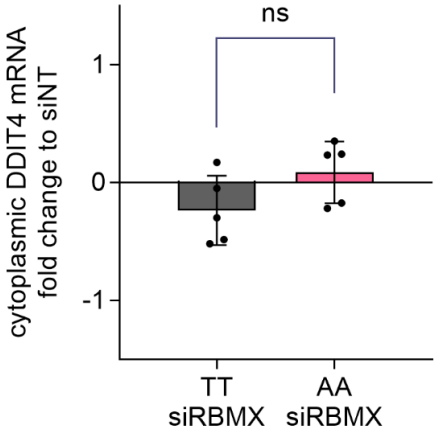

Appendix Figure 2. RBMX silencing significantly affects DDIT4 protein levels, whereas it does not affect DDIT4 mRNA levels.

Cytoplasmic DDIT4 mRNA levels were normalized to cytoplasmic GAPDH levels. ns, not significant, unpaired t-test.

Appendix Figure 3. Appendix to main Figure 17.

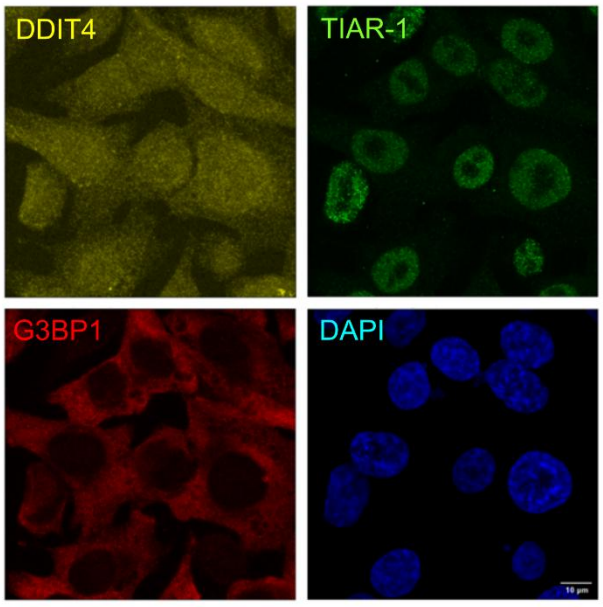

Appendix Figure 3. DDIT4 mRNA spots do not overlap with G3BP1 and TIAR-1.

Representative confocal images of smiFISH-IF of rs1053639 clones. DDIT4 mRNA is shown in yellow, TIAR-1 protein is shown in green, G3BP1 protein is shown in red, and DAPI is shown in blue. Scale bar is 10 µm.

Appendix Figure 4. Appendix to main Figure 23.

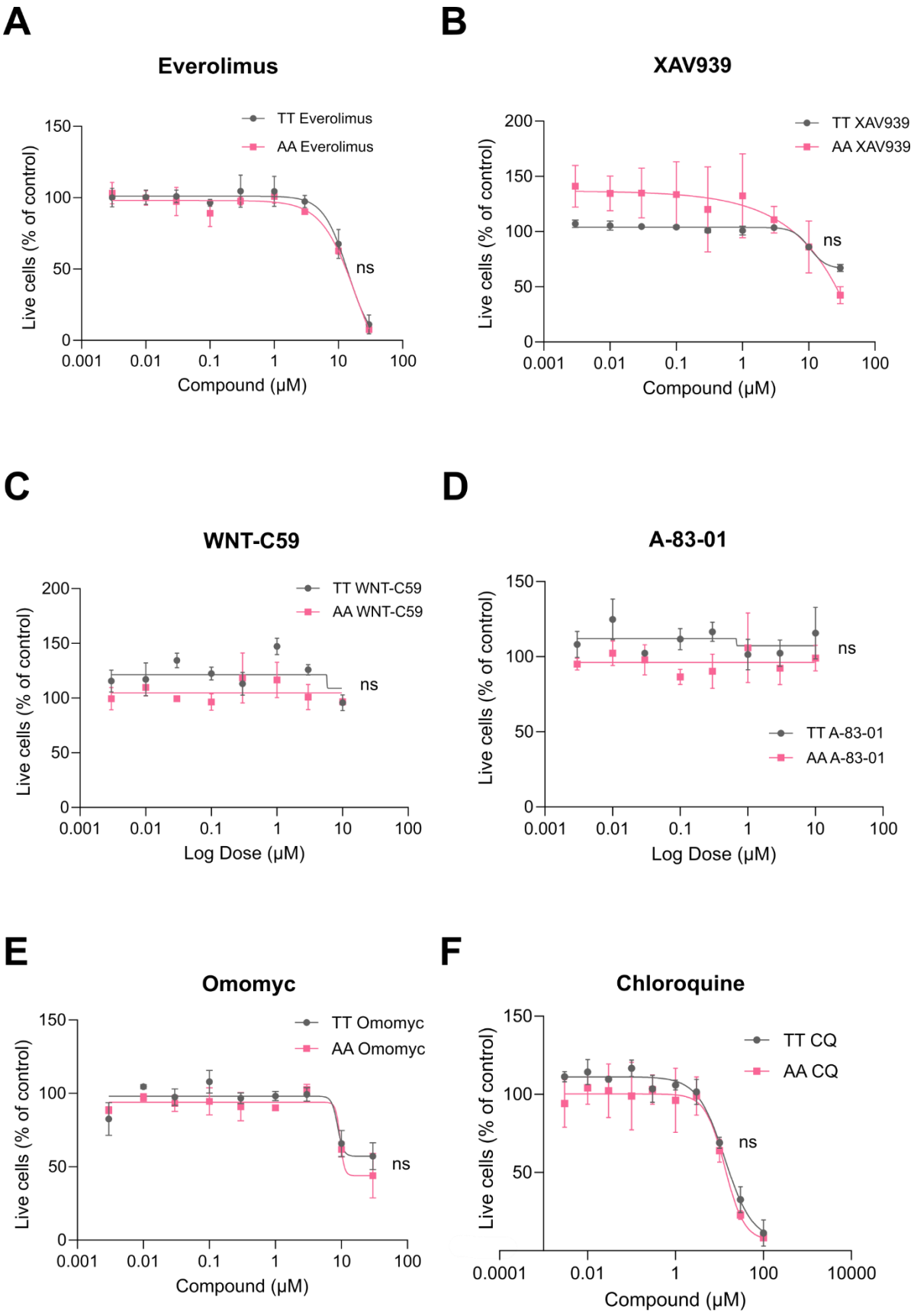

Appendix Figure 4. The rs1053639 genotype determines allele-specific sensitivity to multiple compounds. TT and AA clones were seeded using the automatic VIAFILL dispenser and treated after 24 hours using the Echo Acoustic Liquid Handler with a wide range of concentrations in the nanomolar and micromolar range of either **A)** everolimus **B)** XAV939, **C)** WNT-C59, **D)** A-83-01, **E)** Omomyc, or **F)** Chloroquine (CQ) for 48 hours. Cells were then incubated with Hoechst and PI (1:2000) for at least 40 minutes at 37 °C, and live imaging was performed using the ImageXpress Micro Confocal High-Content Imaging System. Dose-response curve indicating live cells (Hoechst-positive and PI-negative) normalized to the DMSO control on the y-axis and $\log_{10}$ of the compound concentrations on the x-axis are shown for each compound. Since IC50 values could not be calculated for all the tested compounds, dose-response curves were compared using the Extra sum-of-squares F statistical test; ns, not significant.

Appendix Figure 5. Appendix to main Figure 23.

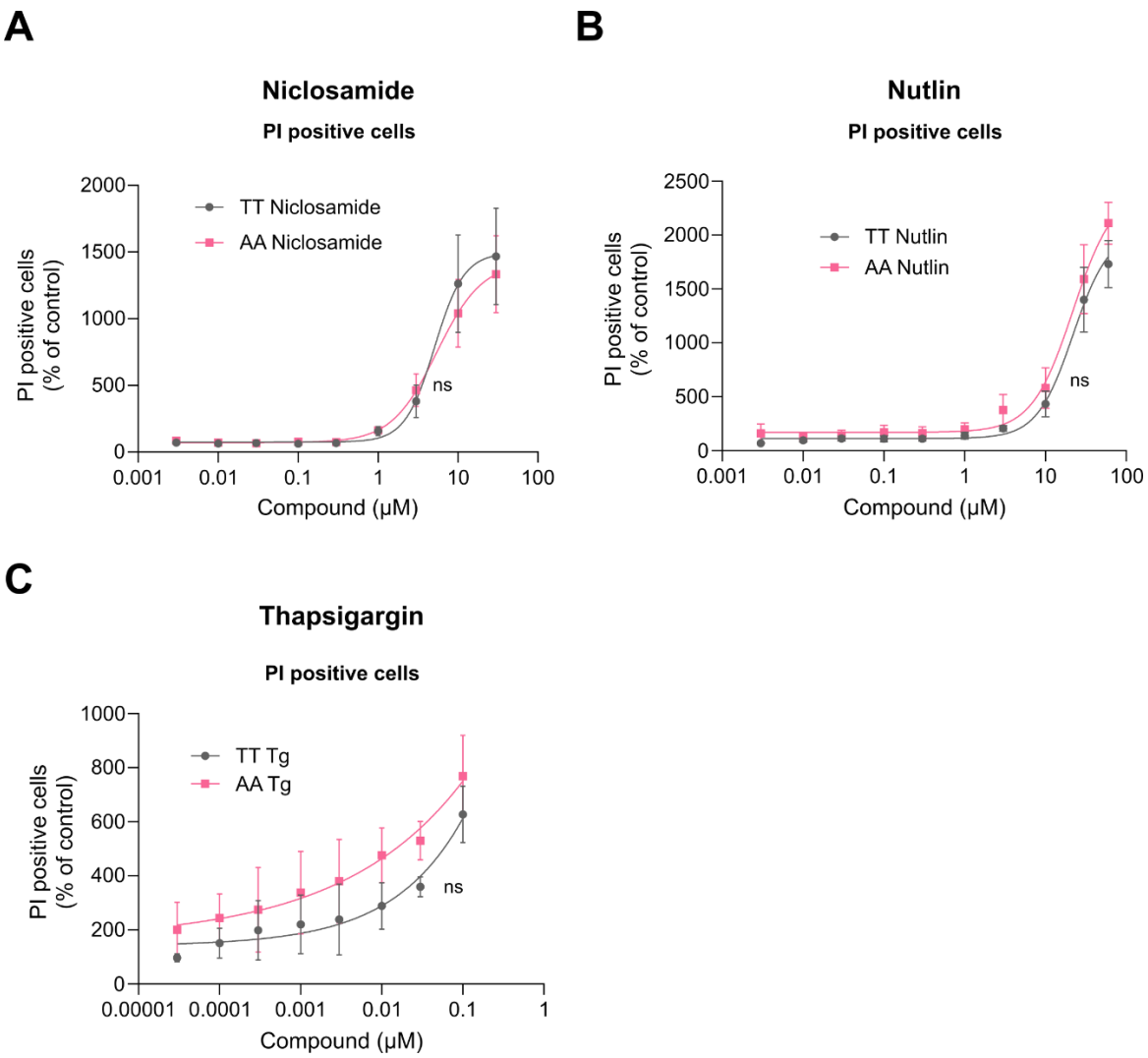

Appendix Figure 5. Evaluation of PI-positive cells upon niclosamide, nutlin, and thapsigargin treatments. TT and AA clones were seeded using the automatic VIAFILL dispenser and treated after 24 hours using the Echo Acoustic Liquid Handler with a wide range of concentrations in the nanomolar and micromolar range of either **A)**

niclosamide, **B)** nutlin, or **C)** thapsigargin for 48 hours. Cells were then incubated with Hoechst and Propidium Iodide (PI) (1:2000) for at least 40 minutes at 37 °C, and live imaging was performed using the ImageXpress Micro Confocal High-Content Imaging System. Curves indicate the percentage of cells positively stained by PI normalized to the DMSO control.

References

Adams-Brown, S.E., Reid, K.Z., 2025. The Central FacilitaTOR: Coordinating Transcription and Translation in Eukaryotes. Int. J. Mol. Sci. 26, 2845. https://doi.org/10.3390/ijms26072845

Adamson, B., Smogorzewska, A., Sigoillot, F.D., King, R.W., Elledge, S.J., 2012. A genome-wide homologous recombination screen identifies the RNA-binding protein RBMX as a component of the DNA-damage response. Nat. Cell Biol. 14, 318–328. https://doi.org/10.1038/ncb2426

Andreotti, V., Bisio, A., Bressac-de Paillerets, B., Harland, M., Cabaret, O., Newton-Bishop, J., Pastorino, L., Bruno, W., Bertorelli, R., De Sanctis, V., Provenzani, A., Menin, C., Fronza, G., Queirolo, P., Spitale, R.C., Bianchi-Scarrà, G., Inga, A., Ghiorzo, P., 2016. The CDKN2A/p16(INK) (4a) 5'UTR sequence and translational regulation: impact of novel variants predisposing to melanoma. Pigment Cell Melanoma Res. 29, 210–221. https://doi.org/10.1111/pcmr.12444

Bahrami-Samani, E., Vo, D.T., de Araujo, P.R., Vogel, C., Smith, A.D., Penalva, L.O.F., Uren, P.J., 2015. Computational challenges, tools, and resources for analyzing co- and post-transcriptional events in high throughput. Wiley Interdiscip. Rev. RNA 6, 291–310. https://doi.org/10.1002/wrna.1274

Batista, P.J., Molinie, B., Wang, J., Qu, K., Zhang, J., Li, L., Bouley, D.M., Lujan, E., Haddad, B., Daneshvar, K., Carter, A.C., Flynn, R.A., Zhou, C., Lim, K.-S., Dedon, P., Wernig, M., Mullen, A.C., Xing, Y., Giallourakis, C.C., Chang, H.Y., 2014. m(6)A RNA modification controls cell fate transition in mammalian embryonic stem cells. Cell Stem Cell 15, 707–719. https://doi.org/10.1016/j.stem.2014.09.019

Bergalet, J., Fawal, M., Lopez, C., Desjobert, C., Lamant, L., Delsol, G., Morello, D., Espinos, E., 2011. HuR-mediated control of C/EBPbeta mRNA stability and translation in ALK-positive anaplastic large cell lymphomas. Mol. Cancer Res. MCR 9, 485–496. https://doi.org/10.1158/1541-7786.MCR-10-0351

Bertoldo, J.B., Müller, S., Hüttelmaier, S., 2023. RNA-binding proteins in cancer drug discovery. Drug Discov. Today 28, 103580. https://doi.org/10.1016/j.drudis.2023.103580

Bertram, R., Schuster, C.F., 2014. Post-transcriptional regulation of gene expression in bacterial pathogens by toxin-antitoxin systems. Front. Cell. Infect. Microbiol. 4, 6. https://doi.org/10.3389/fcimb.2014.00006

Blandy, A., Hopes, T., Vasconcelos, E.J.R., Turner, A., Fatkhullin, B., Agapiou, M., Fontana, J., Aspden, J.L., 2025a. Translational activity of 80S monosomes varies dramatically across different tissues. Nucleic Acids Res. 53, gkaf292. https://doi.org/10.1093/nar/gkaf292

Blandy, A., Hopes, T., Vasconcelos, E.J.R., Turner, A., Fatkhullin, B., Agapiou, M., Fontana, J., Aspden, J.L., 2025b. Translational activity of 80S monosomes varies dramatically across different tissues. Nucleic Acids Res. 53, gkaf292. https://doi.org/10.1093/nar/gkaf292

Bowling, S., Di Gregorio, A., Sancho, M., Pozzi, S., Aarts, M., Signore, M., D. Schneider, M., Martinez-Barbera, J.P., Gil, J., Rodríguez, T.A., 2018. P53 and mTOR signalling determine

fitness selection through cell competition during early mouse embryonic development. Nat. Commun. 9, 1763. https://doi.org/10.1038/s41467-018-04167-y

Brar, G.A., Weissman, J.S., 2015. Ribosome profiling reveals the what, when, where and how of protein synthesis. Nat. Rev. Mol. Cell Biol. 16, 651–664. https://doi.org/10.1038/nrm4069

Brinkman, E.K., van Steensel, B., 2019. Rapid Quantitative Evaluation of CRISPR Genome Editing by TIDE and TIDER. Methods Mol. Biol. Clifton NJ 1961, 29–44. https://doi.org/10.1007/978-1-4939-9170-9_3

Buccitelli, C., Selbach, M., 2020. mRNAs, proteins and the emerging principles of gene expression control. Nat. Rev. Genet. 21, 630–644. https://doi.org/10.1038/s41576-020-0258-4

Buratti, E., Baralle, F.E., 2004. Influence of RNA secondary structure on the pre-mRNA splicing process. Mol. Cell. Biol. 24, 10505–10514. https://doi.org/10.1128/MCB.24.24.10505-10514.2004

Canal, M., Romaní-Aumedes, J., Martín-Flores, N., Pérez-Fernández, V., Malagelada, C., 2014. RTP801/REDD1: a stress coping regulator that turns into a troublemaker in neurodegenerative disorders. Front. Cell. Neurosci. 8, 313. https://doi.org/10.3389/fncel.2014.00313

Capossela, S., Muzio, L., Bertolo, A., Bianchi, V., Dati, G., Chaabane, L., Godi, C., Politi, L.S., Biffo, S., D'Adamo, P., Mallamaci, A., Pannese, M., 2012. Growth defects and impaired cognitive-behavioral abilities in mice with knockout for Eif4h, a gene located in the mouse homolog of the Williams-Beuren syndrome critical region. Am. J. Pathol. 180, 1121–1135. https://doi.org/10.1016/j.ajpath.2011.12.008

Chassé, H., Boulben, S., Costache, V., Cormier, P., Morales, J., 2017. Analysis of translation using polysome profiling. Nucleic Acids Res. 45, e15. https://doi.org/10.1093/nar/gkw907

Chen, A.B., Yu, X., Thapa, K.S., Gao, H., Reiter, J.L., Xuei, X., Tsai, A.P., Landreth, G.E., Lai, D., Wang, Y., Foroud, T.M., Tischfield, J.A., Edenberg, H.J., Liu, Y., 2024. Functional 3'-UTR Variants Identify Regulatory Mechanisms Impacting Alcohol Use Disorder and Related Traits. bioRxiv 2024.01.31.578270. https://doi.org/10.1101/2024.01.31.578270

Chen, T., Hao, Y.-J., Zhang, Y., Li, M.-M., Wang, M., Han, W., Wu, Y., Lv, Y., Hao, J., Wang, L., Li, A., Yang, Y., Jin, K.-X., Zhao, X., Li, Y., Ping, X.-L., Lai, W.-Y., Wu, L.-G., Jiang, G., Wang, H.-L., Sang, L., Wang, X.-J., Yang, Y.-G., Zhou, Q., 2015. m(6)A RNA methylation is regulated by microRNAs and promotes reprogramming to pluripotency. Cell Stem Cell 16, 289–301. https://doi.org/10.1016/j.stem.2015.01.016

Chen, W., Mook, R.A., Premont, R.T., Wang, J., 2018. Niclosamide: Beyond an antihelminthic drug. Cell. Signal. 41, 89–96. https://doi.org/10.1016/j.cellsig.2017.04.001

Chen, X., Li, Z., Liang, M., Zhang, Z., Zhu, D., Lin, B., Zhou, R., Lu, Y., 2023. Identification of DDIT4 as a potential prognostic marker associated with chemotherapeutic and immunotherapeutic response in triple-negative breast cancer. World J. Surg. Oncol. 21, 194. https://doi.org/10.1186/s12957-023-03078-7

Cheng, Z., Dai, Y., Pang, Yifan, Jiao, Y., Liu, Y., Cui, L., Quan, L., Qian, T., Zeng, T., Si, C., Huang, W., Chen, J., Pang, Ying, Ye, X., Shi, J., Fu, L., 2020. Up-regulation of DDIT4 predicts poor

prognosis in acute myeloid leukaemia. J. Cell. Mol. Med. 24, 1067–1075. https://doi.org/10.1111/jcmm.14831

Conant, D., Hsiau, T., Rossi, N., Oki, J., Maures, T., Waite, K., Yang, J., Joshi, S., Kelso, R., Holden, K., Enzmann, B.L., Stoner, R., 2022. Inference of CRISPR Edits from Sanger Trace Data. CRISPR J. 5, 123–130. https://doi.org/10.1089/crispr.2021.0113

Corbett, A.H., 2018. Post-transcriptional regulation of gene expression and human disease. Curr. Opin. Cell Biol. 52, 96–104. https://doi.org/10.1016/j.ceb.2018.02.011

Coronel, L., Häckes, D., Schwab, K., Riege, K., Hoffmann, S., Fischer, M., 2022. p53-mediated AKT and mTOR inhibition requires RFX7 and DDIT4 and depends on nutrient abundance. Oncogene 41, 1063–1069. https://doi.org/10.1038/s41388-021-02147-z

Crighton, D., Woiwode, A., Zhang, C., Mandavia, N., Morton, J.P., Warnock, L.J., Milner, J., White, R.J., Johnson, D.L., 2003. p53 represses RNA polymerase III transcription by targeting TBP and inhibiting promoter occupancy by TFIIIB. EMBO J. 22, 2810–2820. https://doi.org/10.1093/emboj/cdg265

Daran-Lapujade, P., Rossell, S., van Gulik, W.M., Luttik, M.A.H., de Groot, M.J.L., Slijper, M., Heck, A.J.R., Daran, J.-M., de Winde, J.H., Westerhoff, H.V., Pronk, J.T., Bakker, B.M., 2007. The fluxes through glycolytic enzymes in Saccharomyces cerevisiae are predominantly regulated at posttranscriptional levels. Proc. Natl. Acad. Sci. U. S. A. 104, 15753–15758. https://doi.org/10.1073/pnas.0707476104

de Klerk, E., ’t Hoen, P.A.C., 2015. Alternative mRNA transcription, processing, and translation: insights from RNA sequencing. Trends Genet. TIG 31, 128–139. https://doi.org/10.1016/j.tig.2015.01.001

Degtyareva, A.O., Antontseva, E.V., Merkulova, T.I., 2021. Regulatory SNPs: Altered Transcription Factor Binding Sites Implicated in Complex Traits and Diseases. Int. J. Mol. Sci. 22, 6454. https://doi.org/10.3390/ijms22126454

Dehghan Manshadi, M., Tajik, F., Saeednejad Zanjani, L., Hashemi, F., Rahimi, M., Fattahi, F., Safaei, S., Madjd, Z., Ghods, R., 2025. Lower cytoplasmic expression of DDIT4 is associated with poor prognosis in gastric cancer patients. Discov. Oncol. 16, 374. https://doi.org/10.1007/s12672-025-02065-6

DeYoung, M.P., Horak, P., Sofer, A., Sgroi, D., Ellisen, L.W., 2008. Hypoxia regulates TSC1/2-mTOR signaling and tumor suppression through REDD1-mediated 14-3-3 shuttling. Genes Dev. 22, 239–251. https://doi.org/10.1101/gad.1617608

Ding, F., Hong, X., Fan, X., Huang, S., Lian, W., Chen, X., Liu, Q., Chen, Y., Gao, F., 2021. DDIT4 Novel Mutations in Pancreatic Cancer. Gastroenterol. Res. Pract. 2021, 6674404. https://doi.org/10.1155/2021/6674404

Dresios, J., Aschrafi, A., Owens, G.C., Vanderklish, P.W., Edelman, G.M., Mauro, V.P., 2005. Cold stress-induced protein Rbm3 binds 60S ribosomal subunits, alters microRNA levels, and enhances global protein synthesis. Proc. Natl. Acad. Sci. U. S. A. 102, 1865–1870. https://doi.org/10.1073/pnas.0409764102

Dufour, C.R., Scholtes, C., Yan, M., Chen, Y., Han, L., Li, T., Xia, H., Deng, Q., Vernier, M., Giguère, V., 2022. The mTOR chromatin-bound interactome in prostate cancer. Cell Rep. 38, 110534. https://doi.org/10.1016/j.celrep.2022.110534

Elliott, D.J., Dalgliesh, C., Hysenaj, G., Ehrmann, I., 2019. RBMX family proteins connect the fields of nuclear RNA processing, disease and sex chromosome biology. Int. J. Biochem. Cell Biol. 108, 1–6. https://doi.org/10.1016/j.biocel.2018.12.014

Ellisen, L.W., Ramsayer, K.D., Johannessen, C.M., Yang, A., Beppu, H., Minda, K., Oliner, J.D., McKeon, F., Haber, D.A., 2002. REDD1, a developmentally regulated transcriptional target of p63 and p53, links p63 to regulation of reactive oxygen species. Mol. Cell 10, 995–1005. https://doi.org/10.1016/s1097-2765(02)00706-2

Fan, R., Cui, C., Kang, B., Chang, Z., Wang, G., Cui, Q., 2024. A combined deep learning framework for mammalian m6A site prediction. Cell Genomics 4, 100697. https://doi.org/10.1016/j.xgen.2024.100697

Fattahi, F., Saeednejad Zanjani, L., Habibi Shams, Z., Kiani, J., Mehrazma, M., Najafi, M., Madjd, Z., 2021. High expression of DNA damage-inducible transcript 4 (DDIT4) is associated with advanced pathological features in the patients with colorectal cancer. Sci. Rep. 11, 13626. https://doi.org/10.1038/s41598-021-92720-z

Fernández-Calero, T., Davyt, M., Perelmuter, K., Chalar, C., Bampi, G., Persson, H., Tosar, J.P., Hafstað, V., Naya, H., Rovira, C., Bollati-Fogolín, M., Ehrlich, R., Flouriot, G., Ignatova, Z., Marín, M., 2020. Fine-tuning the metabolic rewiring and adaptation of translational machinery during an epithelial-mesenchymal transition in breast cancer cells. Cancer Metab. 8, 8. https://doi.org/10.1186/s40170-020-00216-7

Fitipaldi, H., Franks, P.W., 2023. Ethnic, gender and other sociodemographic biases in genome-wide association studies for the most burdensome non-communicable diseases: 2005–2022. Hum. Mol. Genet. 32, 520–532. https://doi.org/10.1093/hmg/ddac245

Fitzgerald, D.A., Doumit, M., Abel, F., 2018. Changing respiratory expectations with the new disease trajectory of nusinersen treated spinal muscular atrophy [SMA] type 1. Paediatr. Respir. Rev. 28, 11–17. https://doi.org/10.1016/j.prrv.2018.07.002

Foltyn, M., Luger, A.-L., Lorenz, N.I., Sauer, B., Mittelbronn, M., Harter, P.N., Steinbach, J.P., Ronellenfitsch, M.W., 2019. The physiological mTOR complex 1 inhibitor DDIT4 mediates therapy resistance in glioblastoma. Br. J. Cancer 120, 481–487. https://doi.org/10.1038/s41416-018-0368-3

Franks, A., Airoldi, E., Slavov, N., 2017. Post-transcriptional regulation across human tissues. PLoS Comput. Biol. 13, e1005535. https://doi.org/10.1371/journal.pcbi.1005535

Furlan, M., Galeota, E., Gaudio, N.D., Dassi, E., Caselle, M., de Pretis, S., Pelizzola, M., 2020. Genome-wide dynamics of RNA synthesis, processing, and degradation without RNA metabolic labeling. Genome Res. 30, 1492–1507. https://doi.org/10.1101/gr.260984.120

Gagnon, K.T., Li, L., Janowski, B.A., Corey, D.R., 2014. Analysis of nuclear RNA interference in human cells by subcellular fractionation and Argonaute loading. Nat. Protoc. 9, 2045–2060. https://doi.org/10.1038/nprot.2014.135

Gallouzi, I.-E., Brennan, C.M., Stenberg, M.G., Swanson, M.S., Eversole, A., Maizels, N., Steitz, J.A., 2000. HuR binding to cytoplasmic mRNA is perturbed by heat shock. Proc. Natl. Acad. Sci. U. S. A. 97, 3073–3078. https://doi.org/10.1073/pnas.97.7.3073

Gandhi, V., Plunkett, W., Cortes, J.E., 2014. Omacetaxine: a protein translation inhibitor for treatment of chronic myelogenous leukemia. Clin. Cancer Res. Off. J. Am. Assoc. Cancer Res. 20, 1735–1740. https://doi.org/10.1158/1078-0432.CCR-13-1283

Ganley, I.G., Wong, P.-M., Gammoh, N., Jiang, X., 2011. Distinct autophagosomal-lysosomal fusion mechanism revealed by thapsigargin-induced autophagy arrest. Mol. Cell 42, 731–743. https://doi.org/10.1016/j.molcel.2011.04.024

Gao, C., Wang, R., Li, B., Guo, Y., Yin, T., Xia, Y., Zhang, F., Lian, K., Liu, Y., Wang, H., Zhang, L., Gao, E., Yan, W., Tao, L., 2020. TXNIP/Redd1 signalling and excessive autophagy: a novel mechanism of myocardial ischaemia/reperfusion injury in mice. Cardiovasc. Res. 116, 645–657. https://doi.org/10.1093/cvr/cvz152

Garcia-Segura, P., Malagelada, C., 2023. STAT3 and REDD1: an unconventional story of gene repression. FEBS J. 290, 1735–1739. https://doi.org/10.1111/febs.16727

Ghetti, S., Burigotto, M., Mattivi, A., Magnani, G., Casini, A., Bianchi, A., Cereseto, A., Fava, L.L., 2021. CRISPR/Cas9 ribonucleoprotein-mediated knockin generation in hTERT-RPE1 cells. STAR Protoc. 2, 100407. https://doi.org/10.1016/j.xpro.2021.100407

Gordon, B.S., Steiner, J.L., Williamson, D.L., Lang, C.H., Kimball, S.R., 2016. Emerging role for regulated in development and DNA damage 1 (REDD1) in the regulation of skeletal muscle metabolism. Am. J. Physiol. Endocrinol. Metab. 311, E157-174. https://doi.org/10.1152/ajpendo.00059.2016

Gromadka, R., Rytka, J., 2000. The KRR1 gene encodes a protein required for 18S rRNA synthesis and 40S ribosomal subunit assembly in Saccharomyces cerevisiae. Acta Biochim. Pol. 47, 993–1005.

Guirguis, A.A., Ofir-Rosenfeld, Y., Knezevic, K., Blackaby, W., Hardick, D., Chan, Y.-C., Motazedian, A., Gillespie, A., Vassiliadis, D., Lam, E.Y.N., Tran, K., Andrews, B., Harbour, M.E., Vasiliauskaite, L., Saunders, C.J., Tsagkogeorga, G., Azevedo, A., Obacz, J., Pilka, E.S., Carkill, M., MacPherson, L., Wainwright, E.N., Liddicoat, B., Blyth, B.J., Albertella, M.R., Rausch, O., Dawson, M.A., 2023. Inhibition of METTL3 Results in a Cell-Intrinsic Interferon Response That Enhances Antitumor Immunity. Cancer Discov. 13, 2228–2247. https://doi.org/10.1158/2159-8290.CD-23-0007

Gupta, A., Gautam, P., Wennerberg, K., Aittokallio, T., 2020. A normalized drug response metric improves accuracy and consistency of anticancer drug sensitivity quantification in cell-based screening. Commun. Biol. 3, 42. https://doi.org/10.1038/s42003-020-0765-z

Hafner, M., Niepel, M., Chung, M., Sorger, P.K., 2016. Growth rate inhibition metrics correct for confounders in measuring sensitivity to cancer drugs. Nat. Methods 13, 521–527. https://doi.org/10.1038/nmeth.3853

Hahn, M.W., Wray, G.A., 2002. The g-value paradox. Evol. Dev. 4, 73–75. https://doi.org/10.1046/j.1525-142x.2002.01069.x

Hamadou, M.H., Alunno, L., Peroni, D., Pancher, M., Venturelli, T., Belli, R., Dassi, E., Romanel, A., Inga, A., 2025a. Polysomal profiling coupled to allele-specific proteomics reveals an EIF4H tranSNP allele possessing higher mRNA translation potential. https://doi.org/10.1101/2025.04.17.649328

Hamadou, M.H., Alunno, L., Venturelli, T., Valentini, S., Dalfovo, D., Lorenzini, F., Mattivi, A., Vigorito, V., Grupelli, G.P., Matte', A., Gatto, P., Pancher, M., Valentini, C., Sanctis, V.D., Bertorelli, R., Marcel, V., Cusanelli, E., Freddi, S., Bertalot, G., Zaccara, S., Mione, M., Fava, L.L., Romanel, A., Inga, A., 2025b. A TranSNP in the DDIT4 mRNA can impact its translation efficiency and modulate p53-dependent responses in cancer cells. https://doi.org/10.1101/2025.04.02.646512

Hasskarl, J., 2018. Everolimus. Recent Results Cancer Res. Fortschritte Krebsforsch. Progres Dans Rech. Sur Cancer 211, 101–123. https://doi.org/10.1007/978-3-319-91442-8_8

Hay, N., Sonenberg, N., 2004. Upstream and downstream of mTOR. Genes Dev. 18, 1926–1945. https://doi.org/10.1101/gad.1212704

Heck, A.M., Wilusz, J., 2018. The Interplay between the RNA Decay and Translation Machinery in Eukaryotes. Cold Spring Harb. Perspect. Biol. 10, a032839. https://doi.org/10.1101/cshperspect.a032839

Heinrich, B., Zhang, Z., Raitskin, O., Hiller, M., Benderska, N., Hartmann, A.M., Bracco, L., Elliott, D., Ben-Ari, S., Soreq, H., Sperling, J., Sperling, R., Stamm, S., 2009. Heterogeneous nuclear ribonucleoprotein G regulates splice site selection by binding to CC(A/C)-rich regions in pre-mRNA. J. Biol. Chem. 284, 14303–14315. https://doi.org/10.1074/jbc.M901026200

Hennessy, E.J., Moore, K.J., 2013. Using microRNA as an Alternative Treatment for Hyperlipidemia and Cardiovascular Disease: cardio-miRs in the Pipeline. J. Cardiovasc. Pharmacol. 62, 247–254. https://doi.org/10.1097/FJC.0b013e31829d48bf

Heyer, E.E., Moore, M.J., 2016. Redefining the Translational Status of 80S Monosomes. Cell 164, 757–769. https://doi.org/10.1016/j.cell.2016.01.003

Ho, D.S.W., Schierding, W., Wake, M., Saffery, R., O'Sullivan, J., 2019. Machine Learning SNP Based Prediction for Precision Medicine. Front. Genet. 10, 267. https://doi.org/10.3389/fgene.2019.00267

Ho, K.-H., Chen, P.-H., Chou, C.-M., Shih, C.-M., Lee, Y.-T., Cheng, C.-H., Chen, K.-C., 2020. A Key Role of DNA Damage-Inducible Transcript 4 (DDIT4) Connects Autophagy and GLUT3-Mediated Stemness To Desensitize Temozolomide Efficacy in Glioblastomas. Neurother. J. Am. Soc. Exp. Neurother. 17, 1212–1227. https://doi.org/10.1007/s13311-019-00826-0

Horste, E.L., Fansler, M.M., Cai, T., Chen, X., Mitschka, S., Zhen, G., Lee, F.C.Y., Ule, J., Mayr, C., 2023. Subcytoplasmic location of translation controls protein output. Mol. Cell 83, 4509-4523.e11. https://doi.org/10.1016/j.molcel.2023.11.025

Huang, S.-M.A., Mishina, Y.M., Liu, S., Cheung, A., Stegmeier, F., Michaud, G.A., Charlat, O., Wiellette, E., Zhang, Y., Wiessner, S., Hild, M., Shi, X., Wilson, C.J., Mickanin, C., Myer, V., Fazal, A., Tomlinson, R., Serluca, F., Shao, W., Cheng, H., Shultz, M., Rau, C., Schirle, M., Schlegl, J., Ghidelli, S., Fawell, S., Lu, C., Curtis, D., Kirschner, M.W., Lengauer, C., Finan, P.M., Tallarico, J.A., Bouwmeester, T., Porter, J.A., Bauer, A., Cong, F., 2009. Tankyrase inhibition stabilizes axin and antagonizes Wnt signalling. Nature 461, 614–620. https://doi.org/10.1038/nature08356

Hwang, D., Baek, S., Chang, J., Seol, T., Ku, B., Ha, H., Lee, H., Cho, S., Roh, T.-Y., Kim, Y.K., Lim, D.-S., 2024. YAP promotes global mRNA translation to fuel oncogenic growth despite starvation. Exp. Mol. Med. 56, 2202–2215. https://doi.org/10.1038/s12276-024-01316-w

Jalkanen, A.L., Wilusz, J., 2014. Stem cell RNA epigenetics: m(6)arking your territory. Cell Stem Cell 15, 669–670. https://doi.org/10.1016/j.stem.2014.11.011

Janic, A., Valente, L.J., Wakefield, M.J., Di Stefano, L., Milla, L., Wilcox, S., Yang, H., Tai, L., Vandenberg, C.J., Kueh, A.J., Mizutani, S., Brennan, M.S., Schenk, R.L., Lindqvist, L.M., Papenfuss, A.T., O'Connor, L., Strasser, A., Herold, M.J., 2018. DNA repair processes are critical mediators of p53-dependent tumor suppression. Nat. Med. 24, 947–953. https://doi.org/10.1038/s41591-018-0043-5

Jarmoskaite, I., AlSadhan, I., Vaidyanathan, P.P., Herschlag, D., 2020. How to measure and evaluate binding affinities. eLife 9, e57264. https://doi.org/10.7554/eLife.57264

Jhanwar-Uniyal, M., Wainwright, J.V., Mohan, A.L., Tobias, M.E., Murali, R., Gandhi, C.D., Schmidt, M.H., 2019. Diverse signaling mechanisms of mTOR complexes: mTORC1 and mTORC2 in forming a formidable relationship. Adv. Biol. Regul. 72, 51–62. https://doi.org/10.1016/j.jbior.2019.03.003

Jia, B., Xue, Y., Yan, X., Li, J., Wu, Y., Guo, R., Zhang, J., Zhang, L., Li, Y., Liu, Y., Sun, L., 2018. Autophagy inhibitor chloroquine induces apoptosis of cholangiocarcinoma cells via endoplasmic reticulum stress. Oncol. Lett. 16, 3509–3516. https://doi.org/10.3892/ol.2018.9131

Johansson, J., Lidéus, S., Frykholm, C., Gunnarsson, C., Mihalic, F., Gudmundsson, S., Ekvall, S., Molin, A.-M., Pham, M., Vihinen, M., Lagerstedt-Robinson, K., Nordgren, A., Jemth, P., Ameur, A., Annerén, G., Wilbe, M., Bondeson, M.-L., 2024. Gustavson syndrome is caused by an in-frame deletion in RBMX associated with potentially disturbed SH3 domain interactions. Eur. J. Hum. Genet. EJHG 32, 333–341. https://doi.org/10.1038/s41431-023-01392-y

Jung, C.H., Jun, C.B., Ro, S.-H., Kim, Y.-M., Otto, N.M., Cao, J., Kundu, M., Kim, D.-H., 2009. ULK-Atg13-FIP200 complexes mediate mTOR signaling to the autophagy machinery. Mol. Biol. Cell 20, 1992–2003. https://doi.org/10.1091/mbc.e08-12-1249

Kanhoush, R., Beenders, B., Perrin, C., Moreau, J., Bellini, M., Penrad-Mobayed, M., 2010. Novel domains in the hnRNP G/RBMX protein with distinct roles in RNA binding and targeting nascent transcripts. Nucl. Austin Tex 1, 109–122. https://doi.org/10.4161/nucl.1.1.10857

Kantor, A., McClements, M.E., MacLaren, R.E., 2020. CRISPR-Cas9 DNA Base-Editing and Prime-Editing. Int. J. Mol. Sci. 21, 6240. https://doi.org/10.3390/ijms21176240

Katiyar, S., Liu, E., Knutzen, C.A., Lang, E.S., Lombardo, C.R., Sankar, S., Toth, J.I., Petroski, M.D., Ronai, Z., Chiang, G.G., 2009. REDD1, an inhibitor of mTOR signalling, is regulated by the CUL4A-DDB1 ubiquitin ligase. EMBO Rep. 10, 866–872. https://doi.org/10.1038/embor.2009.93

Khong, A., Matheny, T., Jain, S., Mitchell, S.F., Wheeler, J.R., Parker, R., 2017. The Stress Granule Transcriptome Reveals Principles of mRNA Accumulation in Stress Granules. Mol. Cell 68, 808-820.e5. https://doi.org/10.1016/j.molcel.2017.10.015

Kim, W., Kyung Lee, E., 2012. Post-transcriptional regulation in metabolic diseases. RNA Biol. 9, 772–780. https://doi.org/10.4161/rna.20091

Kimball, S.R., Do, A.N.D., Kutzler, L., Cavener, D.R., Jefferson, L.S., 2008. Rapid turnover of the mTOR complex 1 (mTORC1) repressor REDD1 and activation of mTORC1 signaling following inhibition of protein synthesis. J. Biol. Chem. 283, 3465–3475. https://doi.org/10.1074/jbc.M706643200

Kimmel, C.B., Ballard, W.W., Kimmel, S.R., Ullmann, B., Schilling, T.F., 1995. Stages of embryonic development of the zebrafish. Dev. Dyn. Off. Publ. Am. Assoc. Anat. 203, 253–310. https://doi.org/10.1002/aja.1002030302

Klionsky, D.J., Abdalla, F.C., Abeliovich, H., Abraham, R.T., Acevedo-Arozena, A., Adeli, K., Agholme, L., Agnello, M., Agostinis, P., Aguirre-Ghiso, J.A., Ahn, H.J., Ait-Mohamed, O., Ait-Si-Ali, S., Akematsu, T., Akira, S., Al-Younes, H.M., Al-Zeer, M.A., Albert, M.L., Albin, R.L., Alegre-Abarrategui, J., Aleo, M.F., Alirezaei, M., Almasan, A., Almonte-Becerril, M., Amano, A., Amaravadi, R., Amarnath, S., Amer, A.O., Andrieu-Abadie, N., Anantharam, V., Ann, D.K., Anoopkumar-Dukie, S., Aoki, H., Apostolova, N., Arancia, G., Aris, J.P., Asanuma, K., Asare, N.Y.O., Ashida, H., Askanas, V., Askew, D.S., Auberger, P., Baba, M., Backues, S.K., Baehrecke, E.H., Bahr, B.A., Bai, X.-Y., Bailly, Y., Baiocchi, R., Baldini, G., Balduini, W., Ballabio, A., Bamber, B.A., Bampton, E.T.W., Bánhegyi, G., Bartholomew, C.R., Bassham, D.C., Bast, R.C., Batoko, H., Bay, B.-H., Beau, I., Béchet, D.M., Begley, T.J., Behl, C., Behrends, C., Bekri, S., Bellaire, B., Bendall, L.J., Benetti, L., Berliocchi, L., Bernardi, H., Bernassola, F., Besteiro, S., Bhatia-Kissova, I., Bi, X., Biard-Piechaczyk, M., Blum, J.S., Boise, L.H., Bonaldo, P., Boone, D.L., Bornhauser, B.C., Bortoluci, K.R., Bossis, I., Bost, F., Bourquin, J.-P., Boya, P., Boyer-Guittaut, M., Bozhkov, P.V., Brady, N.R., Brancolini, C., Brech, A., Brenman, J.E., Brennand, A., Bresnick, E.H., Brest, P., Bridges, D., Bristol, M.L., Brookes, P.S., Brown, E.J., Brumell, J.H., Brunetti-Pierri, N., Brunk, U.T., Bulman, D.E., Bultman, S.J., Bultynck, G., Burbulla, L.F., Bursch, W., Butchar, J.P., Buzgariu, W., Bydlowski, S.P., Cadwell, K., Cahová, M., Cai, D., Cai, J., Cai, Q., Calabretta, B., Calvo-Garrido, J., Camougrand, N., Campanella, M., Campos-Salinas, J., Candi, E., Cao, L., Caplan, A.B., Carding, S.R., Cardoso, S.M., Carew, J.S., Carlin, C.R., Carmignac, V., Carneiro, L.A.M., Carra, S., Caruso, R.A., Casari, G., Casas, C., Castino,

R., Cebollero, E., Cecconi, F., Celli, J., Chaachouay, H., Chae, H.-J., Chai, C.-Y., Chan, D.C., Chan, E.Y., Chang, R.C.-C., Che, C.-M., Chen, C.-C., Chen, G.-C., Chen, G.-Q., Chen, M., Chen, Q., Chen, S.S.-L., Chen, W., Chen, Xi, Chen, Xiangmei, Chen, Xiequn, Chen, Y.-G., Chen, Yingyu, Chen, Yongqiang, Chen, Y.-J., Chen, Z., Cheng, A., Cheng, C.H.K., Cheng, Y., Cheong, H., Cheong, J.-H., Cherry, S., Chess-Williams, R., Cheung, Z.H., Chevet, E., Chiang, H.-L., Chiarelli, R., Chiba, T., Chin, L.-S., Chiou, S.-H., Chisari, F.V., Cho, C.H., Cho, D.-H., Choi, A.M.K., Choi, D., Choi, K.S., Choi, M.E., Chouaib, S., Choubey, D., Choubey, V., Chu, C.T., Chuang, T.-H., Chueh, S.-H., Chun, T., Chwae, Y.-J., Chye, M.-L., Ciarcia, R., Ciriolo, M.R., Clague, M.J., Clark, R.S.B., Clarke, P.G.H., Clarke, R., Codogno, P., Coller, H.A., Colombo, M.I., Comincini, S., Condello, M., Condorelli, F., Cookson, M.R., Coombs, G.H., Coppens, I., Corbalan, R., Cossart, P., Costelli, P., Costes, S., Coto-Montes, A., Couve, E., Coxon, F.P., Cregg, J.M., Crespo, J.L., Cronjé, M.J., Cuervo, A.M., Cullen, J.J., Czaja, M.J., D'Amelio, M., Darfeuille-Michaud, A., Davids, L.M., Davies, F.E., De Felici, M., de Groot, J.F., de Haan, C.A.M., De Martino, L., De Milito, A., De Tata, V., Debnath, J., Degterev, A., Dehay, B., Delbridge, L.M.D., Demarchi, F., Deng, Y.Z., Dengjel, J., Dent, P., Denton, D., Deretic, V., Desai, S.D., Devenish, R.J., Di Gioacchino, M., Di Paolo, G., Di Pietro, C., Díaz-Araya, G., Díaz-Laviada, I., Diaz-Meco, M.T., Diaz-Nido, J., Dikic, I., Dinesh-Kumar, S.P., Ding, W.-X., Distelhorst, C.W., Diwan, A., Djavaheri-Mergny, M., Dokudovskaya, S., Dong, Z., Dorsey, F.C., Dosenko, V., Dowling, J.J., Doxsey, S., Dreux, M., Drew, M.E., Duan, Q., Duchosal, M.A., Duff, K., Dugail, I., Durbeej, M., Duszenko, M., Edelstein, C.L., Edinger, A.L., Egea, G., Eichinger, L., Eissa, N.T., Ekmekcioglu, S., El-Deiry, W.S., Elazar, Z., Elgendy, M., Ellerby, L.M., Eng, K.E., Engelbrecht, A.-M., Engelender, S., Erenpreisa, J., Escalante, R., Esclatine, A., Eskelinen, E.-L., Espert, L., Espina, V., Fan, H., Fan, J., Fan, Q.-W., Fan, Z., Fang, S., Fang, Y., Fanto, M., Fanzani, A., Farkas, T., Farré, J.-C., Faure, M., Fechheimer, M., Feng, C.G., Feng, J., Feng, Q., Feng, Y., Fésüs, L., Feuer, R., Figueiredo-Pereira, M.E., Fimia, G.M., Fingar, D.C., Finkbeiner, S., Finkel, T., Finley, K.D., Fiorito, F., Fisher, E.A., Fisher, P.B., Flajolet, M., Florez-McClure, M.L., Florio, S., Fon, E.A., Fornai, F., Fortunato, F., Fotedar, R., Fowler, D.H., Fox, H.S., Franco, R., Frankel, L.B., Fransen, M., Fuentes, J.M., Fueyo, J., Fujii, J., Fujisaki, K., Fujita, E., Fukuda, M., Furukawa, R.H., Gaestel, M., Gailly, P., Gajewska, M., Galliot, B., Galy, V., Ganesh, S., Ganetzky, B., Ganley, I.G., Gao, F.-B., Gao, G.F., Gao, J., Garcia, L., Garcia-Manero, G., Garcia-Marcos, M., Garmyn, M., Gartel, A.L., Gatti, E., Gautel, M., Gawriluk, T.R., Gegg, M.E., Geng, J., Germain, M., Gestwicki, J.E., Gewirtz, D.A., Ghavami, S., Ghosh, P., Giammarioli, A.M., Giatromanolaki, A.N., Gibson, S.B., Gilkerson, R.W., Ginger, M.L., Ginsberg, H.N., Golab, J., Goligorsky, M.S., Golstein, P., Gomez-Manzano, C., Goncu, E., Gongora, C., Gonzalez, C.D., Gonzalez, R., González-Estévez, C., González-Polo, R.A., Gonzalez-Rey, E., Gorbunov, N.V., Gorski, S., Goruppi, S., Gottlieb, R.A., Gozuacik, D., Granato, G.E., Grant, G.D., Green, K.N., Gregorc, A., Gros, F., Grose, C., Grunt, T.W., Gual, P., Guan, J.-L., Guan, K.-L., Guichard, S.M., Gukovskaya, A.S., Gukovsky, I., Gunst, J., Gustafsson, A.B., Halayko, A.J., Hale, A.N., Halonen, S.K., Hamasaki, M., Han, F., Han, T., Hancock, M.K., Hansen, M., Harada, H., Harada, M., Hardt, S.E., Harper, J.W., Harris, A.L., Harris, J., Harris, S.D., Hashimoto, M., Haspel, J.A., Hayashi, S., Hazelhurst, L.A., He, C., He, Y.-W., Hébert, M.-J., Heidenreich, K.A., Helfrich, M.H., Helgason, G.V., Henske, E.P., Herman, B., Herman, P.K., Hetz, C., Hilfiker, S., Hill, J.A., Hocking, L.J., Hofman, P., Hofmann, T.G., Höhfeld, J., Holyoake, T.L., Hong, M.-H., Hood, D.A., Hotamisligil, G.S., Houwerzijl, E.J., Høyer-Hansen, M., Hu, B., Hu, C.-A.A., Hu, H.-M., Hua, Y., Huang, C., Huang, J., Huang, S., Huang, W.-P., Huber, T.B., Huh, W.-K., Hung, T.-H., Hupp, T.R., Hur, G.M.,

Hurley, J.B., Hussain, S.N.A., Hussey, P.J., Hwang, J.J., Hwang, S., Ichihara, A., Ilkhanizadeh, S., Inoki, K., Into, T., Iovane, V., Iovanna, J.L., Ip, N.Y., Isaka, Y., Ishida, H., Isidoro, C., Isobe, K., Iwasaki, A., Izquierdo, M., Izumi, Y., Jaakkola, P.M., Jäättelä, M., Jackson, G.R., Jackson, W.T., Janji, B., Jendrach, M., Jeon, J.-H., Jeung, E.-B., Jiang, Hong, Jiang, Hongchi, Jiang, J.X., Jiang, M., Jiang, Q., Jiang, X., Jiang, X., Jiménez, A., Jin, M., Jin, S., Joe, C.O., Johansen, T., Johnson, D.E., Johnson, G.V.W., Jones, N.L., Joseph, B., Joseph, S.K., Joubert, A.M., Juhász, G., Juillerat-Jeanneret, L., Jung, C.H., Jung, Y.-K., Kaarniranta, K., Kaasik, A., Kabuta, T., Kadowaki, M., Kagedal, K., Kamada, Y., Kaminskyy, V.O., Kampinga, H.H., Kanamori, H., Kang, C., Kang, K.B., Kang, K.I., Kang, R., Kang, Y.-A., Kanki, T., Kanneganti, T.-D., Kanno, H., Kanthasamy, A.G., Kanthasamy, A., Karantza, V., Kaushal, G.P., Kaushik, S., Kawazoe, Y., Ke, P.-Y., Kehrl, J.H., Kelekar, A., Kerkhoff, C., Kessel, D.H., Khalil, H., Kiel, J.A.K.W., Kiger, A.A., Kihara, A., Kim, D.R., Kim, Do-Hyung, Kim, Dong-Hou, Kim, E.-K., Kim, H.-R., Kim, J.-S., Kim, J.H., Kim, J.C., Kim, J.K., Kim, P.K., Kim, S.W., Kim, Y.-S., Kim, Y., Kimchi, A., Kimmelman, A.C., King, J.S., Kinsella, T.J., Kirkin, V., Kirshenbaum, L.A., Kitamoto, K., Kitazato, K., Klein, L., Klimecki, W.T., Klucken, J., Knecht, E., Ko, B.C.B., Koch, J.C., Koga, H., Koh, J.-Y., Koh, Y.H., Koike, M., Komatsu, M., Kominami, E., Kong, H.J., Kong, W.-J., Korolchuk, V.I., Kotake, Y., Koukourakis, M.I., Kouri Flores, J.B., Kovács, A.L., Kraft, C., Krainc, D., Krämer, H., Kretz-Remy, C., Krichevsky, A.M., Kroemer, G., Krüger, R., Krut, O., Ktistakis, N.T., Kuan, C.-Y., Kucharczyk, R., Kumar, A., Kumar, R., Kumar, S., Kundu, M., Kung, H.-J., Kurz, T., Kwon, H.J., La Spada, A.R., Lafont, F., Lamark, T., Landry, J., Lane, J.D., Lapaquette, P., Laporte, J.F., László, L., Lavandero, S., Lavoie, J.N., Layfield, R., Lazo, P.A., Le, W., Le Cam, L., Ledbetter, D.J., Lee, A.J.X., Lee, B.-W., Lee, G.M., Lee, J., Lee, J.-H., Lee, M., Lee, M.-S., Lee, S.H., Leeuwenburgh, C., Legembre, P., Legouis, R., Lehmann, M., Lei, H.-Y., Lei, Q.-Y., Leib, D.A., Leiro, J., Lemasters, J.J., Lemoine, A., Lesniak, M.S., Lev, D., Levenson, V.V., Levine, B., Levy, E., Li, F., Li, J.-L., Li, L., Li, S., Li, W., Li, X.-J., Li, Y., Li, Y.-P., Liang, C., Liang, Q., Liao, Y.-F., Liberski, P.P., Lieberman, A., Lim, H.J., Lim, K.-L., Lim, K., Lin, C.-F., Lin, F.-C., Lin, J., Lin, J.D., Lin, K., Lin, W.-W., Lin, W.-C., Lin, Y.-L., Linden, R., Lingor, P., Lippincott-Schwartz, J., Lisanti, M.P., Liton, P.B., Liu, B., Liu, C.-F., Liu, K., Liu, L., Liu, Q.A., Liu, W., Liu, Y.-C., Liu, Y., Lockshin, R.A., Lok, C.-N., Lonial, S., Loos, B., Lopez-Berestein, G., López-Otín, C., Lossi, L., Lotze, M.T., Lőw, P., Lu, Binfeng, Lu, Bingwei, Lu, Bo, Lu, Z., Luciano, F., Lukacs, N.W., Lund, A.H., Lynch-Day, M.A., Ma, Y., Macian, F., MacKeigan, J.P., Macleod, K.F., Madeo, F., Maiuri, L., Maiuri, M.C., Malagoli, D., Malicdan, M.C.V., Malorni, W., Man, N., Mandelkow, E.-M., Manon, S., Manov, I., Mao, K., Mao, X., Mao, Z., Marambaud, P., Marazziti, D., Marcel, Y.L., Marchbank, K., Marchetti, P., Marciniak, S.J., Marcondes, M., Mardi, M., Marfe, G., Mariño, G., Markaki, M., Marten, M.R., Martin, S.J., Martinand-Mari, C., Martinet, W., Martinez-Vicente, M., Masini, M., Matarrese, P., Matsuo, S., Matteoni, R., Mayer, A., Mazure, N.M., McConkey, D.J., McConnell, M.J., McDermott, C., McDonald, C., McInerney, G.M., McKenna, S.L., McLaughlin, B., McLean, P.J., McMaster, C.R., McQuibban, G.A., Meijer, A.J., Meisler, M.H., Meléndez, A., Melia, T.J., Melino, G., Mena, M.A., Menendez, J.A., Menna-Barreto, R.F.S., Menon, M.B., Menzies, F.M., Mercer, C.A., Merighi, A., Merry, D.E., Meschini, S., Meyer, C.G., Meyer, T.F., Miao, C.-Y., Miao, J.-Y., Michels, P.A.M., Michiels, C., Mijaljica, D., Milojkovic, A., Minucci, S., Miracco, C., Miranti, C.K., Mitroulis, I., Miyazawa, K., Mizushima, N., Mograbi, B., Mohseni, S., Molero, X., Mollereau, B., Mollinedo, F., Momoi, T., Monastyrska, I., Monick, M.M., Monteiro, M.J., Moore, M.N., Mora, R., Moreau, K., Moreira, P.I., Moriyasu, Y., Moscat, J., Mostowy, S., Mottram, J.C., Motyl, T., Moussa, C.E.-H., Müller, S., Muller, S., Münger, K., Münz, C., Murphy, L.O., Murphy, M.E., Musarò, A.,

Mysorekar, I., Nagata, E., Nagata, K., Nahimana, A., Nair, U., Nakagawa, T., Nakahira, K., Nakano, H., Nakatogawa, H., Nanjundan, M., Naqvi, N.I., Narendra, D.P., Narita, M., Navarro, M., Nawrocki, S.T., Nazarko, T.Y., Nemchenko, A., Netea, M.G., Neufeld, T.P., Ney, P.A., Nezis, I.P., Nguyen, H.P., Nie, D., Nishino, I., Nislow, C., Nixon, R.A., Noda, T., Noegel, A.A., Nogalska, A., Noguchi, S., Notterpek, L., Novak, I., Nozaki, T., Nukina, N., Nürnberger, T., Nyfeler, B., Obara, K., Oberley, T.D., Oddo, S., Ogawa, M., Ohashi, T., Okamoto, K., Oleinick, N.L., Oliver, F.J., Olsen, L.J., Olsson, S., Opota, O., Osborne, T.F., Ostrander, G.K., Otsu, K., Ou, J.J., Ouimet, M., Overholtzer, M., Ozpolat, B., Paganetti, P., Pagnini, U., Pallet, N., Palmer, G.E., Palumbo, C., Pan, T., Panaretakis, T., Pandey, U.B., Papackova, Z., Papassideri, I., Paris, I., Park, J., Park, O.K., Parys, J.B., Parzych, K.R., Patschan, S., Patterson, C., Pattingre, S., Pawelek, J.M., Peng, J., Perlmutter, D.H., Perrotta, I., Perry, G., Pervaiz, S., Peter, M., Peters, G.J., Petersen, M., Petrovski, G., Phang, J.M., Piacentini, M., Pierre, P., Pierrefite-Carle, V., Pierron, G., Pinkas-Kramarski, R., Piras, A., Piri, N., Platanias, L.C., Pöggeler, S., Poirot, M., Poletti, A., Poüs, C., Pozuelo-Rubio, M., Prætorius-Ibba, M., Prasad, A., Prescott, M., Priault, M., Produit-Zengaffinen, N., Progulske-Fox, A., Proikas-Cezanne, T., Przedborski, S., Przyklenk, K., Puertollano, R., Puyal, J., Qian, S.-B., Qin, L., Qin, Z.-H., Quaggin, S.E., Raben, N., Rabinowich, H., Rabkin, S.W., Rahman, I., Rami, A., Ramm, G., Randall, G., Randow, F., Rao, V.A., Rathmell, J.C., Ravikumar, B., Ray, S.K., Reed, B.H., Reed, J.C., Reggiori, F., Régnier-Vigouroux, A., Reichert, A.S., Reiners, J.J., Reiter, R.J., Ren, J., Revuelta, J.L., Rhodes, C.J., Ritis, K., Rizzo, E., Robbins, J., Roberge, M., Roca, H., Roccheri, M.C., Rocchi, S., Rodemann, H.P., Rodríguez de Córdoba, S., Rohrer, B., Roninson, I.B., Rosen, K., Rost-Roszkowska, M.M., Rouis, M., Rouschop, K.M.A., Rovetta, F., Rubin, B.P., Rubinsztein, D.C., Ruckdeschel, K., Rucker, E.B., Rudich, A., Rudolf, E., Ruiz-Opazo, N., Russo, R., Rusten, T.E., Ryan, K.M., Ryter, S.W., Sabatini, D.M., Sadoshima, J., Saha, T., Saitoh, T., Sakagami, H., Sakai, Y., Salekdeh, G.H., Salomoni, P., Salvaterra, P.M., Salvesen, G., Salvioli, R., Sanchez, A.M.J., Sánchez-Alcázar, J.A., Sánchez-Prieto, R., Sandri, M., Sankar, U., Sansanwal, P., Santambrogio, L., Saran, S., Sarkar, S., Sarwal, M., Sasakawa, C., Sasnauskiene, A., Sass, M., Sato, K., Sato, M., Schapira, A.H.V., Scharl, M., Schätzl, H.M., Scheper, W., Schiaffino, S., Schneider, C., Schneider, M.E., Schneider-Stock, R., Schoenlein, P.V., Schorderet, D.F., Schüller, C., Schwartz, G.K., Scorrano, L., Sealy, L., Seglen, P.O., Segura-Aguilar, J., Seiliez, I., Seleverstov, O., Sell, C., Seo, J.B., Separovic, D., Setaluri, V., Setoguchi, T., Settembre, C., Shacka, J.J., Shanmugam, M., Shapiro, I.M., Shaulian, E., Shaw, R.J., Shelhamer, J.H., Shen, H.-M., Shen, W.-C., Sheng, Z.-H., Shi, Y., Shibuya, K., Shidoji, Y., Shieh, J.-J., Shih, C.-M., Shimada, Y., Shimizu, S., Shintani, T., Shirihai, O.S., Shore, G.C., Sibirny, A.A., Sidhu, S.B., Sikorska, B., Silva-Zacarin, E.C.M., Simmons, A., Simon, A.K., Simon, H.-U., Simone, C., Simonsen, A., Sinclair, D.A., Singh, R., Sinha, D., Sinicrope, F.A., Sirko, A., Siu, P.M., Sivridis, E., Skop, V., Skulachev, V.P., Slack, R.S., Smaili, S.S., Smith, D.R., Soengas, M.S., Soldati, T., Song, X., Sood, A.K., Soong, T.W., Sotgia, F., Spector, S.A., Spies, C.D., Springer, W., Srinivasula, S.M., Stefanis, L., Steffan, J.S., Stendel, R., Stenmark, H., Stephanou, A., Stern, S.T., Sternberg, C., Stork, B., Strålfors, P., Subauste, C.S., Sui, X., Sulzer, D., Sun, J., Sun, S.-Y., Sun, Z.-J., Sung, J.J.Y., Suzuki, K., Suzuki, T., Swanson, M.S., Swanton, C., Sweeney, S.T., Sy, L.-K., Szabadkai, G., Tabas, I., Taegtmeyer, H., Tafani, M., Takács-Vellai, K., Takano, Y., Takegawa, K., Takemura, G., Takeshita, F., Talbot, N.J., Tan, K.S.W., Tanaka, Keiji, Tanaka, Kozo, Tang, Daolin, Tang, Dingzhong, Tanida, I., Tannous, B.A., Tavernarakis, N., Taylor, G.S., Taylor, G.A., Taylor, J.P., Terada, L.S., Terman, A., Tettamanti, G., Thevissen, K., Thompson, C.B., Thorburn, A., Thumm,

M., Tian, F., Tian, Y., Tocchini-Valentini, G., Tolkovsky, A.M., Tomino, Y., Tönges, L., Tooze, S.A., Tournier, C., Tower, J., Towns, R., Trajkovic, V., Travassos, L.H., Tsai, T.-F., Tschan, M.P., Tsubata, T., Tsung, A., Turk, B., Turner, L.S., Tyagi, S.C., Uchiyama, Y., Ueno, T., Umekawa, M., Umemiya-Shirafuji, R., Unni, V.K., Vaccaro, M.I., Valente, E.M., Van den Berghe, G., van der Klei, I.J., van Doorn, W., van Dyk, L.F., van Egmond, M., van Grunsven, L.A., Vandenabeele, P., Vandenberghe, W.P., Vanhorebeek, I., Vaquero, E.C., Velasco, G., Vellai, T., Vicencio, J.M., Vierstra, R.D., Vila, M., Vindis, C., Viola, G., Viscomi, M.T., Voitsekhovskaja, O.V., von Haefen, C., Votruba, M., Wada, K., Wade-Martins, R., Walker, C.L., Walsh, C.M., Walter, J., Wan, X.-B., Wang, A., Wang, C., Wang, D., Wang, Fan, Wang, Fen, Wang, G., Wang, H., Wang, H.-G., Wang, H.-D., Wang, J., Wang, K., Wang, M., Wang, R.C., Wang, Xinglong, Wang, Xuejun, Wang, Y.-J., Wang, Y., Wang, Zhen, Wang, Z.C., Wang, Zhinong, Wansink, D.G., Ward, D.M., Watada, H., Waters, S.L., Webster, P., Wei, L., Weihl, C.C., Weiss, W.A., Welford, S.M., Wen, L.-P., Whitehouse, C.A., Whitton, J.L., Whitworth, A.J., Wileman, T., Wiley, J.W., Wilkinson, S., Willbold, D., Williams, R.L., Williamson, P.R., Wouters, B.G., Wu, C., Wu, D.-C., Wu, W.K.K., Wyttenbach, A., Xavier, R.J., Xi, Z., Xia, P., Xiao, G., Xie, Zhiping, Xie, Zhonglin, Xu, D., Xu, J., Xu, L., Xu, X., Yamamoto, Ai, Yamamoto, Akitsugu, Yamashina, S., Yamashita, M., Yan, X., Yanagida, M., Yang, D.-S., Yang, E., Yang, J.-M., Yang, S.Y., Yang, W., Yang, W.Y., Yang, Z., Yao, M.-C., Yao, T.-P., Yeganeh, B., Yen, W.-L., Yin, J., Yin, X.-M., Yoo, O.-J., Yoon, G., Yoon, S.-Y., Yorimitsu, T., Yoshikawa, Y., Yoshimori, T., Yoshimoto, K., You, H.J., Youle, R.J., Younes, A., Yu, Li, Yu, Long, Yu, S.-W., Yu, W.H., Yuan, Z.-M., Yue, Z., Yun, C.-H., Yuzaki, M., Zabirnyk, O., Silva-Zacarin, E., Zacks, D., Zacksenhaus, E., Zaffaroni, N., Zakeri, Z., Zeh, H.J., Zeitlin, S.O., Zhang, H., Zhang, H.-L., Zhang, J., Zhang, J.-P., Zhang, Lin, Zhang, Long, Zhang, M.-Y., Zhang, X.D., Zhao, M., Zhao, Y.-F., Zhao, Y., Zhao, Z.J., Zheng, X., Zhivotovsky, B., Zhong, Q., Zhou, C.-Z., Zhu, C., Zhu, W.-G., Zhu, X.-F., Zhu, X., Zhu, Y., Zoladek, T., Zong, W.-X., Zorzano, A., Zschocke, J., Zuckerbraun, B., 2012. Guidelines for the use and interpretation of assays for monitoring autophagy. Autophagy 8, 445–544. https://doi.org/10.4161/auto.19496

Kong, Z., Lu, Y., Yang, Y., Chang, K., Lin, Y., Huang, Y., Wang, C., Zhang, L., Xu, W., Zhao, S., Li, Y., 2023. m6A-Mediated Biogenesis of circDDIT4 Inhibits Prostate Cancer Progression by Sequestrating ELAVL1/HuR. Mol. Cancer Res. MCR 21, 1342–1355. https://doi.org/10.1158/1541-7786.MCR-22-0271

Kriachkov, V., Ormsby, A.R., Kusnadi, E.P., McWilliam, H.E.G., Mintern, J.D., Amarasinghe, S.L., Ritchie, M.E., Furic, L., Hatters, D.M., 2023. Arginine-rich C9ORF72 ALS proteins stall ribosomes in a manner distinct from a canonical ribosome-associated quality control substrate. J. Biol. Chem. 299, 102774. https://doi.org/10.1016/j.jbc.2022.102774

Kruglyak, L., Nickerson, D.A., 2001. Variation is the spice of life. Nat. Genet. 27, 234–236. https://doi.org/10.1038/85776

Kucejova, B., Peña-Llopis, S., Yamasaki, T., Sivanand, S., Tran, T.A.T., Alexander, S., Wolff, N.C., Lotan, Y., Xie, X.-J., Kabbani, W., Kapur, P., Brugarolas, J., 2011. Interplay between pVHL and mTORC1 pathways in clear-cell renal cell carcinoma. Mol. Cancer Res. MCR 9, 1255–1265. https://doi.org/10.1158/1541-7786.MCR-11-0302

Kurosaki, T., Cho, H., Abshire, E.T., Pröschel, C., Mitsutomi, S., Sato, H., Simko, E.A.J., Fraser, C.S., Sakano, H., Maquat, L.E., 2025. FMRP drives mRNP targets into translationally silenced complexes. Mol. Cell S1097-2765(25)00512-X. https://doi.org/10.1016/j.molcel.2025.06.012

Laham-Karam, N., Pinto, G.P., Poso, A., Kokkonen, P., 2020. Transcription and Translation Inhibitors in Cancer Treatment. Front. Chem. 8, 276. https://doi.org/10.3389/fchem.2020.00276

Lahiri, V., Hawkins, W.D., Klionsky, D.J., 2019. Watch What You (Self-) Eat: Autophagic Mechanisms that Modulate Metabolism. Cell Metab. 29, 803–826. https://doi.org/10.1016/j.cmet.2019.03.003

Landi, D., Gemignani, F., Naccarati, A., Pardini, B., Vodicka, P., Vodickova, L., Novotny, J., Försti, A., Hemminki, K., Canzian, F., Landi, S., 2008. Polymorphisms within micro-RNA-binding sites and risk of sporadic colorectal cancer. Carcinogenesis 29, 579–584. https://doi.org/10.1093/carcin/bgm304

Lee, T.I., Young, R.A., 2013. Transcriptional regulation and its misregulation in disease. Cell 152, 1237–1251. https://doi.org/10.1016/j.cell.2013.02.014

Li, C., Jiang, Z., Hao, J., Liu, D., Hu, H., Gao, Y., Wang, D., 2021. Role of N6-methyl-adenosine modification in mammalian embryonic development. Genet. Mol. Biol. 44, e20200253. https://doi.org/10.1590/1678-4685-GMB-2020-0253

Li, D., Qian, L., Du, Y., Liu, L., Sun, Z., Han, Y., Guo, X., Shen, C., Zhang, Z., Liu, X., 2025. METTL14-mediated m6A modification of DDIT4 promotes its mRNA stability in aging-related idiopathic pulmonary fibrosis. Epigenetics 20, 2462898. https://doi.org/10.1080/15592294.2025.2462898

Limbu, M.S., Xiong, T., Wang, S., 2024. A review of Ribosome profiling and tools used in Ribo-seq data analysis. Comput. Struct. Biotechnol. J. 23, 1912–1918. https://doi.org/10.1016/j.csbj.2024.04.051

Lin, Y.-J., Huang, L.-H., Huang, C.-T., 2013. Enhancement of heterologous gene expression in Flammulina velutipes using polycistronic vectors containing a viral 2A cleavage sequence. PloS One 8, e59099. https://doi.org/10.1371/journal.pone.0059099

Liu, J., Zheng, T., Chen, D., Huang, J., Zhao, Y., Ma, W., Liu, H., 2023. RBMX involves in telomere stability maintenance by regulating TERRA expression. PLoS Genet. 19, e1010937. https://doi.org/10.1371/journal.pgen.1010937

Liu, N., Zhou, K.I., Parisien, M., Dai, Q., Diatchenko, L., Pan, T., 2017. N6-methyladenosine alters RNA structure to regulate binding of a low-complexity protein. Nucleic Acids Res. 45, 6051–6063. https://doi.org/10.1093/nar/gkx141

Liu, Y., 2020. A code within the genetic code: codon usage regulates co-translational protein folding. Cell Commun. Signal. CCS 18, 145. https://doi.org/10.1186/s12964-020-00642-6

Loayza-Puch, F., Drost, J., Rooijers, K., Lopes, R., Elkon, R., Agami, R., 2013. p53 induces transcriptional and translational programs to suppress cell proliferation and growth. Genome Biol. 14, R32. https://doi.org/10.1186/gb-2013-14-4-r32

Lorenzini, F., Marines, J., Le Friec, J., Do Khoa, N., Nieto, M.A., Sanchez-Laorden, B., Mione, M.C., Fontenille, L., Kissa, K., 2025. Melanoma innervation, noradrenaline and cancer progression in zebrafish xenograft model. Cell Death Discov. 11, 260. https://doi.org/10.1038/s41420-025-02523-8

Louro, M.A.D., Peneda, C., Bank, C., Bettencourt-Dias, M., 2024a. Adaptation of human cell populations to different levels of centriole amplification involves a two-step response. https://doi.org/10.1101/2024.02.15.580424

Louro, M.A.D., Peneda, C., Bank, C., Bettencourt-Dias, M., 2024b. Adaptation of human cell populations to different levels of centriole amplification involves a two-step response. https://doi.org/10.1101/2024.02.15.580424

Maiuri, M.C., Zalckvar, E., Kimchi, A., Kroemer, G., 2007. Self-eating and self-killing: crosstalk between autophagy and apoptosis. Nat. Rev. Mol. Cell Biol. 8, 741–752. https://doi.org/10.1038/nrm2239

Mandic, M., Paunovic, V., Vucicevic, L., Kosic, M., Mijatovic, S., Trajkovic, V., Harhaji-Trajkovic, L., 2024. No energy, no autophagy—Mechanisms and therapeutic implications of autophagic response energy requirements. J. Cell. Physiol. 239, e31366. https://doi.org/10.1002/jcp.31366

Manolio, T.A., Collins, F.S., Cox, N.J., Goldstein, D.B., Hindorff, L.A., Hunter, D.J., McCarthy, M.I., Ramos, E.M., Cardon, L.R., Chakravarti, A., Cho, J.H., Guttmacher, A.E., Kong, A., Kruglyak, L., Mardis, E., Rotimi, C.N., Slatkin, M., Valle, D., Whittemore, A.S., Boehnke, M., Clark, A.G., Eichler, E.E., Gibson, G., Haines, J.L., Mackay, T.F.C., McCarroll, S.A., Visscher, P.M., 2009. Finding the missing heritability of complex diseases. Nature 461, 747–753. https://doi.org/10.1038/nature08494

Marcel, V., Catez, F., Diaz, J.-J., 2015. p53, a translational regulator: contribution to its tumour-suppressor activity. Oncogene 34, 5513–5523. https://doi.org/10.1038/onc.2015.25

Marcel, V., Nguyen Van Long, F., Diaz, J.-J., 2018. 40 Years of Research Put p53 in Translation. Cancers 10, 152. https://doi.org/10.3390/cancers10050152

Marines, J., Lorenzini, F., Kissa, K., Fontenille, L., 2023. Modelling 3D Tumour Microenvironment In Vivo: A Tool to Predict Cancer Fate. Curr. Issues Mol. Biol. 45, 9076–9083. https://doi.org/10.3390/cimb45110569

Marintchev, A., Edmonds, K.A., Marintcheva, B., Hendrickson, E., Oberer, M., Suzuki, C., Herdy, B., Sonenberg, N., Wagner, G., 2009. Topology and regulation of the human eIF4A/4G/4H helicase complex in translation initiation. Cell 136, 447–460. https://doi.org/10.1016/j.cell.2009.01.014

Mas, S., Gassó, P., Ritter, M.A., Malagelada, C., Bernardo, M., Lafuente, A., 2015. Pharmacogenetic predictor of extrapyramidal symptoms induced by antipsychotics: multilocus interaction in the mTOR pathway. Eur. Neuropsychopharmacol. J. Eur. Coll. Neuropsychopharmacol. 25, 51–59. https://doi.org/10.1016/j.euroneuro.2014.11.011

Maston, G.A., Evans, S.K., Green, M.R., 2006. Transcriptional regulatory elements in the human genome. Annu. Rev. Genomics Hum. Genet. 7, 29–59. https://doi.org/10.1146/annurev.genom.7.080505.115623

Matheny, T., Rao, B.S., Parker, R., 2019. Transcriptome-Wide Comparison of Stress Granules and P-Bodies Reveals that Translation Plays a Major Role in RNA Partitioning. Mol. Cell. Biol. 39, e00313-19. https://doi.org/10.1128/MCB.00313-19

Matheny, T., Van Treeck, B., Huynh, T.N., Parker, R., 2021. RNA partitioning into stress granules is based on the summation of multiple interactions. RNA N. Y. N 27, 174–189. https://doi.org/10.1261/rna.078204.120

Mauthe, M., Orhon, I., Rocchi, C., Zhou, X., Luhr, M., Hijlkema, K.-J., Coppes, R.P., Engedal, N., Mari, M., Reggiori, F., 2018. Chloroquine inhibits autophagic flux by decreasing autophagosome-lysosome fusion. Autophagy 14, 1435–1455. https://doi.org/10.1080/15548627.2018.1474314

Mayba, O., Gilbert, H.N., Liu, J., Haverty, P.M., Jhunjhunwala, S., Jiang, Z., Watanabe, C., Zhang, Z., 2014. MBASED: allele-specific expression detection in cancer tissues and cell lines. Genome Biol. 15, 405. https://doi.org/10.1186/s13059-014-0405-3

Mayr, C., 2019. What Are 3' UTRs Doing? Cold Spring Harb. Perspect. Biol. 11, a034728. https://doi.org/10.1101/cshperspect.a034728

Mazan-Mamczarz, K., Lal, A., Martindale, J.L., Kawai, T., Gorospe, M., 2006. Translational Repression by RNA-Binding Protein TIAR. Mol. Cell. Biol. 26, 2716–2727. https://doi.org/10.1128/MCB.26.7.2716-2727.2006

Menendez, D., Inga, A., Snipe, J., Krysiak, O., Schönfelder, G., Resnick, M.A., 2007. A single-nucleotide polymorphism in a half-binding site creates p53 and estrogen receptor control of vascular endothelial growth factor receptor 1. Mol. Cell. Biol. 27, 2590–2600. https://doi.org/10.1128/MCB.01742-06

Menendez, D., Snipe, J., Marzec, J., Innes, C.L., Polack, F.P., Caballero, M.T., Schurman, S.H., Kleeberger, S.R., Resnick, M.A., 2019. p53-responsive TLR8 SNP enhances human innate immune response to respiratory syncytial virus. J. Clin. Invest. 129, 4875–4884. https://doi.org/10.1172/JCI128626

Mijaljica, D., Prescott, M., Devenish, R.J., 2011. V-ATPase engagement in autophagic processes. Autophagy 7, 666–668. https://doi.org/10.4161/auto.7.6.15812

Montero, J.C., Chen, X., Ocaña, A., Pandiella, A., 2012. Predominance of mTORC1 over mTORC2 in the regulation of proliferation of ovarian cancer cells: therapeutic implications. Mol. Cancer Ther. 11, 1342–1352. https://doi.org/10.1158/1535-7163.MCT-11-0723

Motono, M., Ioroi, Y., Ogura, T., Takahashi, J., 2016. WNT-C59, a Small-Molecule WNT Inhibitor, Efficiently Induces Anterior Cortex That Includes Cortical Motor Neurons From Human Pluripotent Stem Cells. Stem Cells Transl. Med. 5, 552–560. https://doi.org/10.5966/sctm.2015-0261

Mulas, C., 2024. Control of cell state transitions by post-transcriptional regulation. Philos. Trans. R. Soc. Lond. B. Biol. Sci. 379, 20230050. https://doi.org/10.1098/rstb.2023.0050

Murakami, S., Olarerin-George, A.O., Liu, J.F., Zaccara, S., Hawley, B., Jaffrey, S.R., 2025. m6A alters ribosome dynamics to initiate mRNA degradation. Cell 188, 3728-3743.e20. https://doi.org/10.1016/j.cell.2025.04.020

Navarro, E., Mallén, A., Hueso, M., 2021. Dynamic Variations of 3'UTR Length Reprogram the mRNA Regulatory Landscape. Biomedicines 9, 1560. https://doi.org/10.3390/biomedicines9111560

Neriec, N., Percipalle, P., 2018. Sorting mRNA Molecules for Cytoplasmic Transport and Localization. Front. Genet. 9. https://doi.org/10.3389/fgene.2018.00510

Panda, A.C., Martindale, J.L., Gorospe, M., 2017. Polysome Fractionation to Analyze mRNA Distribution Profiles. Bio-Protoc. 7, e2126. https://doi.org/10.21769/BioProtoc.2126

Pandey, R.V., Franssen, S.U., Futschik, A., Schlötterer, C., 2013. Allelic imbalance metre (Allim), a new tool for measuring allele-specific gene expression with RNA-seq data. Mol. Ecol. Resour. 13, 740–745. https://doi.org/10.1111/1755-0998.12110

Plomp, P.J., Gordon, P.B., Meijer, A.J., Høyvik, H., Seglen, P.O., 1989. Energy dependence of different steps in the autophagic-lysosomal pathway. J. Biol. Chem. 264, 6699–6704.

Polymenis, M., Schmidt, E.V., 1997. Coupling of cell division to cell growth by translational control of the G1 cyclin CLN3 in yeast. Genes Dev. 11, 2522–2531. https://doi.org/10.1101/gad.11.19.2522

Qin, Y., Li, B., Arumugam, S., Lu, Q., Mankash, S.M., Li, Junzi, Sun, B., Li, Jiansheng, Flavell, R.A., Li, H.-B., Ouyang, X., 2021. m6A mRNA methylation-directed myeloid cell activation controls progression of NAFLD and obesity. Cell Rep. 37, 109968. https://doi.org/10.1016/j.celrep.2021.109968

Qiu, Y., Pu, C., Wang, C., Quan, Z., 2025. The RNA-Binding Protein RBMX Mediates the Immunosuppressive Microenvironment of Osteosarcoma by Regulating CD8+T Cells. Cancers 17, 2928. https://doi.org/10.3390/cancers17172928

Querido, E., Sfeir, A., Chartrand, P., 2020. Imaging of Telomerase RNA by Single-Molecule Inexpensive FISH Combined with Immunofluorescence. STAR Protoc. 1, 100104. https://doi.org/10.1016/j.xpro.2020.100104

Raj, N., Wang, M., Seoane, J.A., Zhao, R.L., Kaiser, A.M., Moonie, N.A., Demeter, J., Boutelle, A.M., Kerr, C.H., Mulligan, A.S., Moffatt, C., Zeng, S.X., Lu, H., Barna, M., Curtis, C., Chang, H.Y., Jackson, P.K., Attardi, L.D., 2022. The Mettl3 epitranscriptomic writer amplifies p53 stress responses. Mol. Cell 82, 2370-2384.e10. https://doi.org/10.1016/j.molcel.2022.04.010

Reshef, Y.A., Finucane, H.K., Kelley, D.R., Gusev, A., Kotliar, D., Ulirsch, J.C., Hormozdiari, F., Nasser, J., O'Connor, L., van de Geijn, B., Loh, P.-R., Grossman, S.R., Bhatia, G., Gazal, S., Palamara, P.F., Pinello, L., Patterson, N., Adams, R.P., Price, A.L., 2018. Detecting genome-wide directional effects of transcription factor binding on polygenic disease risk. Nat. Genet. 50, 1483–1493. https://doi.org/10.1038/s41588-018-0196-7

Richter, N.J., Rogers, G.W., Hensold, J.O., Merrick, W.C., 1999. Further biochemical and kinetic characterization of human eukaryotic initiation factor 4H. J. Biol. Chem. 274, 35415–35424. https://doi.org/10.1074/jbc.274.50.35415

Rodriguez-Martinez, A., Young-Baird, S.K., 2025. Polysome profiling is an extensible tool for the analysis of bulk protein synthesis, ribosome biogenesis, and the specific steps in translation. Mol. Biol. Cell 36, mr2. https://doi.org/10.1091/mbc.E24-08-0341

Romanel, A., 2019. Allele-Specific Expression Analysis in Cancer Using Next-Generation Sequencing Data. Methods Mol. Biol. Clifton NJ 1878, 125–137. https://doi.org/10.1007/978-1-4939-8868-6_7

Romo, L., Findlay, S.D., Burge, C.B., 2024. Regulatory features aid interpretation of 3'UTR variants. Am. J. Hum. Genet. 111, 350–363. https://doi.org/10.1016/j.ajhg.2023.12.017

Rozovsky, N., Butterworth, A.C., Moore, M.J., 2008. Interactions between eIF4AI and its accessory factors eIF4B and eIF4H. RNA 14, 2136–2148. https://doi.org/10.1261/rna.1049608

Sato, K., Akiyama, M., Sakakibara, Y., 2021. RNA secondary structure prediction using deep learning with thermodynamic integration. Nat. Commun. 12, 941. https://doi.org/10.1038/s41467-021-21194-4

Savino, M., Annibali, D., Carucci, N., Favuzzi, E., Cole, M.D., Evan, G.I., Soucek, L., Nasi, S., 2011. The action mechanism of the Myc inhibitor termed Omomyc may give clues on how to target Myc for cancer therapy. PloS One 6, e22284. https://doi.org/10.1371/journal.pone.0022284

Schug, J., 2008. Using TESS to predict transcription factor binding sites in DNA sequence. Curr. Protoc. Bioinforma. Chapter 2, Unit 2.6. https://doi.org/10.1002/0471250953.bi0206s21

Shenasa, H., Bentley, D.L., 2023. Pre-mRNA splicing and its cotranscriptional connections. Trends Genet. 39, 672–685. https://doi.org/10.1016/j.tig.2023.04.008

Sheng, Y., Lei, K., Sun, C., Liu, J., Tu, Z., Zhu, X., Huang, K., 2024. Aberrant RBMX expression is relevant for cancer prognosis and immunotherapy response. Aging. https://doi.org/10.18632/aging.205363

Sheng, Y., Tu, Z., Sun, C., Long, X., Wu, L., Huang, K., Zhu, X., 2022. Prognostic and Immunological Role of RBMX in cancers. https://doi.org/10.21203/rs.3.rs-2179142/v1

Shin, K.-H., Kim, Reuben H., Kim, Roy H., Kang, M.K., Park, N.-H., 2008a. hnRNP G elicits tumor-suppressive activity in part by upregulating the expression of Txnip. Biochem. Biophys. Res. Commun. 372, 880–885. https://doi.org/10.1016/j.bbrc.2008.05.175

Shin, K.-H., Kim, Reuben H., Kim, Roy H., Kang, M.K., Park, N.-H., 2008b. hnRNP G elicits tumor suppressive activity in part by upregulating the expression of Txnip. Biochem. Biophys. Res. Commun. 372, 880–885. https://doi.org/10.1016/j.bbrc.2008.05.175

Shoshani, T., Faerman, A., Mett, I., Zelin, E., Tenne, T., Gorodin, S., Moshel, Y., Elbaz, S., Budanov, A., Chajut, A., Kalinski, H., Kamer, I., Rozen, A., Mor, O., Keshet, E., Leshkowitz, D., Einat, P., Skaliter, R., Feinstein, E., 2002. Identification of a novel hypoxia-inducible factor 1-

responsive gene, RTP801, involved in apoptosis. Mol. Cell. Biol. 22, 2283–2293. https://doi.org/10.1128/MCB.22.7.2283-2293.2002

Siachisumo, C., Luzzi, S., Aldalaqan, S., Hysenaj, G., Dalgliesh, C., Cheung, K., Gazzara, M.R., Yonchev, I.D., James, K., Kheirollahi Chadegani, M., Ehrmann, I.E., Smith, G.R., Cockell, S.J., Munkley, J., Wilson, S.A., Barash, Y., Elliott, D.J., 2024a. An anciently diverged family of RNA binding proteins maintain correct splicing of a class of ultra-long exons through cryptic splice site repression. eLife 12, RP89705. https://doi.org/10.7554/eLife.89705

Siachisumo, C., Luzzi, S., Aldalaqan, S., Hysenaj, G., Dalgliesh, C., Cheung, K., Gazzara, M.R., Yonchev, I.D., James, K., Kheirollahi Chadegani, M., Ehrmann, I.E., Smith, G.R., Cockell, S.J., Munkley, J., Wilson, S.A., Barash, Y., Elliott, D.J., 2024b. An anciently diverged family of RNA binding proteins maintain correct splicing of a class of ultra-long exons through cryptic splice site repression. eLife 12, RP89705. https://doi.org/10.7554/eLife.89705

Singh, S., Vanden Broeck, A., Miller, L., Chaker-Margot, M., Klinge, S., 2021. Nucleolar maturation of the human small subunit processome. Science 373, eabj5338. https://doi.org/10.1126/science.abj5338

Sinnamon, J.R., Waddell, C.B., Nik, S., Chen, E.I., Czaplinski, K., 2012. Hnrpab regulates neural development and neuron cell survival after glutamate stimulation. RNA N. Y. N 18, 704–719. https://doi.org/10.1261/rna.030742.111

Sofer, A., Lei, K., Johannessen, C.M., Ellisen, L.W., 2005. Regulation of mTOR and cell growth in response to energy stress by REDD1. Mol. Cell. Biol. 25, 5834–5845. https://doi.org/10.1128/MCB.25.14.5834-5845.2005

Solem, A.C., Halvorsen, M., Ramos, S.B.V., Laederach, A., 2015. The potential of the riboSNitch in personalized medicine. Wiley Interdiscip. Rev. RNA 6, 517–532. https://doi.org/10.1002/wrna.1291

Sun, K., Deng, W., Zhang, S., Cai, N., Jiao, S., Song, J., Wei, L., 2013. Paradoxical roles of autophagy in different stages of tumorigenesis: protector for normal or cancer cells. Cell Biosci. 3, 35. https://doi.org/10.1186/2045-3701-3-35

Sun, Y., Zhang, J., Wang, Y., Wang, L., Song, M., Khan, A., Zhang, L., Niu, B., Zhao, H., Li, M., Luo, T., He, Q., Xie, X., Liu, Z., Xie, J., 2021. miR-222-3p is involved in neural tube closure by directly targeting Ddit4 in RA induced NTDs mouse model. Cell Cycle Georget. Tex 20, 2372–2386. https://doi.org/10.1080/15384101.2021.1982506

Susanto, T.T., Hung, V., Levine, A.G., Chen, Y., Kerr, C.H., Yoo, Y., Oses-Prieto, J.A., Fromm, L., Zhang, Z., Lantz, T.C., Fujii, K., Wernig, M., Burlingame, A.L., Ruggero, D., Barna, M., 2024. RAPIDASH: Tag-free enrichment of ribosome-associated proteins reveals composition dynamics in embryonic tissue, cancer cells, and macrophages. Mol. Cell 84, 3545-3563.e25. https://doi.org/10.1016/j.molcel.2024.08.023

Suzuki, K., Bose, P., Leong-Quong, R.Y., Fujita, D.J., Riabowol, K., 2010. REAP: A two minute cell fractionation method. BMC Res. Notes 3, 294. https://doi.org/10.1186/1756-0500-3-294

Tajik, F., Fattahi, F., Rezagholizadeh, F., Bouzari, B., Babaheidarian, P., Baghai Wadji, M., Madjd, Z., 2023. Nuclear overexpression of DNA damage-inducible transcript 4 (DDIT4) is associated with aggressive tumor behavior in patients with pancreatic tumors. Sci. Rep. 13, 19403. https://doi.org/10.1038/s41598-023-46484-3

Tam, V., Patel, N., Turcotte, M., Bossé, Y., Paré, G., Meyre, D., 2019. Benefits and limitations of genome-wide association studies. Nat. Rev. Genet. 20, 467–484. https://doi.org/10.1038/s41576-019-0127-1

Thastrup, O., Cullen, P.J., Drøbak, B.K., Hanley, M.R., Dawson, A.P., 1990. Thapsigargin, a tumor promoter, discharges intracellular Ca2+ stores by specific inhibition of the endoplasmic reticulum Ca2(+)-ATPase. Proc. Natl. Acad. Sci. U. S. A. 87, 2466–2470. https://doi.org/10.1073/pnas.87.7.2466

Thomas, C.A., 1971. The genetic organization of chromosomes. Annu. Rev. Genet. 5, 237–256. https://doi.org/10.1146/annurev.ge.05.120171.001321

Tirado-Hurtado, I., Fajardo, W., Pinto, J.A., 2018. DNA Damage Inducible Transcript 4 Gene: The Switch of the Metabolism as Potential Target in Cancer. Front. Oncol. 8, 106. https://doi.org/10.3389/fonc.2018.00106

Tiu, G.C., Kerr, C.H., Forester, C.M., Krishnarao, P.S., Rosenblatt, H.D., Raj, N., Lantz, T.C., Zhulyn, O., Bowen, M.E., Shokat, L., Attardi, L.D., Ruggero, D., Barna, M., 2021. A p53-dependent translational program directs tissue-selective phenotypes in a model of ribosomopathies. Dev. Cell 56, 2089-2102.e11. https://doi.org/10.1016/j.devcel.2021.06.013

Tojo, M., Hamashima, Y., Hanyu, A., Kajimoto, T., Saitoh, M., Miyazono, K., Node, M., Imamura, T., 2005. The ALK-5 inhibitor A-83-01 inhibits Smad signaling and epithelial-to-mesenchymal transition by transforming growth factor-beta. Cancer Sci. 96, 791–800. https://doi.org/10.1111/j.1349-7006.2005.00103.x

Tovar, C., Rosinski, J., Filipovic, Z., Higgins, B., Kolinsky, K., Hilton, H., Zhao, X., Vu, B.T., Qing, W., Packman, K., Myklebost, O., Heimbrook, D.C., Vassilev, L.T., 2006. Small-molecule MDM2 antagonists reveal aberrant p53 signaling in cancer: implications for therapy. Proc. Natl. Acad. Sci. U. S. A. 103, 1888–1893. https://doi.org/10.1073/pnas.0507493103

Tsai, C.-J., Sauna, Z.E., Kimchi-Sarfaty, C., Ambudkar, S.V., Gottesman, M.M., Nussinov, R., 2008. Synonymous Mutations and Ribosome Stalling Can Lead to Altered Folding Pathways and Distinct Minima. J. Mol. Biol. 383, 281–291. https://doi.org/10.1016/j.jmb.2008.08.012

Tuersun, H., Liu, L., Zhang, J., Maimaitizunong, R., Tang, X., Li, H., 2023a. m6A reading protein RBMX as a biomarker for prognosis and tumor progression in esophageal cancer. Transl. Cancer Res. 12, 2319–2335. https://doi.org/10.21037/tcr-23-84

Tuersun, H., Liu, L., Zhang, J., Maimaitizunong, R., Tang, X., Li, H., 2023b. m6A reading protein RBMX as a biomarker for prognosis and tumor progression in esophageal cancer. Transl. Cancer Res. 12, 2319–2335. https://doi.org/10.21037/tcr-23-84

Valentini, S., Marchioretti, C., Bisio, A., Rossi, A., Zaccara, S., Romanel, A., Inga, A., 2021. TranSNPs: A class of functional SNPs affecting mRNA translation potential revealed by

fraction-based allelic imbalance. iScience 24, 103531. https://doi.org/10.1016/j.isci.2021.103531

Vassilev, L.T., Vu, B.T., Graves, B., Carvajal, D., Podlaski, F., Filipovic, Z., Kong, N., Kammlott, U., Lukacs, C., Klein, C., Fotouhi, N., Liu, E.A., 2004. In vivo activation of the p53 pathway by small-molecule antagonists of MDM2. Science 303, 844–848. https://doi.org/10.1126/science.1092472

Vaysse, C., Philippe, C., Martineau, Y., Quelen, C., Hieblot, C., Renaud, C., Nicaise, Y., Desquesnes, A., Pannese, M., Filleron, T., Escourrou, G., Lawson, M., Rintoul, R.C., Delisle, M.B., Pyronnet, S., Brousset, P., Prats, H., Touriol, C., 2015. Key contribution of eIF4H-mediated translational control in tumor promotion. Oncotarget 6, 39924–39940. https://doi.org/10.18632/oncotarget.5442

Vega-Rubin-de-Celis, S., Abdallah, Z., Kinch, L., Grishin, N.V., Brugarolas, J., Zhang, X., 2010. Structural analysis and functional implications of the negative mTORC1 regulator REDD1. Biochemistry 49, 2491–2501. https://doi.org/10.1021/bi902135e

Volpe, E., Colantoni, A., Corda, L., Di Tommaso, E., Pelliccia, F., Ottalevi, R., Guarracino, A., Licastro, D., Faino, L., Capulli, M., Formenti, G., Tassone, E., Giunta, S., 2025. The reference genome of the human diploid cell line RPE-1. Nat. Commun. 16, 7751. https://doi.org/10.1038/s41467-025-62428-z

Wang, Q., Zhao, G., Yang, Z., Liu, X., Xie, P., 2018. Downregulation of microRNA-124-3p suppresses the mTOR signaling pathway by targeting DDIT4 in males with major depressive disorder. Int. J. Mol. Med. 41, 493–500. https://doi.org/10.3892/ijmm.2017.3235

Wang, Y., Han, E., Xing, Q., Yan, J., Arrington, A., Wang, C., Tully, D., Kowolik, C.M., Lu, D.M., Frankel, P.H., Zhai, J., Wen, W., Horne, D., Yip, M.L.R., Yim, J.H., 2015. Baicalein upregulates DDIT4 expression which mediates mTOR inhibition and growth inhibition in cancer cells. Cancer Lett. 358, 170–179. https://doi.org/10.1016/j.canlet.2014.12.033

Wang, Y., Yang, S., Hao, C., Chen, J., Wang, J., Xu, L., 2023. DDIT4 is essential for DINP-induced autophagy of ovarian granulosa cells. Ecotoxicol. Environ. Saf. 268, 115686. https://doi.org/10.1016/j.ecoenv.2023.115686

Wang, Y., Zhang, H., Lu, J., 2020. Recent advances in ribosome profiling for deciphering translational regulation. Methods San Diego Calif 176, 46–54. https://doi.org/10.1016/j.ymeth.2019.05.011

Wayment-Steele, H.K., Kladwang, W., Strom, A.I., Lee, J., Treuille, A., Becka, A., Eterna Participants, Das, R., 2022. RNA secondary structure packages evaluated and improved by high-throughput experiments. Nat. Methods 19, 1234–1242. https://doi.org/10.1038/s41592-022-01605-0

Weitzel, J.N., Blazer, K.R., MacDonald, D.J., Culver, J.O., Offit, K., 2011. Genetics, genomics, and cancer risk assessment: State of the Art and Future Directions in the Era of Personalized Medicine. CA. Cancer J. Clin. 61, 327–359. https://doi.org/10.3322/caac.20128

White, R.M., Sessa, A., Burke, C., Bowman, T., LeBlanc, J., Ceol, C., Bourque, C., Dovey, M., Goessling, W., Burns, C.E., Zon, L.I., 2008. Transparent adult zebrafish as a tool for in vivo transplantation analysis. Cell Stem Cell 2, 183–189. https://doi.org/10.1016/j.stem.2007.11.002

Whitney, M.L., Jefferson, L.S., Kimball, S.R., 2009a. ATF4 is necessary and sufficient for ER stress-induced upregulation of REDD1 expression. Biochem. Biophys. Res. Commun. 379, 451–455. https://doi.org/10.1016/j.bbrc.2008.12.079

Whitney, M.L., Jefferson, L.S., Kimball, S.R., 2009b. ATF4 is necessary and sufficient for ER stress-induced upregulation of REDD1 expression. Biochem. Biophys. Res. Commun. 379, 451–455. https://doi.org/10.1016/j.bbrc.2008.12.079

Wieder, N., D'Souza, E.N., Dawes, R., Chan, A., Martin-Geary, A., Whiffin, N., 2025. The role of untranslated region variants in Mendelian disease: a review. Eur. J. Hum. Genet. 33, 1096–1105. https://doi.org/10.1038/s41431-025-01905-x

Xu, Z., Yang, H., Zhou, X., Li, J., Jiang, L., Li, D., Wu, L., Huang, Y., Xu, N., 2019. Genetic variants in mTOR-pathway-related genes contribute to osteoarthritis susceptibility. Int. Immunopharmacol. 77, 105960. https://doi.org/10.1016/j.intimp.2019.105960

Yan, Q., Zeng, P., Zhou, X., Zhao, X., Chen, R., Qiao, J., Feng, L., Zhu, Z., Zhang, G., Chen, C., 2021a. RBMX suppresses tumorigenicity and progression of bladder cancer by interacting with the hnRNP A1 protein to regulate PKM alternative splicing. Oncogene 40, 2635–2650. https://doi.org/10.1038/s41388-021-01666-z

Yan, Q., Zeng, P., Zhou, X., Zhao, X., Chen, R., Qiao, J., Feng, L., Zhu, Z., Zhang, G., Chen, C., 2021b. RBMX suppresses tumorigenicity and progression of bladder cancer by interacting with the hnRNP A1 protein to regulate PKM alternative splicing. Oncogene 40, 2635–2650. https://doi.org/10.1038/s41388-021-01666-z

Yeh, H.-S., Yong, J., 2020. mTOR-coordinated Post-Transcriptional Gene Regulations: from Fundamental to Pathogenic Insights. J. Lipid Atheroscler. 9, 8–22. https://doi.org/10.12997/jla.2020.9.1.8

Yengo, L., Vedantam, S., Marouli, E., Sidorenko, J., Bartell, E., Sakaue, S., Graff, M., Eliasen, A.U., Jiang, Y., Raghavan, S., Miao, J., Arias, J.D., Graham, S.E., Mukamel, R.E., Spracklen, C.N., Yin, X., Chen, S.-H., Ferreira, T., Highland, H.H., Ji, Y., Karaderi, T., Lin, K., Lüll, K., Malden, D.E., Medina-Gomez, C., Machado, M., Moore, A., Rüeger, S., Sim, X., Vrieze, S., Ahluwalia, T.S., Akiyama, M., Allison, M.A., Alvarez, M., Andersen, M.K., Ani, A., Appadurai, V., Arbeeva, L., Bhaskar, S., Bielak, L.F., Bollepalli, S., Bonnycastle, L.L., Bork-Jensen, J., Bradfield, J.P., Bradford, Y., Braund, P.S., Brody, J.A., Burgdorf, K.S., Cade, B.E., Cai, H., Cai, Q., Campbell, A., Cañadas-Garre, M., Catamo, E., Chai, J.-F., Chai, X., Chang, L.-C., Chang, Y.-C., Chen, C.-H., Chesi, A., Choi, S.H., Chung, R.-H., Cocca, M., Concas, M.P., Couture, C., Cuellar-Partida, G., Danning, R., Daw, E.W., Degenhard, F., Delgado, G.E., Delitala, A., Demirkan, A., Deng, X., Devineni, P., Dietl, A., Dimitriou, M., Dimitrov, L., Dorajoo, R., Ekici, A.B., Engmann, J.E., Fairhurst-Hunter, Z., Farmaki, A.-E., Faul, J.D., Fernandez-Lopez, J.-C., Forer, L., Francescatto, M., Freitag-Wolf, S., Fuchsberger, C., Galesloot, T.E., Gao, Y., Gao, Z., Geller, F., Giannakopoulou, O., Giulianini, F., Gjesing, A.P., Goel, A., Gordon, S.D., Gorski, M.,

Grove, J., Guo, X., Gustafsson, S., Haessler, J., Hansen, T.F., Havulinna, A.S., Haworth, S.J., He, J., Heard-Costa, N., Hebbar, P., Hindy, G., Ho, Y.-L.A., Hofer, E., Holliday, E., Horn, K., Hornsby, W.E., Hottenga, J.-J., Huang, H., Huang, J., Huerta-Chagoya, A., Huffman, J.E., Hung, Y.-J., Huo, S., Hwang, M.Y., Iha, H., Ikeda, D.D., Isono, M., Jackson, A.U., Jäger, S., Jansen, I.E., Johansson, I., Jonas, J.B., Jonsson, A., Jørgensen, T., Kalafati, I.-P., Kanai, M., Kanoni, S., Kårhus, L.L., Kasturiratne, A., Katsuya, T., Kawaguchi, T., Kember, R.L., Kentistou, K.A., Kim, H.-N., Kim, Y.J., Kleber, M.E., Knol, M.J., Kurbasic, A., Lauzon, M., Le, P., Lea, R., Lee, J.-Y., Leonard, H.L., Li, S.A., Li, Xiaohui, Li, Xiaoyin, Liang, J., Lin, H., Lin, S.-Y., Liu, Jun, Liu, X., Lo, K.S., Long, J., Lores-Motta, L., Luan, J., Lyssenko, V., Lyytikäinen, L.-P., Mahajan, A., Mamakou, V., Mangino, M., Manichaikul, A., Marten, J., Mattheisen, M., Mavarani, L., McDaid, A.F., Meidtner, K., Melendez, T.L., Mercader, J.M., Milaneschi, Y., Miller, J.E., Millwood, I.Y., Mishra, P.P., Mitchell, R.E., Møllehave, L.T., Morgan, A., Mucha, S., Munz, M., Nakatochi, M., Nelson, C.P., Nethander, M., Nho, C.W., Nielsen, A.A., Nolte, I.M., Nongmaithem, S.S., Noordam, R., Ntalla, I., Nutile, T., Pandit, A., Christofidou, P., Pärna, K., Pauper, M., Petersen, E.R.B., Petersen, L.V., Pitkänen, N., Polašek, O., Poveda, A., Preuss, M.H., Pyarajan, S., Raffield, L.M., Rakugi, H., Ramirez, J., Rasheed, A., Raven, D., Rayner, N.W., Riveros, C., Rohde, R., Ruggiero, D., Ruotsalainen, S.E., Ryan, K.A., Sabater-Lleal, M., Saxena, R., Scholz, M., Sendamarai, A., Shen, B., Shi, J., Shin, J.H., Sidore, C., Sitlani, C.M., Slieker, R.C., Smit, R.A.J., Smith, A.V., Smith, J.A., Smyth, L.J., Southam, L., Steinthorsdottir, V., Sun, L., Takeuchi, F., Tallapragada, D.S.P., Taylor, K.D., Tayo, B.O., Tcheandjieu, C., Terzikhan, N., Tesolin, P., Teumer, A., Theusch, E., Thompson, D.J., Thorleifsson, G., Timmers, P.R.H.J., Trompet, S., Turman, C., Vaccargiu, S., van der Laan, S.W., van der Most, P.J., van Klinken, J.B., van Setten, J., Verma, S.S., Verweij, N., Veturi, Y., Wang, C.A., Wang, C., Wang, L., Wang, Z., Warren, H.R., Bin Wei, W., Wickremasinghe, A.R., Wielscher, M., Wiggins, K.L., Winsvold, B.S., Wong, A., Wu, Y., Wuttke, M., Xia, R., Xie, T., Yamamoto, K., Yang, Jingyun, Yao, J., Young, H., Yousri, N.A., Yu, L., Zeng, L., Zhang, W., Zhang, X., Zhao, J.-H., Zhao, W., Zhou, W., Zimmermann, M.E., Zoledziewska, M., Adair, L.S., Adams, H.H.H., Aguilar-Salinas, C.A., Al-Mulla, F., Arnett, D.K., Asselbergs, F.W., Åsvold, B.O., Attia, J., Banas, B., Bandinelli, S., Bennett, D.A., Bergler, T., Bharadwaj, D., Biino, G., Bisgaard, H., Boerwinkle, E., Böger, C.A., Bønnelykke, K., Boomsma, D.I., Børglum, A.D., Borja, J.B., Bouchard, C., Bowden, D.W., Brandslund, I., Brumpton, B., Buring, J.E., Caulfield, M.J., Chambers, J.C., Chandak, G.R., Chanock, S.J., Chaturvedi, N., Chen, Y.-D.I., Chen, Z., Cheng, C.-Y., Christophersen, I.E., Ciullo, M., Cole, J.W., Collins, F.S., Cooper, R.S., Cruz, M., Cucca, F., Cupples, L.A., Cutler, M.J., Damrauer, S.M., Dantoft, T.M., de Borst, G.J., de Groot, L.C.P.G.M., De Jager, P.L., de Kleijn, D.P.V., Janaka de Silva, H., Dedoussis, G.V., den Hollander, A.I., Du, S., Easton, D.F., Elders, P.J.M., Eliassen, A.H., Ellinor, P.T., Elmståhl, S., Erdmann, J., Evans, M.K., Fatkin, D., Feenstra, B., Feitosa, M.F., Ferrucci, L., Ford, I., Fornage, M., Franke, A., Franks, P.W., Freedman, B.I., Gasparini, P., Gieger, C., Girotto, G., Goddard, M.E., Golightly, Y.M., Gonzalez-Villalpando, C., Gordon-Larsen, P., Grallert, H., Grant, S.F.A., Grarup, N., Griffiths, L., Gudnason, V., Haiman, C., Hakonarson, H., Hansen, T., Hartman, C.A., Hattersley, A.T., Hayward, C., Heckbert, S.R., Heng, C.-K., Hengstenberg, C., Hewitt, A.W., Hishigaki, H., Hoyng, C.B., Huang, P.L., Huang, W., Hunt, S.C., Hveem, K., Hyppönen, E., Iacono, W.G., Ichihara, S., Ikram, M.A., Isasi, C.R., Jackson, R.D., Jarvelin, M.-R., Jin, Z.-B., Jöckel, K.-H., Joshi, P.K., Jousilahti, P., Jukema, J.W., Kähönen, M., Kamatani, Y., Kang, K.D., Kaprio, J., Kardia, S.L.R., Karpe, F., Kato, N., Kee, F., Kessler, T., Khera, A.V., Khor, C.C., Kiemeney, L.A.L.M., Kim, B.-J., Kim, E.K., Kim, H.-L., Kirchhof, P., Kivimaki, M., Koh, W.-P.,

Koistinen, H.A., Kolovou, G.D., Kooner, J.S., Kooperberg, C., Köttgen, A., Kovacs, P., Kraaijeveld, A., Kraft, P., Krauss, R.M., Kumari, M., Kutalik, Z., Laakso, M., Lange, L.A., Langenberg, C., Launer, L.J., Le Marchand, L., Lee, H., Lee, N.R., Lehtimäki, T., Li, H., Li, L., Lieb, W., Lin, X., Lind, L., Linneberg, A., Liu, C.-T., Liu, Jianjun, Loeffler, M., London, B., Lubitz, S.A., Lye, S.J., Mackey, D.A., Mägi, R., Magnusson, P.K.E., Marcus, G.M., Vidal, P.M., Martin, N.G., März, W., Matsuda, F., McGarrah, R.W., McGue, M., McKnight, A.J., Medland, S.E., Mellström, D., Metspalu, A., Mitchell, B.D., Mitchell, P., Mook-Kanamori, D.O., Morris, A.D., Mucci, L.A., Munroe, P.B., Nalls, M.A., Nazarian, S., Nelson, A.E., Neville, M.J., Newton-Cheh, C., Nielsen, C.S., Nöthen, M.M., Ohlsson, C., Oldehinkel, A.J., Orozco, L., Pahkala, K., Pajukanta, P., Palmer, C.N.A., Parra, E.J., Pattaro, C., Pedersen, O., Pennell, C.E., Penninx, B.W.J.H., Perusse, L., Peters, A., Peyser, P.A., Porteous, D.J., Posthuma, D., Power, C., Pramstaller, P.P., Province, M.A., Qi, Q., Qu, J., Rader, D.J., Raitakari, O.T., Ralhan, S., Rallidis, L.S., Rao, D.C., Redline, S., Reilly, D.F., Reiner, A.P., Rhee, S.Y., Ridker, P.M., Rienstra, M., Ripatti, S., Ritchie, M.D., Roden, D.M., Rosendaal, F.R., Rotter, J.I., Rudan, I., Rutters, F., Sabanayagam, C., Saleheen, D., Salomaa, V., Samani, N.J., Sanghera, D.K., Sattar, N., Schmidt, B., Schmidt, H., Schmidt, R., Schulze, M.B., Schunkert, H., Scott, L.J., Scott, R.J., Sever, P., Shiroma, E.J., Shoemaker, M.B., Shu, X.-O., Simonsick, E.M., Sims, M., Singh, J.R., Singleton, A.B., Sinner, M.F., Smith, J.G., Snieder, H., Spector, T.D., Stampfer, M.J., Stark, K.J., Strachan, D.P., 't Hart, L.M., Tabara, Y., Tang, H., Tardif, J.-C., Thanaraj, T.A., Timpson, N.J., Tönjes, A., Tremblay, A., Tuomi, T., Tuomilehto, J., Tusié-Luna, M.-T., Uitterlinden, A.G., van Dam, R.M., van der Harst, P., Van der Velde, N., van Duijn, C.M., van Schoor, N.M., Vitart, V., Völker, U., Vollenweider, P., Völzke, H., Wacher-Rodarte, N.H., Walker, M., Wang, Y.X., Wareham, N.J., Watanabe, R.M., Watkins, H., Weir, D.R., Werge, T.M., Widen, E., Wilkens, L.R., Willemsen, G., Willett, W.C., Wilson, J.F., Wong, T.-Y., Woo, J.-T., Wright, A.F., Wu, J.-Y., Xu, H., Yajnik, C.S., Yokota, M., Yuan, J.-M., Zeggini, E., Zemel, B.S., Zheng, W., Zhu, X., Zmuda, J.M., Zonderman, A.B., Zwart, J.-A., 23andMe Research Team, VA Million Veteran Program, DiscovEHR (DiscovEHR and MyCode Community Health Initiative), eMERGE (Electronic Medical Records and Genomics Network), Lifelines Cohort Study, PRACTICAL Consortium, Understanding Society Scientific Group, Chasman, D.I., Cho, Y.S., Heid, I.M., McCarthy, M.I., Ng, M.C.Y., O'Donnell, C.J., Rivadeneira, F., Thorsteinsdottir, U., Sun, Y.V., Tai, E.S., Boehnke, M., Deloukas, P., Justice, A.E., Lindgren, C.M., Loos, R.J.F., Mohlke, K.L., North, K.E., Stefansson, K., Walters, R.G., Winkler, T.W., Young, K.L., Loh, P.-R., Yang, Jian, Esko, T., Assimes, T.L., Auton, A., Abecasis, G.R., Willer, C.J., Locke, A.E., Berndt, S.I., Lettre, G., Frayling, T.M., Okada, Y., Wood, A.R., Visscher, P.M., Hirschhorn, J.N., 2022. A saturated map of common genetic variants associated with human height. Nature 610, 704–712. https://doi.org/10.1038/s41586-022-05275-y

Yu, F., Zhu, A.C., Liu, S., Gao, B., Wang, Y., Khudaverdyan, N., Yu, C., Wu, Q., Jiang, Y., Song, J., Jin, L., He, C., Qian, Z., 2023. RBM33 is a unique m6A RNA-binding protein that regulates ALKBH5 demethylase activity and substrate selectivity. Mol. Cell 83, 2003-2019.e6. https://doi.org/10.1016/j.molcel.2023.05.010

Zhang, P., Cheng, S., Sheng, X., Dai, H., He, K., Du, Y., 2023. The role of autophagy in regulating metabolism in the tumor microenvironment. Genes Dis. 10, 447–456. https://doi.org/10.1016/j.gendis.2021.10.010

Zhang, Y., Liu, L., Hou, X., Zhang, Z., Zhou, X., Gao, W., 2023. Role of Autophagy Mediated by AMPK/DDiT4/mTOR Axis in HT22 Cells Under Oxygen and Glucose Deprivation/Reoxygenation. ACS Omega 8, 9221–9229. https://doi.org/10.1021/acsomega.2c07280

Zhao, Y., Hu, X., Yu, H., Sun, H., Zhang, L., Shao, C., 2024. The FTO Mediated N6-Methyladenosine Modification of DDIT4 Regulation with Tumorigenesis and Metastasis in Prostate Cancer. Res. Wash. DC 7, 0313. https://doi.org/10.34133/research.0313

Zhou, K.I., Shi, H., Lyu, R., Wylder, A.C., Matuszek, Ż., Pan, J.N., He, C., Parisien, M., Pan, T., 2019. Regulation of co-transcriptional pre-mRNA splicing by m6A through the low-complexity protein hnRNPG. Mol. Cell 76, 70-81.e9. https://doi.org/10.1016/j.molcel.2019.07.005

Zuccotti, P., Peroni, D., Potrich, V., Quattrone, A., Dassi, E., 2020. Hyperconserved Elements in Human 5'UTRs Shape Essential Post-transcriptional Regulatory Networks. Front. Mol. Biosci. 7, 220. https://doi.org/10.3389/fmolb.2020.00220